

Human Brain Project
Education Programme

1ST HBP STUDENT CONFERENCE

TRANSDISCIPLINARY RESEARCH LINKING NEUROSCIENCE,
BRAIN MEDICINE AND COMPUTER SCIENCE

8-10 FEBRUARY 2017
CAMPUS OF THE UNIVERSITY OF VIENNA, AUSTRIA

BOOK OF ABSTRACTS

Conference Programme Committee:

Nikola Simidjievski | JSI, Slovenia
Andrea Santuy | UPM, Spain
Miriam Menzel | FZ JUELICH, Germany
Jovan Tanevski | JSI, Slovenia
Vitali Karasenko | UHEI, Germany
Tara Mahfoud | KCL, UK

Organiser:

HBP Education Programme Office
Innsbruck, Austria



MEDIZINISCHE
UNIVERSITÄT
INNSBRUCK



Co-funded by
the European Union

1st Human Brain Project Student Conference

ISBN: 978-2-88945-421-1

DOI: 10.3389/978-2-88945-421-1

February 8th 2017 – February 10th 2017, Vienna, Austria.

The text of the abstracts is reproduced as submitted. The opinions and views expressed are those of the authors and have not been verified by the meeting Organisers, who accept no responsibility for the statements made or the accuracy of the data presented.

This project has received funding from the European Union's Horizon 2020 Research and Innovation Programme under Grant Agreement No. 720270 (HBP SGA1).

We are pleased to present the proceedings of the 1st Human Brain Project Student Conference - Transdisciplinary Research Linking Neuroscience, Brain Medicine and Computer Science - held in Vienna, Austria from 8 to 10 February 2017. The conference provides an open forum for exchange of new ideas among young researchers working on various aspects of neuroscience relevant to the Human Brain Project (HBP). The scope of the conference offers a plethora of opportunities for extensive scientific discussions, both intra- and inter-disciplinary, among peers and faculty through a variety of discussion sessions, lectures and social events.

We invited original high quality submissions describing innovative research in all research disciplines addressing the HBP research program. Particularly encouraged were submissions with a potential to inspire the research community by introducing new and relevant problems, concepts, and ideas, even if the work was at an early stage of development. The accepted abstracts cover a wide range of topics that emphasize theoretical and empirical foundations as well as novel approaches to specific problems with respect to the subprojects of the Human Brain Project.

We would like to use this opportunity to thank all authors for submitting their work to the 1st HBP Student Conference. We hope that the readers will enjoy the selected set of abstracts and that these contributions will inspire and encourage new interactions, discussions and opportunities beneficial to the authors, the Human Brain Project community as well as the communities of neuroscience, brain medicine and computer science.

Nikola Simidjievski,
Program Committee Chair of the 1st HBP Student Conference

List of Editors

Nikola Simidjievski, Jozef Stefan Institute, Slovenia

Andrea Santuy, Universidad Politécnica de Madrid, Spain

Miriam Menzel, Forschungszentrum Jülich, Germany

Jovan Tanevski, Jozef Stefan Institute, Slovenia

Vitali Karasenko, Heidelberg University, Germany

Tara Mahfoud, King's College London, United Kingdom

List of Organizers

Nikola Simidjievski, Jozef Stefan Institute, Slovenia

Andrea Santuy, Universidad Politécnica de Madrid, Spain

Miriam Menzel, Forschungszentrum Jülich, Germany

Jovan Tanevski, Jozef Stefan Institute, Slovenia

Vitali Karasenko, Heidelberg University, Germany

Tara Mahfoud, King's College London, UK

Viktoria Tipotsch, Medical University Innsbruck, Austria

Theresa Rass, Medical University Innsbruck, Austria

Alois Saria, Medical University Innsbruck, Austria

Table of Contents

- 9** Combining Robots with Neuromorphic Hardware: Case Study of a Visual Tracking Controller Embedding a Retina Circuit
 - 14** Computer Aided Diagnosis System Based on Random Forests for the Prognosis of Alzheimer’s Disease
 - 19** Convergent Analysis of Genome-Wide Data Suggests Association of Zinc Finger Genes with Lithium Response in Bipolar Disorder
 - 25** Probabilistic Framework Simulating Artificially-Induced Neural Plasticity by a Bidirectional Brain-Computer-Spinal Cord Interface
 - 27** Multi-Target Prediction of Motor Impairment Caused by Parkinson’s Disease Using Imaging Scans
 - 29** Deep Networks Using Auto-Encoders for PD Prodromal Analysis
 - 33** Dependency of Neural Tracts’ Curvature Estimations on Tractography Methods
 - 39** Earphone-Shaped EEG Instrument for Real-Time Brain State Monitoring
 - 43** Towards Modeling Metabolic and Communication Dysfunctions in Neurodegenerative Diseases
 - 47** Sharing Electrophysiological Data and Metadata on HBP Platforms – An Example Collaboratory Workflow
 - 50** ASSET for JULIA: Executing Massively Parallel Spike Correlation Analysis on KNL Cluster
 - 52** A Three-Dimensional Bayesian Spatial Variable Selection Model with Estimated HRF on fMRI Time Series Data
 - 56** A Compressing Auto-Encoder as a Developmental Model of Grid Cells
-

60	Quantitative Relations between CRAIIM Human Brain Atlases
68	Activation Likelihood Estimation Based Analysis of Memory-Related in Alzheimer Disease and Mild Cognitive Impairment Patients Using fMRI and PET Data
71	NestMC: A Morphologically Detailed Neural Network Simulator for Modern High Performance Computer Architectures
73	Real-Time Neuromorphic Encoding of Visual Stimuli Acquired with a Camera through Labview Interface
75	Neurogenesis on SpiNNaker
78	Short-Term Plasticity for Neuromorphic Hardware
80	Neuronal Dynamics: Silicon vs. Biology
82	Forging an Ensemble of Neuromorphic Chips into a Large-Scale Neural Network Emulation Platform
84	Bayesian Computing with Spikes
86	Efficiently Navigating through Structural Connectivity Parameter Spaces for Multiscale Whole Brain Simulations
88	The Dynamical Response Properties of Cortical Neurons in Silico
89	Developing Software Tools for Parameter Fitting and Validation of Neuronal Models
92	Consciousness and Cortical Connectivity in Subanaesthetic Ketamine Measured by TMS and EEG
95	Evidence for a Novel Connectivity Gradient of Executive Function in the Mammalian Brain
97	Markers of Consciousness before, during, and after Anesthesia; A TMS-EEG Study
100	Spatio-Temporal Spike Pattern Recognition in Massively Parallel Spike Trains

-
- 102** Spatiotemporal Patterns of a Population Burst in Cultured Neuronal Networks
- 105** Biophysical Modeling of Single-Neuron Contributions to EEG and ECoG Signals
- 107** Abnormalities of Walking as a Sign of Non-Alzheimer's Dementia
- 108** Analysis on Link and Motif Asymmetry of *C. elegans* Connectome
- 110** Native Architecture for Artificial Intelligence
- 113** An Evolutionary Machine Learning Algorithm to Enhance Language Processing
- 116** Creating Patterns for Machine Learning Using Multiple Alignment
- 119** The Basal Ganglia of the Hemispheres: Physiology, Function and Clinical Syndromes of Defeat
- 120** Modeling of Blood Flow in Branching Vessels of the Human Brain
- 121** Neural Dynamics and Inter-Brain Synchronization Underlying the Use of Nonverbal Social Cues to Read Other's Intentions to Cooperate
- 122** Dissecting the Effect of 16p11.2 Gene Dosage on Brain Structure
- 128** Cytoarchitectonic Mapping and Ultrahigh-Resolution 3D Reconstruction of the Bed Nucleus of Stria Terminalis
- 131** Synaptology of Layer II of the Transentorhinal Cortex in Alzheimer's Disease
- 134** A Fusion Mechanism for Depth Cues in the Primate Brain
- 136** Pre-Stimulus Brain State: A Possible Key to Vision Restoration?
- 139** A Study Based on the Reconstruction of Multivesicular Bodies in the Rodent Somatosensory Cortex
-

-
- 141** Comparing Synaptic Connectivity of Stress-Resilient and Stress-Susceptible Rats in the Default Network after Applying Learned-Helplessness Paradigm
 - 145** Neuropeptide Y and Y2R in Emotional and Non-Emotional Learning
 - 147** Assessment of Mid-Level Vision Segregation in Mice
 - 148** The Presence of Corpora Amylacea and Microglial Cells in Individuals with Unspecified Encephalopathy
 - 151** From Membranes to Transistors: A Physical Model of Spiking Neurons
 - 153** The Play Pen – Accelerated Embodiment for Accelerated Hardware
-

Combining Robots with Neuromorphic Hardware: Case Study of a Visual Tracking Controller Embedding a Retina Circuit

**Alessandro Ambrosano, Lorenzo Vannucci, Ugo Albanese,
Egidio Falotico, Cecilia Laschi**

*Scuola Superiore Sant'Anna – The Biorobotics Institute, Pontedera, Italy
a.ambrosano@sssup.it*

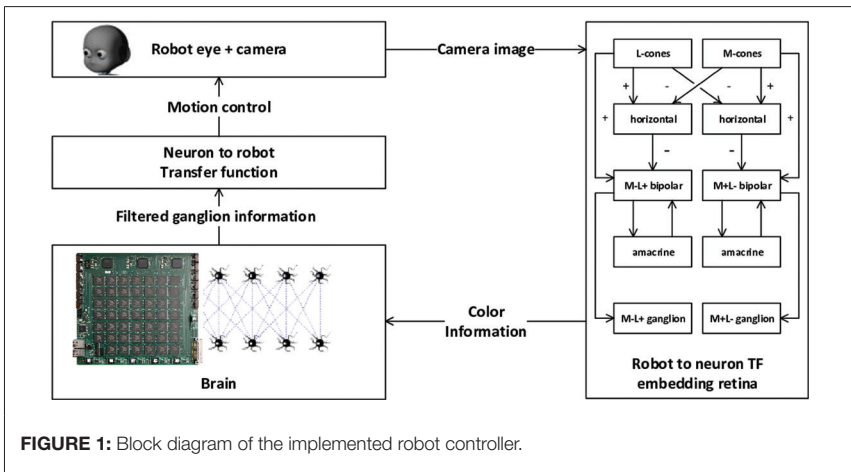
Introduction: One of the most important characteristics of the mammalian visual system is represented by the space-variant resolution retina with a high-resolution fovea that is fundamental for a detailed analysis of visual stimuli. The space-variant resolution of the retina requires efficient eye movements for correct vision. Two types of eye movements—saccades and smooth pursuit—enable us to fixate objects on the fovea. Saccades are high-velocity gaze shifts that bring the image of an object of interest onto the fovea, while the purpose of smooth pursuit eye movements is to minimize the retinal slip, i.e., the target velocity projected onto the retina, stabilizing the image of the moving object on the fovea. Shibata and colleagues suggested a control circuit for the integration of the most basic oculomotor behaviors (Shibata et al., 2001) including the smooth pursuit eye movement. A similar model of smooth pursuit and catch-up saccade (Falotico et al., 2010) was implemented on the iCub robot.

Robotic autonomy in unstructured environments is a challenging goal of great interest for many fields, with applications ranging from fully independent robots in a factory to self-driving cars. However, classical robotic controllers do not provide enough reliability for unpredictable variables that occur often, if not always, in such environments. For this reason many tracking controllers (Falotico et al., 2009; Zambrano et al., 2010; Vannucci et al., 2014, 2015) have been implemented embedding artificial neural networks components, providing, to a certain extent, the ability to learn and some robustness with respect to environment changes. A special category of neural networks, the Spiking Neural Networks (SNNs), models every neuron in the network with a biologically inspired dynamic model, and represents the communication between neurons with synaptic action potentials, also known as spikes. Such a low level description detail makes this model suitable for biologically inspired controllers.

In this work our aim is to validate the visual pursuit controller described in (Ambrosano et al., 2016), by implementing a similar closed loop mechanism using the iCub humanoid robot (Metta et al., 2010) and a SpiNNaker board (Painkras et al., 2013). The controller is embedding a retina modelling framework, which we used for wiring a

software circuit mimicking the red-green opponency pathway of the human retina, and a spiking neural network, executed on the SpiNNaker, for elaborating the retinal information.

Methods: In order to validate our controller on hardware, we tried to reproduce the same conditions we had on the simulated experiment (Ambrosano et al., 2016). We kept the same validation task, the smooth pursuit of a green target on a red background, where one single horizontal stripe near the center of the target is processed for implementing the tracking algorithm. The controller we used for the proposed experiment, depicted in Figure 1, includes four components: an iCub humanoid robot, a red-green opponency software retinal circuit, a SpiNNaker board and a special module (transfer function) translating neural spikes to robotic motor commands. The retinal circuit has been developed using COREM (Computational framework for realistic REtina Modelling), a framework developed at the University of Granada by Martínez-Cañada et al. (2016). The framework includes a set of microcircuits that can be combined together in a complex circuit simulating one or more retina pathways. The SpiNNaker board is a biologically inspired, massively parallel computing engine designed facilitate the modelling and the simulation of large-scale spiking neural networks of up to a billion neurons and a trillion synapses in biological real time.



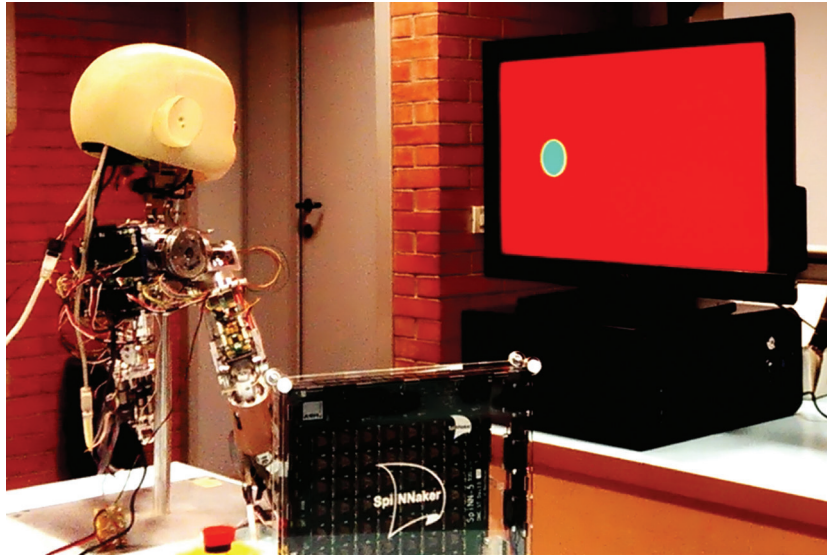


FIGURE 2: Experiment setup for the pursuit task.

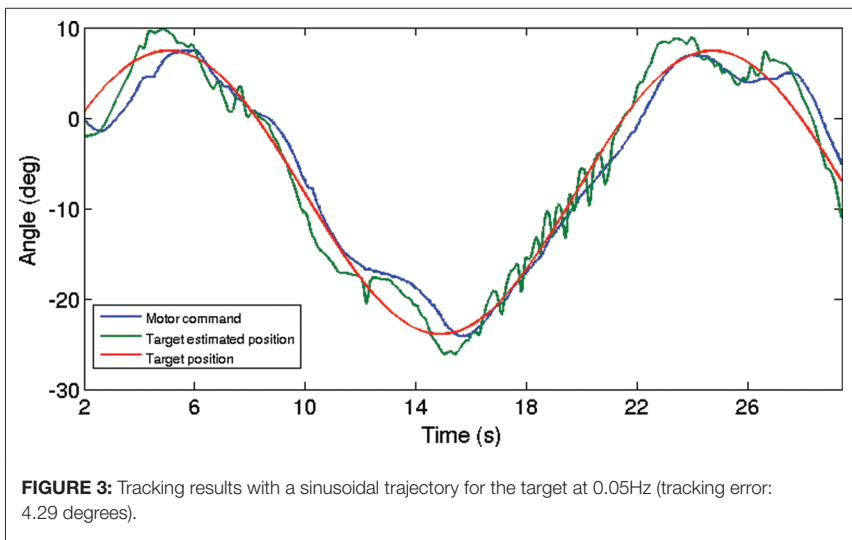
Input from an iCub eye camera is forwarded to the opponency retinal circuit, implemented using the COREM retina modelling framework, which transforms visual stimuli into a series of spike trains, suitable for being processed by the SpiNNaker board. A Spiking Neural Network implemented on the board processes the spike trains arriving from the retina model and outputs spike trains localizing the moving target offset on the retina. The resulting spikes are eventually translated to motor commands for the eye version of the robot. Two different retinal sub-circuits have been implemented, one more sensitive to red objects entering green background and one more sensitive to green objects entering red background. The functional separation is kept in the neural networks, where each sub-circuit is processed by a two tier network, implementing a filter focusing the spike processing near the center of the eye by modulating the synaptic weight. Figure 2 depicts the final setup for the described controller.

We obtained the hardware controller rewiring the closed loop mechanism of the Neurobotics Platform using a custom message passing library, deploying the original brain model on the SpiNNaker board and keeping the original transfer function. In order to connect properly the SpiNNaker board to the retina circuit, we had to

implement DC generator devices, which were provided by the platform in the software implementation, and integrate and fire neuron dynamics.

The major difference between the original controller and our implementation is the lack of real-time requirements of the former, as the closed loop mechanism of the Neurorobotics Platform waits for every component of the loop to terminate a time step before running the next one. In particular, the COREM framework was able to provide output with a frequency of 16 to 18Hz, which is lower than our target processing frequency (30Hz). A possible source of error could also be identified in the different frequencies at which the components of the hardware controller receive or send messages. These frequency differences were not present in the software implementation.

Results: We tested the controller with a target moving along a horizontal sinusoidal trajectory with a frequency (0.05 Hz). Figure 3 shows the target position and estimation, and the motor command generated by the controller during the pursuit task. The target estimation proved to be effective for the tracking task, even though it is not comparable to a classical image processing-based estimate.



Discussion: In this work we presented a hardware implementation of an existing software visual tracking controller embedding a retina model. The transition from a simulated to a hardware implementation validated the suitability of the controller for

the pursuit task, even though there is still some lack of generality, because only one horizontal strip of pixel is processed by the controller. We plan to extend the same mechanism to the whole image to test the controller for 2-dimensional pursuit.

Due to the low frame rate achievable using COREM, in order to track faster targets, or implement more complex retinal circuits, it will be necessary to optimize the framework or implement the framework to work on faster hardware (e.g., GPU).

REFERENCES

- Ambrosano, A., Vannucci, L., Albanese, U., Kirtay, M., Falotico, E., Martínez-Cañada, P., et al. (2016). “Retina color-opponency based pursuit implemented through spiking neural networks in the neurobotics platform,” in *Biomimetic and Biohybrid Systems: 5th International Conference, Living Machines 2016*, eds N. F. Lepora, A. Mura, M. Mangan, P. F. M. J. Verschure, M. Desmulliez, and T. J. Prescott (Edinburgh, UK: Springer International Publishing), 16–27.
- Falotico, E., Taiana, M., Zambrano, D., Bernardino, A., Santos-Victor, J., Dario, P., et al. (2009). “Predictive tracking across occlusions in the iCub robot,” in *Proceedings of the 9th IEEE-RAS International Conference on Humanoid Robots* (Paris, France).
- Falotico, E., Zambrano, D., Muscolo, G. G., Marazzato, L., Dario, P., and Laschi, C. (2010). “Implementation of a bio-inspired visual tracking model on the iCub robot,” in *Proc. 19th IEEE International Symposium on Robot and Human Interactive Communication (RO-MAN’10)* (Viareggio, Italy).
- Martínez-Cañada, P., Morillas, C., Pino, B., Ros, E., and Pelayo, F. (2016). A computational framework for realistic retina modeling. *Int. J. Neural Syst.* 26, 1650030. doi: 10.1142/S0129065716500301 PMID:27354192
- Metta, G., Natale, L., Nori, F., Sandini, G., Vernon, D., Fadiga, L., et al. (2010). The iCub humanoid robot: an open-systems platform for research in cognitive development. *Neural Net.* 23, 1125–1134. doi: 10.1016/j.neunet.2010.08.010 PMID:NOPMID
- Painkras, E., Plana, L. A., Garside, J., Temple, S., Galluppi, F., Patterson, C., et al. (2013). SpiNNaker: A 1-W 18-core system-on-chip for massively-parallel neural network simulation. *IEEE J. Solid State Circ.* 48, 1943–1953. doi: 10.1109/JSSC.2013.2259038 PMID:NOPMID
- Shibata, T., Vijayakumar, S., Conradt, J., and Schaal, S. (2001). Biomimetic oculomotor control. *Adapt. Behav.* 9, 189–207. doi: 10.1177/10597123010093005 PMID:NOPMID
- Vannucci, L., Cauli, N., Falotico, E., Bernardino, A., and Laschi, C. (2014). “Adaptive visual pursuit involving eye-head coordination and prediction of the target motion,” in *Proceedings of the 14th IEEE-RAS International Conference on Humanoid Robots* (Madrid, Spain).
- Vannucci, L., Falotico, E., Di Lecce, N., Dario, P., and Laschi, C. (2015). “Integrating feedback and predictive control in a bio-inspired model of visual pursuit implemented on a humanoid robot,” in *Biomimetic and Biohybrid Systems* (Springer).
- Zambrano, D., Falotico, E., Manfredi, L., and Laschi, C. (2010). A model of the smooth pursuit eye movement with prediction and learning. *Appl. Bionics Biomech.* 7, 109–118. doi: 10.1080/11762321003760944 PMID:NOPMID

Computer Aided Diagnosis System Based on Random Forests for the Prognosis of Alzheimer's Disease

M. Wehenkel^{1,2}, C. Bastin², P. Geurts¹, C. Phillips²

¹Department of Electrical Engineering and Computer Science, University of Liège, Liège, Belgium

²GIGAResearch, University of Liège, Liège, Belgium

m.wehenkel@ulg.ac.be

Introduction: Over the last decade, a large number of computer aided diagnosis (CAD) systems have been developed by researchers in neuroimaging to study neurodegenerative diseases or other kinds of brain disorders (Klöppel et al., 2008; Garraux et al., 2013; Fu et al., 2008). Briefly, machine-learning (ML) techniques help doctors to distinguish groups of people (e.g., healthy vs. diseased) by automatically identifying characteristics in the images that discriminate the groups. The challenge in the modelling of CAD systems is not only to perform well in terms of prediction but also to provide relevant information about the diagnosis, such as regions of interest in the brain that are affected by the disease.

In this abstract, we propose an original CAD system consisting in the combination of brain parcelling, ensemble of trees methods, and selection of (groups of) features using the importance scores embedded in tree-based methods. Indeed, on top of their ease of use and accuracy without *ad hoc* parameter tuning, tree ensemble methods such as random forests (RF) (Breiman, 2001) or extremely randomized trees (ET) (Geurts et al., 2006) provide interpretable results in the form of feature importance scores. We also compare the performance and interpretability of our proposed method to standard RF and ET approaches, without feature selection, and to multiple kernel learning (MKL) (Bach et al., 2004). The latter was shown to be an efficient method notably capable of dealing with anatomically defined regions of the brain by the use of multiple kernels.

Methods: Our CAD system is designed to discriminate older adults with Mild Cognitive Impairments (MCI) in terms of their clinical outcome 4 years later, based on their current PET images. More precisely, 45 individuals presenting mild cognitive impairments (MCI) at the beginning of the study were followed during 4 years and their diagnostic updated based on neuropsychology tests (no further imaging was performed). Among those subjects, 22 patients were eventually diagnosed with Alzheimer's disease (AD) in the course of the study. These were labelled "MCI converters" (MCIc). The others showed no cognitive decline and are thus denominated stable MCI (sMCI). The aim of such a CAD system is thus to predict the likelihood of progression to dementia based on the images acquired before the onset of the disease.

The PET images were pre-processed using SPM8 (<http://www.fil.ion.ucl.ac.uk/spm/software/>). This included spatial normalization to the MNI reference space and intensity normalization by the cerebellar intensities. Then a feature vector for each individual was built by extracting the voxel values within the brain volume.

The first step of our diagnosis system consists in learning a tree ensemble model and attributing a score per AAL region (Tzourio-Mazoyer et al., 2002) from the mean of the voxel importance scores in each region. In a second step, the k best regions according to these scores are selected and used to learn a new model (with k set to 10 in our experiments). This approach is thus a combination of group selection and ensemble methods. The procedure used for its assessment is summarized in Figure 1. We evaluate it with a “leave 10% of subjects per group out” cross validation (CV) procedure for RF and ET respectively with default parameter values ($M = 500$ trees and $K = \sqrt{N}$ where N is the total number of features). Standard RF and ET (without feature selection) and MKL, all with default parameter setting, are also assessed for comparison with the same CV procedure. As RF and ET involve randomization, experiments were repeated ten times, called runs here under, to obtain mean and standard deviation of performance metrics.

Algorithm Protocol of model assessment.

Require: Divide the learning set (LS) into X folds.

for $i = 1 : X$ **do**

 Remove the i^{th} fold from LS.

 Fit an ensemble of trees from the learning set $LS \setminus \{i^{\text{th}} \text{ fold}\}$ to obtain importance scores.

 Compute a score W_R for each set of features.

 Rank the groups of features and choose the ten best groups.

 Build an ensemble model using the ten groups and the set $LS \setminus \{i^{\text{th}} \text{ fold}\}$.

 Test the model on the i^{th} fold.

end for

FIGURE 1: Protocol to assess the proposed CAD system.

To interpret the results of the proposed method and to have insights about regions involved in the prognosis, we compute importance scores for each ensemble of trees. We then average the scores over the folds and the runs and we subsequently compute a score for each brain region. For MKL, we use the weights attributed to each brain area. Finally, as our proposed method embeds a selection process, we also analyze the frequency of selection of brain areas over the folds and the runs to have additional information about important regions.

Results: Table 1 summarizes the accuracy, sensitivity and specificity obtained with each method. MKL is less efficient in terms of accuracy than tree-based approaches. Moreover, we observe that extremely randomized trees, which include supplementary randomization, provide better accuracy than RF. Our proposed CAD system obtains also a better accuracy with ET than RF. The preliminary step of group selection slightly increases mean values of accuracies and sensitivities of ensemble methods and decreases the variance caused by randomization with a large number of features (more or less 200,000 voxels to consider).

In terms of interpretability with weights for MKL and importance scores for the ensemble methods, we can observe in Table 2 the listing of the ten most contributing regions for each method for the discrimination between MCIc and sMCI. The areas TemporalMidR, AngularR, and TemporalMidL are common to the five models. Moreover, ParietalInfR, Vermis7, and TemporalInfR are identified among the most important by each of the tree-based methods. Finally, we analyse the regions that have been selected the most frequently over the folds and the runs during the selection process of our procedure. For RF, in order of decreasing frequency, the ten most frequent are TemporalMidR, AngularR, ParietalInfR, TemporalMidL, TemporalInfR, CuneusL, Vermis7, TemporalInfL, Cerebelum6R, and Vermis8 whereas ET identifies TemporalMidR, AngularR, TemporalMidL, ParietalInfR, TemporalInfR, Vermis7, TemporalInfL, Cerebelum6R, Vermis8, Vermis6 as the first ten. Nevertheless, the frequency of selection for the last three listed areas for both methods is at most half the time. Given this information, those regions should likely not be considered as informative to decide if an individual will convert to AD within 4 years following the start of cognitive impairments.

TABLE 1: Summary of method performance and corresponding *p*-values (obtained using a permutation test with 100 repetitions). The asterisk indicates a *p*-value <0.05. GS abbreviation is used for group selection.

Method	Accuracy (%)	Sensitivity (%)	Specificity (%)
MKL	68.89 (0.02)*	59.09 (0.23)	78.26 (0.01)*
RF	77.11 ± 2.58 (0.01)*	71.82 ± 4.18 (0.02)*	82.17 ± 2.47 (0.03)*
ET	80.22 ± 3.22 (0.01)*	77.73 ± 5.85 (0.01)*	82.61 ± 4.10 (0.01)*
GS and RF	78.00 ± 1.26 (0.01)*	76.36 ± 1.92 (0.01)*	79.57 ± 2.93 (0.01)*
GS and ET	80.44 ± 1.75 (0.01)*	78.18 ± 3.59 (0.01)*	82.61 ± 0(0.01)*

TABLE 2: Ranking of the first ten most contributing regions of AAL brain atlas.

Rk	Method				
	MKL	RF	ET	GS and RF	GS and ET
1	TemporalMidR	AngularR	TemporalMidR	AngularR	TemporalMidR
2	AngularR	TemporalMidR	AngularR	TemporalMidR	AngularR
3	Vermis6	ParietalInFR	TemporalMidL	ParietalInFR	ParietalInFR
4	ParietalSupR	TemporalMidL	ParietalInFR	TemporalMidL	TemporalMidL
5	TemporalMidL	Vermis7	Vermis7	CuneusL	Vermis7
6	FrontalSupMedialR	CuneusL	TemporalInFR	Cerebelum10L	TemporalInFR
7	Vermis8	TemporalInFR	TemporalInFL	Vermis7	Cerebelum6R
8	OlfactoryL	Vermis 8	Vermis8	TemporalInFR	Cerebelum10L
9	Cerebelum10L	TemporalInFL	Vermis6	ThalamusL	TemporalInFL
10	ThalamusL	TemporalSupR	Cerebelum6R	Cerebelum6R	Vermis6

Discussion: We have shown that, at least for the data and problem considered here, tree-based ensemble methods are competitive methods and that they can outperform other advanced methods like MKL. They exhibit better accuracy, sensitivity and specificity and provide good interpretability through importance scores. Furthermore, group selection combined with ensemble of trees adds more insight about the regions that are relevant to diagnose a MCI patient who is likely to develop Alzheimer's disease within 4 years. Indeed, group selection enables us to study the frequency of selection of a brain area among the whole set. It should also be noted that the results regarding the most involved regions are coherent with studies showing that MCI patients who are about to develop Alzheimer's disease exhibit more hypometabolic temporoparietal areas than MCI patients who remain stable in the next few years (Chételat et al., 2003). Another advantage of feature selection is that it improves the sensitivity of the diagnosis, which is the quantity relative to true positive (i.e., MCI converters), and largely reduces the variance induced by the initial huge number of features and the randomization process. Finally, the ET approach, with or without group selection, gives rise to accuracy slightly higher than that of RF. Nevertheless, supplementary tests are needed to assess if the differences of accuracy between the distinct methods are statistically significant.

To conclude, we show that using group selection combined with ensemble of trees compose a good CAD system which can help making a correct early prognosis of people suffering of mild cognitive impairments.

REFERENCES

- Bach, F., Lanckriet, G., and Jordan, M. (2004). "Multiple kernel learning, conic duality, and the SMO algorithm," in *Proceedings of the 21st International Conference on Machine Learning* (p. 6). (Banff, Canada: ACM).
- Breiman, L. (2001). Random forests. *Mach. Learn.* 45, 5–32. doi: 10.1023/A:1010933404324 PMID:NOPMID
- Chételat, G., Desgranges, B., De La Sayette, V., Viader, F., Eustache, F., and Baron, J. C. (2003). Mild cognitive impairment: can FDG-PET predict who is to rapidly convert to Alzheimer's disease? *Neurology* 60, 1374–1377. doi: 10.1212/01.WNL.0000055847.17752.E6 PMID:12707450
- Fu, C. H., Mourao-Miranda, J., Costafreda, S. G., Khanna, A., Marquand, A. F., Williams, S. C., et al. (2008). Pattern classification of sad facial processing: toward the development of neurobiological markers in depression. *Biol. Psychiatry* 63, 656–662. doi: 10.1016/j.biopsych.2007.08.020 PMID:17949689
- Garraux, G., Phillips, C., Schrouff, J., Kreisler, A., Lemaire, C., Degueldre, C., et al. (2013). Multiclass classification of FDG PET scans for the distinction between Parkinson's disease and atypical Parkinsonian syndromes. *Neuroimage Clin.* 2, 883–893. doi: 10.1016/j.nicl.2013.06.004 PMID:24179839
- Geurts, P., Ernst, D., and Wehenkel, L. (2006). Extremely randomized trees. *Mach. Learn.* 63, 3–42. doi: 10.1007/s10994-006-6226-1 PMID:NOPMID
- Klöppel, S., Stonnington, C. M., Chu, C., Draganski, B., Scahill, R. I., Rohrer, J. D., et al. (2008). Automatic classification of MR scans in Alzheimer's disease. *Brain* 131, 681–689. doi: 10.1093/brain/awm319 PMID:18202106
- Tzourio-Mazoyer, N., Landeau, B., Papathanassiou, D., Crivello, F., Etard, O., Delcroix, N., et al. (2002). Automated anatomical labeling of activations in SPM using a macroscopic anatomical parcellation of the MNI MRI single-subject brain. *Neuroimage* 15, 273–289. doi: 10.1006/nimg.2001.0978 PMID:11771995

Convergent Analysis of Genome-Wide Data Suggests Association of Zinc Finger Genes with Lithium Response in Bipolar Disorder

Claudia Pisanu¹, Donatella Congiu¹, Marta Costa^{1,2}, Caterina Chillotti³, Raffaella Ardaù³, Giovanni Severino¹, Andrea Angius⁴, Urs Heilbronner⁵, Liping Hou⁶, Francis J. McMahon⁶, Thomas G. Schulze^{5,6}, Maria Del Zompo^{1,3}, Alessio Squassina¹

¹Department of Biomedical Sciences, Section of Neuroscience and Clinical Pharmacology, University of Cagliari, Cagliari, Italy

²The Francis Crick Institute, London, United Kingdom

³Unit of Clinical Pharmacology of the University Hospital of Cagliari, Cagliari, Italy

⁴Istituto di Ricerca Genetica e Biomedica, Consiglio Nazionale delle Ricerche (CNR), Cagliari, Italy

⁵Institute of Psychiatric Phenomics and Genomics (IPPG), Medical Center of the University of Munich, Campus Innenstadt, Innenstadt, Germany

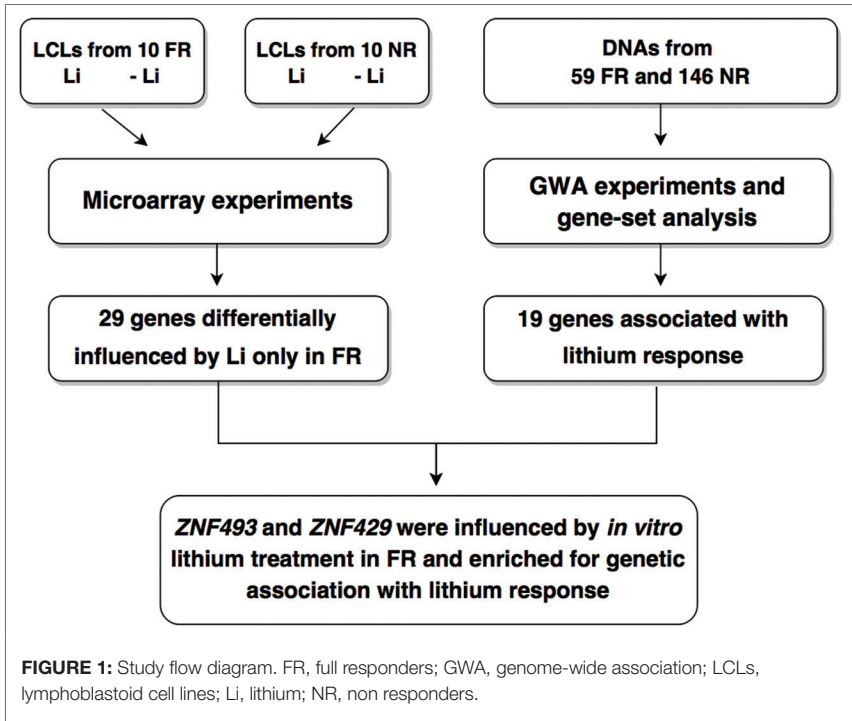
⁶Intramural Research Program, National Institute of Mental Health, National Institutes of Health, U.S. Department of Health & Human Services, Bethesda, MD, United States

claudia.pisanu@unica.it

Introduction: Lithium has been used for over 50 years in the management of bipolar disorder (BD) for its effectiveness in the acute phases of illness and in the prevention of manic and depressive recurrences (Grof et al., 2002). Response to lithium is highly variable, and although 30% of patients are excellent responders, 70% show partial or no response (Malhi et al., 2012). The identification of reliable biomarkers to predict the clinical outcome would be of great help to limit side effects and toxicity in unresponsive BD patients. Response to lithium treatment is heritable, and a large body of evidence suggests that genetics plays a key role in modulating the degree of response (Malhi et al., 2012). Although genome-wide association studies (GWAS) are starting to provide promising results, the genetic bases of variability in lithium response are far from being elucidated. GWAS allow exploring the genome for genetic variants associated with the phenotypic trait, but their power is limited in that the function of many variants is not known. On the other hand, transcriptome studies allow investigating the role of differentially expressed genes in the phenotype under study. Deeper information on the genetics of lithium response would be given by the integration of data from multiple omic datasets. In this study we used a convergent approach integrating, for the first time, genome-wide expression and genome-wide genotyping data from BD patients characterized for lithium response to identify genes potentially involved in modulating the clinical efficacy of lithium.

Methods

Sample: A study flow diagram is reported in Figure 1. We used two datasets: (1) genome-wide genotyping data from 205 BD patients characterized for lithium response; (2) transcriptome data from lymphoblastoid cell lines (LCLs) of a subsample of 10 full responders (FR) and 10 non responders (NR) to lithium, cultured with or without lithium chloride 1 mM for 1 week.



Patients with a diagnosis of BD according to Research Diagnostic Criteria and DSM-IV criteria were recruited at the Lithium Clinic of the University Hospital of Cagliari, Italy. Lithium response was evaluated using the “Retrospective Criteria of Long-Term Treatment Response in Research Subjects with Bipolar Disorder” scale (Malhi et al., 2012). The research protocol followed the principles of the Declaration of Helsinki and was approved by the Ethics Committee of the University of Cagliari, Italy. All participants signed informed written consent.

Genome-wide association: DNA was extracted from peripheral blood samples. The sample is part of the Consortium on Lithium Genetics (ConLiGen) (Mangino et al., 2012), and genome wide genotyping was carried out at the National Institute of Mental Health (Bethesda, USA), with Illumina 2.5 M Omni Chip arrays according to the manufacturers' protocols.

Genome-wide gene expression and validation with quantitative real-time PCR: Microarrays were run using RNA extracted from LCLs. For each sample, complementary DNAs (cDNAs) were obtained and hybridized to GeneChip® Human Gene 1.0 ST Arrays (Affymetrix, CA, USA). Genes showing convergent evidence for involvement in lithium response were validated with quantitative real-time PCR (qRT-PCR).

Statistical analyses: Transcriptome data were normalized using the Robust Multi-array Average algorithm. Genes were tested for differential expression after *in vitro* lithium treatment in both FR and NR using the paired *t*-test implemented in limma (Mishra and Macgregor, 2015), in R (v. 3.3.1). In order to include the largest possible number of genes at this step, significance was defined based on a false discovery rate threshold of 20%. We created a list of genes altered by lithium exclusively in FR, as these genes could be involved in modulating clinical efficacy of lithium.

Quality control of GWAS data was performed with PLINK 1.07 (Purcell et al., 2007). Single nucleotide polymorphisms (SNP) were excluded in case of minor allele frequency <0.05 or deviation from Hardy–Weinberg equilibrium with $p < 0.0001$. Population outliers were identified with principal component analysis using EIGENSOFT and removed. Association with lithium response was tested using logistic regression with lithium response as the outcome variable.

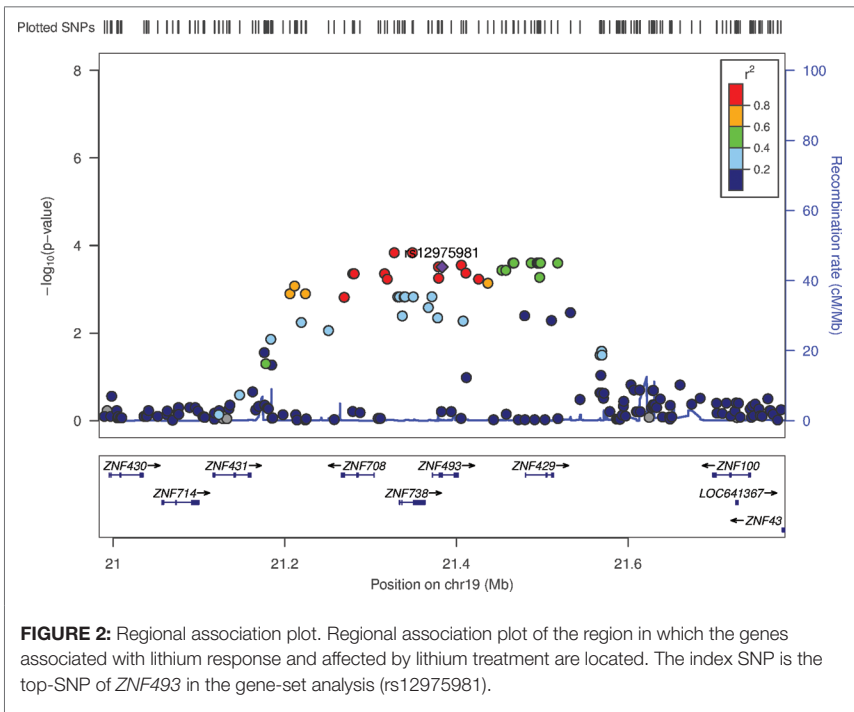
Gene-based analysis was performed with VEGAS2 (Schulze et al., 2010) using the list of SNPs and *p*-values generated by PLINK. VEGAS2 calculates the gene-based empirical association *p*-values taking into account gene-size, SNP density and linkage disequilibrium between SNPs. We focused the analyses on the genes differentially expressed after lithium treatment exclusively in FR ($n = 29$) and applied a Bonferroni-corrected threshold of $p = 0.0017$ (i.e., $0.05/29$).

Genes which were (1) differentially expressed after lithium treatment in FR but not in NR and (2) enriched for association with lithium response from the gene-based association analyses were selected for validation with qRT-PCR. Relative expression levels were calculated with the $\Delta\Delta C_t$ method and differences between baseline and lithium-treated samples were analyzed with a paired *t*-test using R.

Results: Lithium influenced the expression of 33 genes in FR and 15 genes in NR with a FDR <20%. Twenty-nine genes were altered by lithium exclusively in FR.

Gene-set analyses identified 19 genes as significantly associated with lithium response. Of these genes, two were also regulated by lithium exclusively in FR: zinc finger protein 429 (ZNF429, gene-set $p = 0.0003$) and zinc finger protein 493 (ZNF493, gene-set $p = 0.0005$).

The region in which *ZNF493* and *ZNF429* are located hosts several members of the zinc finger proteins genes cluster (Figure 2). Findings from qRT-PCR validated the lithium-induced underexpression of *ZNF493* in FR [fold change (FC) = 0.71, $p = 0.036$], while *ZNF429* showed a trend for downregulation (FC = 0.82, $p = 0.06$).



Discussion: This study suggests for the first time that zinc finger proteins could be involved in lithium response and mechanism of action. We showed that *ZNF429* and *ZNF493* are downregulated by lithium treatment in LCLs of BD patients responders to lithium, while these genes were not affected by *in vitro* treatment in NR. Moreover, the two genes were enriched in genetic variants associated with lithium response,

suggesting that the differential sensitivity to lithium of these genes in FR and NR might be mediated by genetic variants located in their region.

Zinc finger proteins are a large family of small functional domains involved in several functions comprising transcriptional activation, regulation of apoptosis and protein folding. Another member of the Cys2His2 zinc finger class, zinc finger protein 804A (ZNF804A), was associated with BD and schizophrenia (Smyth, 2004). Both *ZNF429* and *ZNF493* are located at 19p12, a region previously associated with telomere homeostasis (Squassina et al., 2015). Zinc finger proteins could modulate the expression of genes involved in telomere maintenance through their interaction with DNA or influence the posttranslational expression of a gene *via* binding with RNA or proteins (Squassina et al., 2015). Interestingly, lithium might normalize telomere dysfunction (Williams et al., 2011). It could be speculated that the impact exerted by lithium on telomere length could be partly mediated by its action on zinc finger proteins.

Limitations of this study include the limited sample size and the use of LCLs. Although LCLs represent a valuable model to test peripheral effects of medications, they do not constitute a brain model. The strengths of our study include the integration of genotyping and gene expression data from subjects characterized for lithium response using a well validated scale and the choice to include only subjects of Sardinian origin, a population with a high genetic homogeneity and a low level of stratification.

To our knowledge, this is the first evidence supporting the involvement of zinc finger genes in lithium's mechanism of action and response.

REFERENCES

- Grof, P., Duffy, A., Cavazzoni, P., Grof, E., Garnham, J., MacDougall, M., et al. (2002). Is response to prophylactic lithium a familial trait? *J. Clin. Psychiatry* 63, 942–947. doi: 10.4088/JCP.v63n1013 PMID:12416605
- Malhi, G. S., Tanious, M., Das, P., and Berk, M. (2012). The science and practice of lithium therapy. *Aust. N. Z. J. Psychiatry* 46, 192–211. doi: 10.1177/0004867412437346 PMID:22391277
- Mangino, M., Hwang, S. J., Spector, T. D., Hunt, S. C., Kimura, M., Fitzpatrick, A. L., et al. (2012). Genome-wide meta-analysis points to CTC1 and ZNF676 as genes regulating telomere homeostasis in humans. *Hum. Mol. Genet.* 21, 5385–5394. doi: 10.1093/hmg/dd3382 PMID:23001564
- Mishra, A., and Macgregor, S. (2015). VEGAS2: software for more flexible gene-based testing. *Twin. Res. Hum. Genet.* 18, 86–91. doi: 10.1017/thg.2014.79 PMID:25518859
- Purcell, S., Neale, B., Todd-Brown, K., Thomas, L., Ferreira, M. A., Bender, D., et al. (2007). PLINK: a tool set for whole-genome association and population-based linkage analyses. *Am. J. Hum. Genet.* 81, 559–575. doi: 10.1086/519795 PMID:17701901

- Schulze, T. G., Alda, M., Adli, M., Akula, N., Arda, R., Bui, E. T., et al. (2010). The international consortium on lithium genetics (ConLiGen): an initiative by the NIMH and IGSLI to study the genetic basis of response to lithium treatment. *Neuropsychobiology* 62, 72–78. doi: 10.1159/000314708 PMID:20453537
- Smyth, G. K. (2004). Linear models and empirical bayes methods for assessing differential expression in microarray experiments. *Stat. Appl. Genet. Mol. Biol.* 2004, Article3. doi: 10.2202/1544-6115.1027
- Squassina, A., Pisanu, C., Corbett, N., and Alda, M. (2015). Telomere length in bipolar disorder and lithium response. *Eur. Neuropsychopharmacol.* 27, 560–567. doi: 10.1016/j.euroneuro.2015.10.008 PMID:NOPMID
- Williams, H. J., Norton, N., Dwyer, S., Moskvina, V., Nikolov, I., Carroll, L., et al. (2011). Fine mapping of ZNF804A and genome-wide significant evidence for its involvement in schizophrenia and bipolar disorder. *Mol. Psychiatry* 16, 429–441. doi: 10.1038/mp.2010.36 PMID:20368704

Probabilistic Framework Simulating Artificially-Induced Neural Plasticity by a Bidirectional Brain-Computer-Spinal Cord Interface

Stefano Vrizzi^{1,2,3,4}, **Guillaume Lajoie**^{3,4,5}, **Adrienne Fairhall**^{3,4}

¹*University of Tübingen, Tübingen, Germany*

²*Faculty of Biological Sciences, School of Biomedical Sciences, University of Leeds, Leeds, United Kingdom*

³*Department of Applied Mathematics, University of Washington, Seattle, WA, United States*

⁴*Department of Physiology and Biophysics, University of Washington, Seattle, WA, United States*

⁵*University of Washington Institute for Neuroengineering, Seattle, WA, United States*

stefano.vrizzi@student.uni-tuebingen.de

Introduction: Brain-Computer-Interfaces (BCIs) are a family of devices that process recorded brain activity to perform a desired output. Recent development of Bidirectional Brain-Computer Interface (BBCI), neural implants that not only record single-neuron activity at precise spike-time resolution, but also stimulates neuronal sites, open the door to direct interaction with the dynamics of neural circuits in the brain and in the nervous system at large. Specifically, Bidirectional-Brain-Computer-Spinal Cord Interfaces (BBCSIs) are implemented to record motor cortex (MC) activity and stimulate spinal cord (SC) sites to promote rehabilitation following spinal cord injury (SCI). Stimulation by implantable electronic circuits, named the Neurochip (Mavoori et al., 2005), aims at triggering neural plasticity to restore disrupted pathways by exploiting Spike-Timing Dependent Plasticity (STDP) rules. Our first goal was to capture artificially-induced neural plasticity by mimicking the BBCSI spike-triggered stimulation protocol on STDP-driven neural networks modelled by probabilistic firing rates modulated by external driving rates. Second, we investigated the differences in stimulating one site, either in MC or SC, or in both sites, modelling healthy and or SCI conditions. The aims of our study converged to the ultimate goal of contributing to the technological development of the Neurochip, in order to help restore impaired motor functions in human beings.

Methods: In a probabilistic model that we numerically simulate, MC and SC were represented by excitatory and inhibitory neurons, which were recurrently connected according to set connectivity probabilities schematising the corticospinal tract (CST). We investigated how spike-triggered stimulation protocols changed mean synaptic strength of existing excitatory synapses through a simple multiplicative STDP rule. We run different simulations stimulating either a group of neurons in MC or SC, or both, after set delays from the time of spiking of a recording neuron. Finally, we also

explored effects on SCI by testing a double-site stimulation protocol, after setting a low probability of connection between MC and SC.

Results: (1) Results were qualitatively matched previous experimental findings (Nishimura et al., 2013), by evolving in time consistently with the original computational model (Lajoie et al., 2017), while incorporating higher complexity, such as inhibitory populations. (2) As we hypothesised, synapses strengthened between recording group and stimulated groups, as well as between stimulated groups. The model indeed allowed to explore how stimulation of multiple groups, both in MC and SC, may cause linear and non-linear interactions of mean synaptic strengths between groups of neurons. (3) Investigation of SCI conditions suggested that temporal evolution of mean synaptic strength may depend on the mean probability of connection among groups of neurons.

Discussion: Although our research is in progress, these simulations highlight possible implications of eliciting plasticity along descending pathways of different size and by double-site stimulation protocols.

REFERENCES

- Lajoie, G., Krouchev, N. I., Kalaska, J. F., Fairhall, A. L., and Fetz, E. E. (2017). Correlation-based model of artificially induced plasticity in motor cortex by a bidirectional brain-computer interface. *PLoS Comput. Biol.* 13(2), e1005343. doi: 10.1371/journal.pcbi.1005343
- Mavoori, J., Jackson, A., Diorio, C., and Fetz, E. (2005). An autonomous implantable computer for neural recording and stimulation in unrestrained primates. *J. Neurosci. Methods* 148, 71–77. doi: 10.1016/j.jneumeth.2005.04.017 PMID:16102841
- Nishimura, Y., Perlmutter, S. I., Eaton, R. W., and Fetz, E. E. (2013). Spike-timing-dependent plasticity in primate corticospinal connections induced during free behavior. *Neuron* 80, 1301–1309. doi: 10.1016/j.neuron.2013.08.028 PMID:24210907

Multi-Target Prediction of Motor Impairment Caused by Parkinson's Disease Using Imaging Scans

Vanja Mileski^{1,2}, Dragi Kocev^{1,2}, Bogdan Draganski³, Sašo Džeroski^{1,2}

¹Jožef Stefan Institute, Ljubljana, Slovenia

²International Postgraduate School Jožef Stefan, Ljubljana, Slovenia

³Centre Hospitalier Universitaire, Lausanne, Switzerland

saso.dzeroski@ijs.si

Introduction: The Parkinson's disease progression is typically described with motor assessment scores of the motor impact of the disease on the patients (MDS-UPDRS). The goal of this work is to search for groups of subjects that exhibit similar behavior in terms of the multiple motor assessment scores. The identified groups/clusters of subjects are then described using image features including Regions of Interest (ROIs) from fMRI scans, as well as DaT scans. This can save time, money and effort from specialists and can also provide an insight or even detect the biomarkers that indicate Parkinson's disease at an early stage of the disease.

Methods: The three data sets used were acquired from the Parkinson's Progression Markers Initiative (PPMI) database. We distinguish two variants of the merged dataset: baseline, where we consider only the earliest scores and imaging data for each patient resulting in 374 examples, and complete dataset, where we take all scores and imaging data for each patient resulting in 716 examples.

The task at hand is multi-target regression: the goal is to predict all of the scores for the motor impairment assessments from the extracted ROIs (of the fMRIs) and the DaT scans features. To this end, we use CLUS—a system for multi-target prediction based on the predictive clustering framework where we use predictive clustering trees (PCTs)—a generalization of the decision trees towards predicting structure outputs including multiple continuous target variables. Furthermore, we use two tree-based ensemble methods: bagging and random forests. The results from the predictive modelling methods applied on the two datasets reveal that the lowest error (as estimated with 10-fold cross-validation) is achieved using random forests on the complete dataset that uses all of the imaging data and scores with performances ranging from 0.603 to 0.883 as opposed to 0.889 to 0.926 for the baseline (measured as normalized root mean squared error—nRMSE). We also introduced a hierarchy in the output space and discovered that the introduction of such a hierarchy slightly improves the predictive performance.

Results: The results from the analysis are indicative that both the descriptive and predictive power of all of the obtained models is good. The improved performance obtained on the complete dataset is mainly due to the fact that by using the additional samples, we introduced more variability in the target space. Namely, the baseline dataset contains measurements from subjects that are, more or less, at an earlier stage of the disease, hence the motor assessment scores are lower. Moreover, since it is impossible to investigate subjects that are the same stage of disease simultaneously, including information obtained throughout various disease stages helps to construct a better predictive model.

Deep Networks Using Auto-Encoders for PD Prodromal Analysis

Eleni Kroupi¹, Aureli Soria-Frisch¹, Marta Castellano¹, David Ibáñez¹, Jacques Montplaisir², Jean-Francois Gagnon², Ron Postuma², Stephen Dunne¹, Giulio Ruffini¹

¹Starlab, Barcelona, Spain

²CARSM, Montréal, QC, Canada

Introduction: Accurate diagnosis of the sleep disorder known as Rapid-eye movement behavior disorder (RBD) is a clinically relevant problem given its predictive role in years-later neurodegeneration (Postuma et al., 2015). Concretely RBD can evolve with a very large probability into various α -synucleinopathies, from which Parkinson's Disease (PD), and Dementia with Lewy Bodies (DLB) are the most common ones. We aim to develop tools for diagnosis of RBD and even prognosis of PD and DLB based on the analysis of electroencephalography (EEG). We analyze therefore a data set acquired at the Center for Advanced Research in Sleep Medicine (CARSM) in Montreal while patients were exclusively diagnosed as RBD. Machine Learning (ML) algorithms have been already proposed to automatically discriminate across the different disorders (Soria-Frisch et al., 2014). However, there is still need for improving the accuracy of discrimination across these disorders. Especially the reduction of the feature space needs further attention. To this regard, it is necessary to find ways to extract the most meaningful information of the EEG extracted features in order to train the classifiers based on the most relevant representation of the data. Compression methods based on ML can serve as a tool to extract the most meaningful feature signatures. Among various ML methods, neural networks have been used for image compression (Jiang, 1999). We are interested in investigating whether a particular type of deep neural networks known as auto encoders, which have been used for compression in images (Jiang, 1999), can serve for feature dimensionality reduction in prognostic and diagnostic tools of the aforementioned disorders, and whether they can complement or improve state-of-the-art ML methods.

Auto-encoders are a form of unsupervised neural networks, whose application may reveal interesting data structures by introducing constraints on the network. Moreover, it is not until recent years that deep neural networks have outperformed many conventionally used learning algorithms. This is due to their capability of learning complex relationships within the data by using several levels of data representation through multiple layers. This study aims at exploring the accuracy of using auto-encoders as a feature projection tool, which is compared to a conventional feature selection method

based on a wrapper. Both types of feature reduction procedures are applied to EEG features.

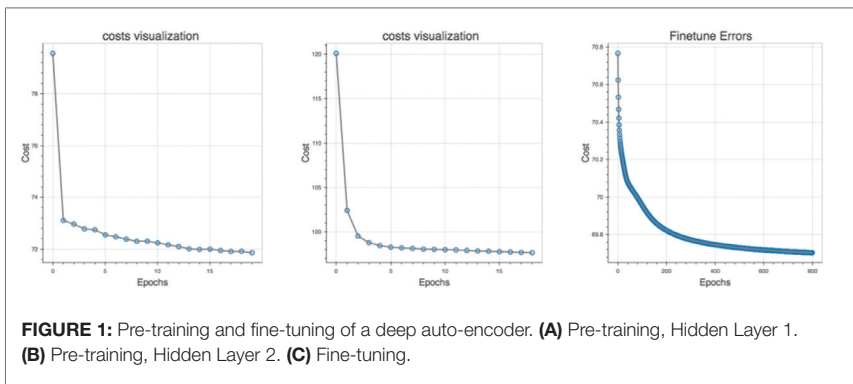
Methods: Many types of auto-encoders exist, of which the most common is the de-noising auto-encoder. Auto-encoders are neural networks used to find a mapping function from the training data into itself. Its characterizing trait is the corruption of the data at the input layer, in order to avoid learning the identity function, and in order for the achieved mapping to be more robust to slight modifications of the input data. Auto-encoders can form deep neural networks, known as stacked auto-encoders. The latter include auto-encoders one on the top of the other. Typically, it is suggested to use an unsupervised criterion to pre-train each layer in order to produce a higher-level representation of the feature space based on the lower-level representation of the previous layer. The rationale is to avoid getting stuck on poor solutions that may appear due to random initializations (Hinton and Salakhutdinov, 2006). Once this is carried out, a fine-tuning step is performed, in which all the network parameters are updated. In our case we used a deep auto-encoder with two hidden layers with 200 nodes in the first layer and {10, 20, 40, 60, 80, 100} nodes in the second layer. Each layer was pre-trained using a mini-batch gradient descent method with mini-batches of size 10, 20 pre-training epochs and 800 fine-tuning epochs, a corruption level of 0.1 for each layer, the sigmoid function as the activation function, and the cross-entropy function as the cost function.

The data was whitened in terms of mean and standard deviation, i.e., so that to have zero mean and standard deviation 1, and then scaled so that they belong to the [0,1] space. The rationale for scaling in the [0,1] space is that given we use the cross entropy, which is a measure of similarity between two distributions, as error function, each distribution should be represented in the unit hypercube.

Regarding the input to the deep auto-encoder, the awake eyes-closed EEG signals of 224 subjects (99 Healthy Controls—HC-, 21 PD, 15 DLB, and 98 RBD) were analyzed. All patients were diagnosed with RBD at the recording time, and some of them developed PD or DLB after 8 years in average. EEG data was recorded at 250 Hz, from 14 electrodes (F3, F4, F7, F8, C3, C4, P3, P4, O1, O2, T3, T4, T5, T6, in the 10–20 EEG system). The signals were segmented into epochs of 30-s with 50% overlapping, and the noisy epochs were excluded from the analysis. The power of ten EEG frequency bands, namely delta (1–4 Hz), theta (4–8 Hz), alpha (8–13 Hz), alpha1 (8–10 Hz), alpha2 (10–13 Hz), beta1 (13–22 Hz), beta2 (22–32 Hz), gamma (30–40 Hz), and custom (13–18 Hz) was estimated for each epoch and electrode. Relative band power, i.e., dividing the power in the bands by the total power, was thence computed. The concatenated vector of electrodes and bands, which presents 140 components, i.e., 14×10 , was used as the input feature to the deep network.

In order to evaluate the performance of the deep auto-encoders, we also compare its performance with this of a wrapper feature selection method. The wrapper was based on sequential forward feature selection. In both cases classification was carried out using a Support Vector Machine (SVM) classifier in a leave-pair-subjects out cross validation scheme. This cross-fold validation scheme allows the computation of the Area Under Curve (AUC) using the Wilcoxon-Mann-Whitney statistic without representing the ROC space (Postuma et al., 2015). Hence the wrapper feature selection was performed on the training set and tested on the pair of subjects that was left out as the test set. This procedure was repeated until all pair of subjects had been left out as the test set. The AUC and the optimal average accuracy were estimated to evaluate the performance of each method.

Results: Figure 1 presents an example of the convergence of a deep auto-encoder with 200 nodes in the first layer and 10 nodes in the second layer. One can observe in Figure 1 the convergence of all layers minimizing the cost function.



The classification performance was estimated wrt the different tested number of nodes in the second layer, i.e., {10, 20, 40, 60, 80, 100}. 80 was the optimal number of nodes, which was selected as the one providing the largest average AUC across all classification scenarios. The AUC and averaged accuracy for the deep auto-encoder and the wrapper is presented in Table 1.

One may notice from Table 1 that the deep auto-encoder outperforms the conventional feature selection using a wrapper, for all classification scenarios, and significantly improves classification performance.

TABLE 1: AUC and averaged accuracy (in brackets) achieved with SVM classification.

AUC (ACC)%	Wrapper	Deep Auto-encoder
HC vs. PD	63 (81.5)	75.5 (87.7)
HC vs. PD+RBD+DLB	63 (81)	71.5 (85.7)
PD vs. DLB	57 (78.4)	66.5 (83.2)
PD vs. RBD	67 (83.2)	71.4 (85.7)
RBD vs. PD+DLB	65.9 (82.9)	75.5 (87.7)

Discussion: In this study a deep auto-encoder with two hidden layers was applied to the relative band-power features extracted from EEG signals of patients with RBD, PD, and DLB. The results revealed that the deep-auto-encoder outperforms conventional feature selection using a wrapper, and it significantly improves classification performance. This finding indicates that deep auto-encoders can right serve as a useful feature reduction scheme in RBD diagnostic and a-synucleinopathies (PD, DLB) prognostic tools. Further improvement of the AUC with deep auto-encoders is related to the parameterization of the deep network. For instance, mini-batch randomization, which is expected to improve classification performance by undertaking gradient descent in different subspaces, was not taken into account in this study. Moreover, some papers suggest to use dropout, i.e., to use only a part of the data, for extracting the network parameters in order for the model to be more generalizable. As a final improvement we plan to use regularization and a sparse parameter in the hidden layer. All these improvements are currently being investigated and will be communicated in the future.

Acknowledgments: The research work described herein has been partially funded by the Michael J. Fox Foundation (Grant Nr. 8140.01). EEG data was collected at the CARSM in Montreal with grant support from the Canadian Institute of Health Research and the Garfield Weston Foundation.

REFERENCES

- Hinton, G. E., and Salakhutdinov, R. R. (2006). Reducing the dimensionality of data with neural networks. *Science* 313, 504–507. doi: 10.1126/science.1127647 PMID:16873662
- Jiang, J. (1999). Image compression with neural networks – a survey. *Sig. Process. Image Commun.* 14, 737–760. doi: 10.1016/S0923-5965(98)00041-1 PMID:NOPMID
- Postuma, R. B., Gagnon, J.-F., Bertrand, J.-A., Marchand, D. G., and Montplaisir, J. Y. (2015). Parkinson risk in idiopathic REM sleep behavior disorder preparing for neuroprotective trials. *Neurology* 84, 1104–1113. doi: 10.1212/WNL.0000000000001364 PMID:NOPMID
- Soria-Frisch, A., Marin, J., Ibanez, D., Dunne, S., Grau, C., Ruffini, G., et al. (2014). Machine learning for a Parkinsons prognosis and diagnosis system based on EEG. in: *Proceedings of the International Pharmacoe-EEG Society Meeting, IPEG 2014*, Leipzig, Germany.

Dependency of Neural Tracts' Curvature Estimations on Tractography Methods

Irene Brusini, Daniel Jörgens, Örjan Smedby, Rodrigo Moreno

*Department of Biomedical Engineering and Health Systems, KTH Royal Institute of Technology, Hälsövägen 11C, 14157, Huddinge, Stockholm, Sweden
brusini@kth.se*

Introduction: For investigating brain structure and neural tracts, one of the most widely used techniques is tractography, which creates a 3D model of the neural fiber bundles using the voxel-wise fiber orientation distributions (FODs) estimated from diffusion magnetic resonance imaging (dMRI) data. Tractography methods can be divided into two classes: deterministic and probabilistic algorithms. The first ones model the neural tracts in small successive steps by following the main direction of the fibers in every voxel, while probabilistic algorithms consider also other possible directions.

Various geometrical descriptors can be extracted from the modeled neuronal pathways to investigate the properties of white matter (WM). However, the configurations of the modeled tracts, and thus their geometry, may vary depending on which algorithm (probabilistic or deterministic) is used.

A tract is represented by a discrete 3D curve, so curvature can be extracted in each of its points and used in various applications. For example, fiber curvature has been employed for finding differences between patients with autism spectrum disorder and controls (Jeong et al., 2011). Moreover, curvature has been suggested as a local shape property for characterizing tracts' diffusion properties (Gerig et al., 2004). Furthermore, it has been used to assess its role on the outcome of brain injuries (Zappalà, 2016) and it could be employed as a prior for preprocessing diffusion data (Jörgens et al., 2016). In our study, we investigate whether the choice of the tractography method can affect the local estimations of fiber curvature.

Methods: The data used in this study are two healthy adult subjects randomly selected from the 500 Subjects + MEG2 data release (November 2014) of the Human Connectome Project (HCP) (Van et al., 2012; WU-Minn Consortium Human Connectome Project, 2014). Multishell HARDI data were available, consisting of 3×90 gradient directions at b -values 1,000, 2,000, and 3,000 s/mm^2 and 18 $b = 0$ acquisitions. The data were affine registered as described by Zappalà (2016), obtaining images with voxel size of $1 \text{ mm} \times 1 \text{ mm} \times 1 \text{ mm}$.

The FOD of both subjects was reconstructed by applying constrained spherical deconvolution (CSD) (Tournier et al., 2007), already implemented in the software package MRtrix (J-D Tournier, Brain Research Institute, Melbourne, Australia, <https://www.mrtrix.org>) (Tournier et al., 2012). CSD was applied using a maximum harmonic order of 8 and combining the shells at $b = 1,000 \text{ s/mm}^2$ and $b = 3,000 \text{ s/mm}^2$.

The fiber trajectories of the two subjects were obtained by applying both a deterministic and a probabilistic tractography algorithm compiled in MRtrix: SD_STREAM (Tournier et al., 2012) and iFOD2 (Tournier et al., 2010), respectively. For each of the two algorithms, the following step sizes were tested: 0.1, 0.3, 0.5, and 0.7 mm. Default values were then set for most of the parameters of the tractography, such as the FOD amplitude cutoff ($=0.1$) for terminating tracks or the maximum angle between successive steps ($90^\circ \text{ stepsize/voxelsize}$). Finally, the number of modeled tracks per subject was set to 300,000.

For every tract of every tractography dataset, the angle of curvature θ_i was extracted in each of its 3D points \mathbf{P}_i and the corresponding curvature κ_i was computed as $\kappa_i = 2 \cdot \sin(\theta_i) / s$ (Moreno et al., 2011), where s is the step size. This procedure was carried out on MATLAB (MATLAB R2015a, The MathWorks Inc., Natick, MA, USA). The final voxel-wise curvature κ of a given tract was computed as the average of all the curvatures κ_i associated to the tract's points in that specific voxel.

Results: A large set of voxel-wise curvature values was obtained, each one corresponding to a single tract of one subject in one of the tested tractography settings. From such values, it was possible to analyze the distributions of the voxel-wise curvatures κ for every experimental setting, which are shown in Figure 1. In Table 1, the 95% confidence intervals of the mean values of curvature are presented.

Discussion: From our results, it can be observed that the estimated local values of curvature are strongly dependent on both the choice of the tractography algorithm (probabilistic or deterministic) and its settings. The statistics obtained in this study are based on values of curvature computed from whole brain tractography results. In the future, more in-depth research may be performed by focusing on specific regions of interest.

In our work, very similar values were obtained between the two subjects when the same tractography algorithms and settings were applied. It remains to be seen whether the same finding will be made when running similar experiments on a larger number of subjects.

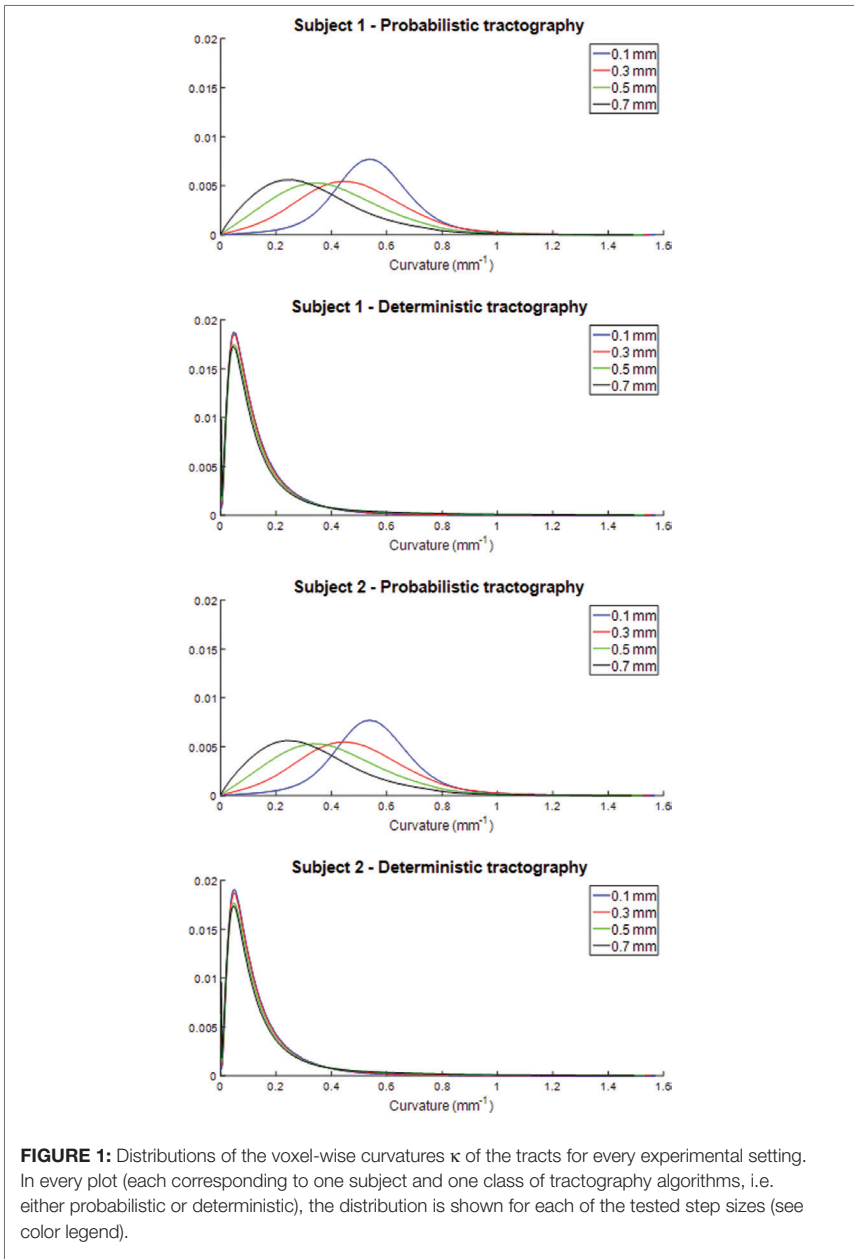


FIGURE 1: Distributions of the voxel-wise curvatures κ of the tracts for every experimental setting. In every plot (each corresponding to one subject and one class of tractography algorithms, i.e. either probabilistic or deterministic), the distribution is shown for each of the tested step sizes (see color legend).

TABLE 1: 95% confidence intervals of the mean values of curvature κ computed from the voxel-wise curvature values of each tract in each of the tested tractography settings. The confidence interval is expressed as mean \pm 1.96·SEM, where SEM is the standard error of the mean.

Step-size	Probabilistic		Deterministic	
	Subject 1	Subject 2	Subject 1	Subject 2
0.1 mm	0.5494 \pm 6.86·10 ⁻⁵ mm ⁻¹	0.5495 \pm 6.81·10 ⁻⁵ mm ⁻¹	0.1301 \pm 7.79·10 ⁻⁵ mm ⁻¹	0.1302 \pm 7.70·10 ⁻⁵ mm ⁻¹
0.3 mm	0.4765 \pm 8.45·10 ⁻⁵ mm ⁻¹	0.4763 \pm 8.33·10 ⁻⁵ mm ⁻¹	0.1330 \pm 8.39·10 ⁻⁵ mm ⁻¹	0.1336 \pm 8.33·10 ⁻⁵ mm ⁻¹
0.5 mm	0.3986 \pm 9.12·10 ⁻⁵ mm ⁻¹	0.3980 \pm 9.04·10 ⁻⁵ mm ⁻¹	0.1519 \pm 9.46·10 ⁻⁵ mm ⁻¹	0.1521 \pm 9.29·10 ⁻⁵ mm ⁻¹
0.7 mm	0.3328 \pm 8.37·10 ⁻⁵ mm ⁻¹	0.3319 \pm 8.27·10 ⁻⁵ mm ⁻¹	0.1522 \pm 8.38·10 ⁻⁵ mm ⁻¹	0.1531 \pm 8.29·10 ⁻⁵ mm ⁻¹

In general, the curvatures obtained from probabilistic tractography are larger than those from deterministic one. Moreover, in the probabilistic datasets, the estimated mean of κ decreases almost linearly with increasing step size. On the other hand, in the deterministic case, κ increases with the step size, showing also similar mean values between the step sizes 0.1 and 0.3 mm and between 0.5 and 0.7 mm. These results could suggest that the probabilistic tracking tends to be more irregular and curved at a smaller scale, since it tests a larger number of possible directions, and becomes smoother as soon as the step size is increased. Instead, in deterministic tractography, the fitting may be quite smooth if small steps are used, but an increase in the step size yields larger variations in the directions, which are reflected in a larger curvature. We aim at conducting more experiments to test these hypotheses, for example by increasing the FOD amplitude cutoff in probabilistic tractography to reduce the number of possible tracking directions. Another possible approach could consist in computing curvature regarding more tracts' segments, i.e., more than three subsequent points of the pathway.

We can conclude that, in studies where local curvature information is required, it is important to apply exactly the same tractography method to get comparable results. Curvature estimations are very sensitive to the choice of tractography parameters, and particular attention should be paid if curvature is studied at a small scale. Moreover, further investigations on the actual reliability of local curvature estimations should be performed.

Acknowledgments: Data were provided [in part] by the Human Connectome Project, WU-Minn Consortium (Principal Investigators: David Van Essen and Kamil Ugurbil; 1U54\ -MH091657) funded by the 16 NIH Institutes and Centers that support the NIH Blueprint for Neuroscience Research; and by the McDonnell Center for Systems Neuroscience at Washington University. This research has partially been funded by the Swedish Research Council (VR), grants no. 2014-6153 and 2012-3512, and the Swedish Heart-Lung Foundation (HLF), grant no. 2011-0376.

REFERENCES

- Gerig, G., Gouttard, S., and Corouge, I. (2004). "Analysis of brain white matter via fiber tract modeling," in: *Annual International Conference of the IEEE Engineering in Medicine and Biology Society*, San Francisco, CA, USA, Vol. 6, 4421–4424.
- Jeong, J. W., Kumar, A. K., Sundaram, S. K., Chugani, H. T., and Chugani, D. C. (2011). Sharp curvature of frontal lobe white matter pathways in children with autism spectrum disorders: Tract-based morphometry analysis. *Am. J. Neuroradiol.* 32, 1600–1606. doi: 10.3174/ajnr.A2557 PMID:21757519
- Jörgens, D., Smedby, Ö. and Moreno, R. (2016). "Steering second-order tensor voting by vote clustering," in *IEEE International Symposium on Biomedical Imaging*, Prague, Czech Republic, 1245–1248. doi: 10.1109/ISBI.2016.7493492

- Moreno, R., Garcia, M. A., Puig, D., Pizarro, L., Burgeth, B., and Weickert, J. (2011). On improving the efficiency of tensor voting. *IEEE Trans. Pattern Anal. Mach. Intell.* 33, 2215–2228. doi: 10.1109/TPAMI.2011.23 PMID:21282853
- Tournier, J. D., Calamante, F., and Connelly, A. (2007). Robust determination of the fibre orientation distribution in diffusion MRI: non-negativity constrained super-resolved spherical deconvolution. *Neuroimage* 35, 1459–1472. doi: 10.1016/j.neuroimage.2007.02.016 PMID:17379540
- Tournier, J.D., Calamante, F. and Connelly, A. (2010). “Improved probabilistic streamlines tractography by 2nd order integration over fibre orientation distributions,” in *Proceedings of the 18th Annual Meeting of the International Society for Magnetic Resonance in Medicine (ISMRM)*, 1670.
- Tournier, J. D., Calamante, F. and Connelly, A. (2012). MRtrix: diffusion tractography in crossing fiber regions. *Int. J. Imag. Syst. Technol.* 22, 53–66. doi: 10.1002/ima.22005 PMID:NOPMID
- Van Essen, DC, Ugurbil, K., Auerbach, E., Barch, D., Behrens, T. E., Bucholz, R., et al. (2012). The Human Connectome Project: a data acquisition perspective. *Neuroimage* 62, 2222–2231. doi: 10.1016/j.neuroimage.2012.02.018 PMID:22366334
- WU-Minn Consortium Human Connectome Project. (2014). *WU-Minn HCP 500 Subjects Data Release: Reference Manual*. Available at: <https://www.humanconnectome.org/storage/app/media/documentation/s500/hcps500meg2releasereferencemanual.pdf>
- Zappalà, S. (2016). “Exploring the inter-subject variability of neuronal tracts orientation and its effect on FE simulation of anisotropic brain tissue,” in *Master’s thesis at the School of Technology and Health of KTH Royal Institute of Technology* (Stockholm, Sweden).

Earphone-Shaped EEG Instrument for Real-Time Brain State Monitoring

Dong-Hwa Jeong¹, Jaeseung Jeong¹, Yongwook Chae², Jeeun Lee², Hyeonyoung Choi²

¹Department of Bio and Brain Engineering, KAIST, Daejeon, South Korea

²Looxid Labs, Seoul, South Korea

donghwa@kaist.ac.kr

Introduction: Conventional EEG instruments were difficult to be used for real-time monitoring because they are uncomfortable to wear in daily life. In recent, most smart-phone users widely wear earphones even they fall asleep. Therefore, a novel Earphone-shaped EEG instrument, which measures EEG signals around the ear and in the ear canal while playing music, can help enable real-time brain state monitoring.

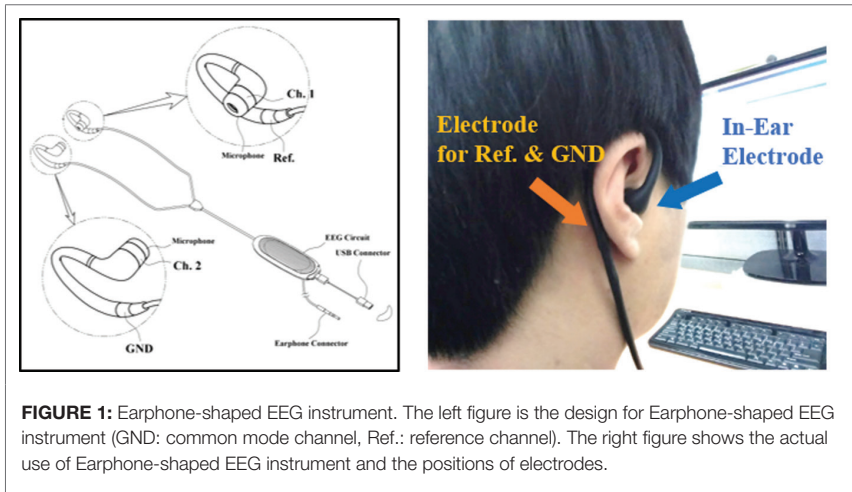
Since in-ear EEG concept was first introduced by Looney et al., a few research groups reported in-ear EEG prototypes and their signal properties (Looney et al., 2011; Looney et al., 2012; Kidmose et al., 2013; Hoon Lee et al., 2014; Mikkelsen et al., 2015; Bleichner et al., 2015). However, there are few reports on single trial signal analysis of in-ear EEG and no research on combining earphone and in-ear EEG acquisition system.

In this study, the signal validity of in-ear EEG signals was examined and their possible application of mental state monitoring was suggested using simple attention state classification.

Methods: Earphone-shaped EEG instrument was designed as the form of canal type and earhook earphone (Figures 1A,B). Electrodes to record ear-EEG signals and microphones were put on the canal part (Figure 1A, Ch. 1, Ch. 2, and Microphone). Electrodes were put on the earhook part to contact ear lobes and mastoid processes. The left electrodes on the earhook part was used for the reference channel and the right one was used for the common mode channel (Figure 1A, Ref. and GND). Lead wires connected to each channel and microphone were connected to the 2-channel circuit board for amplifying and filtering signals (Looxid Labs, sampling frequency 125 Hz). Finally, preprocessed EEG signals were sent to computer with USB connector and earphone connector.

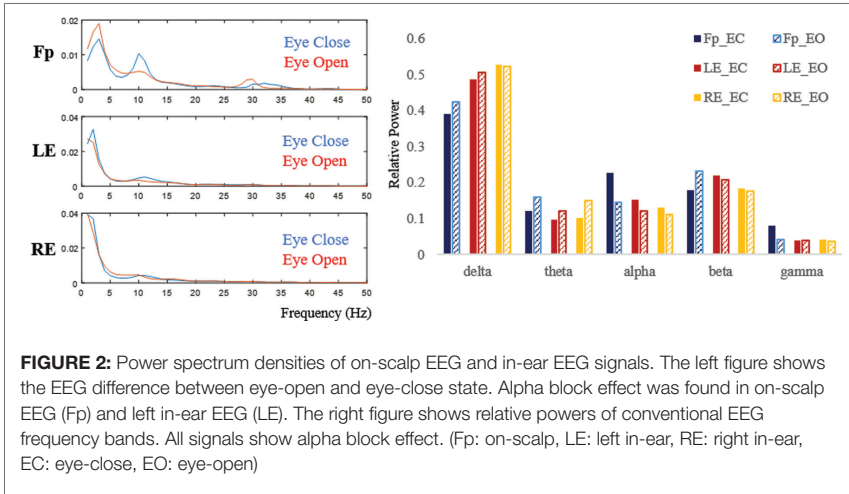
Ear-EEG signals were recorded from a 29-year-old male subjects for three states; eye-closed resting state, eye-opened resting state, and eye-opened attention state in the both ear canals. In addition, to compare Ear-EEG and on-scalp EEG signals, the same

experiments were performed using on-scalp electrodes on the forehead (Fp2 according to 10–20 International Systems).



Acquired EEG signals were segmented into 1-s epoch (125 data points) with the Hanning window and filtered with 0.5 Hz high-pass filter and 50 Hz low-pass filter. The power spectrum analysis was performed using the AR Burg method. As a result, 50 frequency components (1–50 Hz) were obtained from the power spectrum analysis. To discriminate attention state and resting state, Fisher ratio and support vector machines (SVM) were adopted. Attention states were distinguished from eye-opened resting state using SVM with most discriminable frequency bands selected by Fisher ratio. To avoid over-fitting problem, the classification was repeated 100 times based on 10-fold cross validation.

Results: Power spectral densities obtained using the AR Burg method showed similar EEG patterns in both on-scalp EEG and in-ear EEG signals (Figure 2). In particular, alpha block and attenuation effect around 10Hz frequency was clearly observed in on-scalp EEG signals. Alpha waves are generally dominant during closing eye and reduce when opening eye. Although differences of in-ear EEG between eye-close and eye-open state were relatively smaller than those in on-scalp EEG, alpha power decrease during opening eye was observed.



Attention state was distinguished from resting state using Fisher ratio and SVM. The 10 frequency components which have the largest Fisher ratio were selected as features for SVM. Alpha frequency (11 Hz), beta frequency (23–25 Hz), and gamma frequency (37–38, 44–46 Hz) components were selected. The average classification accuracy using 10-fold cross-validation was 73.35%.

Discussion: In this study, a novel Earphone-shaped EEG instrument was developed and their signal properties were examined. In-ear EEG signals showed similar characteristics with those from on-scalp EEG signals. Besides, attention state could be distinguished from resting state using machine learning techniques. Inspired from those results, in-ear EEG signals and Earphone-shaped EEG instrument can be a useful device for real-time brain state monitoring.

This study has some limitations of the number of subject, insufficient classification accuracy, and offline experiment and analysis. In the previous study, our group made individually-fitted in-ear electrodes using ear-canal impressions. Acquired signals from those electrodes were finer than those from Earphone-shaped EEG instrument. They showed clear alpha peaks and successful classification of attention state (81.3%). In our ongoing study, well-contacted in-ear electrodes are going to be applied. Then, subject variability problem will be examined by performing experiment on multiple subjects. Furthermore, online experiments and adaptive algorithms will be performed for the

use of real-time brain state monitoring. After improvement of in-ear EEG instruments, various mental states, clinical features of neurological diseases, and influences of sound on in-ear EEG signals will be examined using these devices.

Acknowledgments: This work was supported by the National Research Foundation of Korea Grant funded by the Korean Government (MEST) (NRF-2015-R1D1A1A02062365).

REFERENCES

- Bleichner, M. G., Lundbeck, M., Selisky, M., Minow, F., Jager, M., Emkes, R., et al. (2015). Exploring miniaturized EEG electrodes for brain-computer interfaces. An EEG you do not see? *Physiol. Rep.* 3, e12362–e12362. doi: 10.14814/phy2.12362 PMID:NOPMID
- Hoon Lee, J., Min Lee, S., Jin Byeon, H., Sook Hong, J., Suk Park, K., and Lee, S.-H. (2014). CNT/PDMS-based canal-typed ear electrodes for inconspicuous EEG recording. *J. Neural Eng.* 11, 046014. doi: 10.1088/1741-2560/11/4/046014 PMID:NOPMID
- Kidmose, P., Looney, D., Ungstrup, M., Rank, M. L., and Mandic, D. P. (2013). A study of evoked potentials from ear-EEG. *IEEE Trans. Biomed. Eng.* 60, 2824–2830. doi: 10.1109/TBME.2013.2264956 PMID:NOPMID
- Looney, D., Kidmose, P., Park, C., Ungstrup, M., Rank, M. L., and Rosenkranz, K. (2012). The in-the-ear recording concept: user-centered and wearable brain monitoring. *IEEE Pulse* 3(6), 32–42.
- Looney, D., Park, C., Kidmose, P., Rank, M. L., Ungstrup, M., Rosenkranz, K., et al. (2011). An in-the-ear platform for recording electroencephalogram. *Proc. Annu. Int. Conf. IEEE Eng. Med. Biol. Soc.* 1, 6882–6885. doi:10.1109/IEMBS.2011.6091733 PMID:NOPMID
- Mikkelsen, K. B., Kappel, S. L., Mandic, D. P., and Kidmose, P. (2015). EEG recorded from the ear: characterizing the Ear-EEG method. *Front. Neurosci.* 9:1–8. doi: 10.3389/fnins.2015.00438 PMID:NOPMID

Towards Modeling Metabolic and Communication Dysfunctions in Neurodegenerative Diseases

Tiago Azevedo, Pietro Lio

*Computer Laboratory, University of Cambridge, Cambridge, United Kingdom
tmla2@cl.cam.ac.uk*

Patients are often characterized by multiple, complex, and interrelated conditions, disorders, or diseases often driven by a general inflammatory state. In the past 5 years we have developed methodology to model multi omic metabolic networks. We have shown the effectiveness of using multi omic metabolic models to identify pathways involved in phenotype changes, clustering environmental conditions, compute sensitivity and robustness. Now we would like to develop further the methodology to investigate the relation between drugs and pathways at the multi organ level and at the multi drug levels.

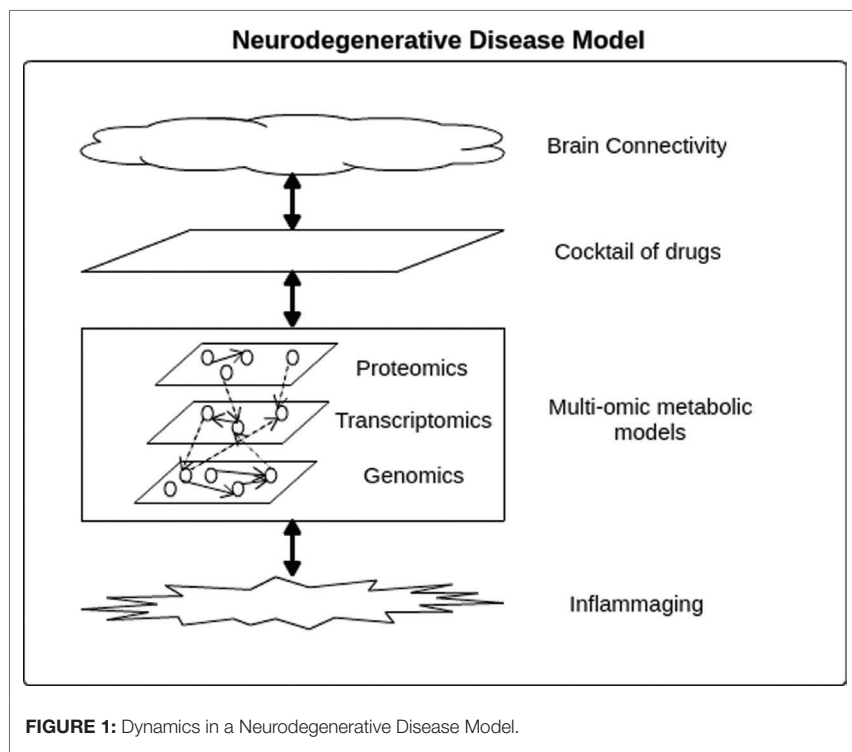
This project addresses an important need in current biomedical engineering studies. The main aim is to identify principles in predicting effects when using cocktails of drugs and treatments at systemic level. We believe that the most meaningful way is to use multi omic metabolic models based on dynamic flux balance analysis that integrate transcriptomics, proteomic and pathway data. The methodology will be based on multi layer networks and multi objective optimisation approaches. We will consider Parkinson together with brain inflammatory factors for which we have obtained data from collaborations within UK and Europe. A second aim is to build a software platform that will allow predictive analytics on multiple drugs that consider targets in different organs. The omics era has generated a new approach to medicine, i.e., systems medicine. The definition of systems medicine is deeply related to complex networks: it involves a systemic view of the organism where the various building elements are considered in their interplay. A paradigmatic example is the networks of human diseases. The diseaseome is a bipartite network that connects human diseases (disease phenome) and human genes (disease genome). The strong connectivity of molecular systems implies that a specific dysfunction of an element propagates throughout the network of interactions and affects the activity of other components. Therefore, different dysfunctions can lead to the same effect through different pathways. The concept of disease module has been proposed to indicate a group of network components the disruption of which leads to a particular disease phenotype. Single-target therapies may fail because they are not contemplating the underlying network characteristics during target identification. On the other side, a drug used for a disease could reveal itself of valuable use also for other diseases strongly connected to the original target node. The novelty is also in the fact that each patient status can be described by several networks, e.g., related to its genomic, proteomic or transcriptomic profile. For example, when gene

expression data are available, they can be mapped onto protein-protein networks, thus integrating general biological knowledge and sample-specific information at multiple levels (from whole network to single gene or pathway). By combining data coming from heterogeneous sources, the resulting networks will be very large in size.

The Parkinson's Progression Markers Initiative (PPMI) is a large study that collects data from hundreds of people in an effort to identify the causes of Parkinson's disease. Zeighami et al. have analysed MRI scans that were collected as part of this initiative, which show the structure of the brains of 230 people in the early stages of Parkinson's disease (Zeighami et al., 2015). Moreover, the Brain Connectome Project maps networks in the living human brain, and a disease-causing agent might spread in such networks. Although we know a lot about brain's structural connectivity, we can derive a better Parkinson disease model by integrating these connectivity information with transcriptomic, proteomic and pathway data collected through collaborations at the U.K. and Europe. A similar integrative approach has already been taken by Riedl et al. (2016), where researchers traced the directionality of the connectome based on where metabolic energy was being used. Tau proteins should be considered in the metabolic model as they are involved in motor proteins (which require more energy that could be used as in the Riedl et al. research (Riedl et al., 2016)) and there are studies that correlate them with the Parkinson disease (Spillantini and Goedert, 2013). In order to build a software platform that will allow predictive analytics on multiple drugs, statistical and machine learning techniques such as Bayesian networks will be used. There is no optimal machine learning algorithm that works best for all problems (Libbrecht and Noble, 2015). So, some approaches that were done already should be taken into account. For instance, Menden et al. (2013) developed machine learning models to predict the response of cancer cell lines to drug treatment, based on both the genomic features of the cell lines and the chemical properties of the considered drugs. Vidyasagar (2015) reviewed several techniques from machine learning in order to predict a drug response.

Figure 1 summarises how there could be many interactions and factors when modelling a neurodegenerative disease. This project is in an early stage of a PhD research program funded by the W. D. Armstrong Trust Fund. The student will develop expertise in machine learning (particularly Bayesian approaches), network science (particularly multiplex and multi layer network models) and multi objective optimisation and control theory. As a preliminary result we want to show other a paradigm shift from the analytic to the systemic approach when dealing with neurodegenerative diseases, stating that it is important to consider the interactions of multiple factors. For instance, Zuddas et al. (Pierpaolo et al., 2013) suspect that even magnetic nanocrystals, possibly produced by cars, could have an important role in the nervous system, more specifically in causing diseases such as Alzheimer. Mankia and Emery (Kulveer and Emery, 2016) showed that it was possible to combine the predictive abilities of clinical, genetic, immunologic

and imaging biomarkers in order to identify the individuals with higher risk of having Rheumatoid Arthritis. This is a new vision appearing in medicine where the preclinical phase of a disease can be started much earlier, using machine learning and modelling capabilities for predictability but also to see its causalities.



REFERENCES

- Kulveer, M., and Emery, P. (2016). Review: preclinical rheumatoid arthritis progress toward prevention. *Arthritis Rheumatol.* 68, 779–788. doi: 10.1002/art.39603 PMID:NOPMID
- Libbrecht, M. W., and Noble, W. S. (2015). Machine learning applications in genetics and genomics. *Nat. Rev. Genet.* 16, 321–332. doi: 10.1038/nrg3920 PMID:25948244
- Menden, M. P., Iorio, F., Garnett, M., McDermott, U., Benes, C. H., Ballester, P. J., et al. (2013). Machine learning prediction of cancer cell sensitivity to drugs based on genomic and chemical properties. *PLoS ONE* 8:e61318. doi: 10.1371/journal.pone.0061318 PMID:23646105

- Pierpaolo, Z., Favre, D., and Duhamel, J. R. (2013). "Magnetite minerals in the human brain: what is their role?" in *Medical Geochemistry* (Netherlands: Springer), 91–99.
- Riedl, V., Utz, L., Castrillón, G., Grimmer, T., Rauschecker, J. P., Ploner, M., et al. (2016). Metabolic connectivity mapping reveals effective connectivity in the resting human brain. *Proc. Natl. Acad. Sci. U S A* 113, 428–433. doi: 10.1073/pnas.1513752113 PMID:26712010
- Spillantini, M. G., and Goedert, M. (2013). Tau pathology and neurodegeneration. *Lancet Neurol.* 12, 609–622. doi: 10.1016/S1474-4422(13)70090-5 PMID:NOPMID
- Vidyasagar, M. (2015). Identifying predictive features in drug response using machine learning: opportunities and challenges. *Ann. Rev. Pharmacol. Toxicol.* 55, 15–34. doi: 10.1146/annurev-pharmtox-010814-124502 PMID:25423479
- Zeighami, Y., Ulla, M., Iturria-Medina, Y., Dadar, M., Zhang, Y., Larcher, K. M., et al. (2015). Network structure of brain atrophy in de novo Parkinson's disease. *Elife* 4, e08440. doi: 10.7554/eLife.08440 PMID:NOPMID

Sharing Electrophysiological Data and Metadata on HBP Platforms – An Example Collaboratory Workflow

Julia Sprenger¹, Alper Yegenoglu¹, Sonja Grün^{1,2}, Michael Denker¹

¹*Institute of Neuroscience and Medicine (INM-6), Institute for Advanced Simulation (IAS-6), and JARA Brain Institute I (INM-10), Jülich Research Centre Jülich, Germany*

²*Theoretical Systems Neurobiology, RWTH Aachen University, Aachen, Germany*
j.sprenger@fz-juelich.de

Introduction: The Human Brain Project (HBP)¹ aims at creating and operating a European scientific Research Infrastructure for the neurosciences. A main goal is to gather, organise and disseminate data describing the brain and its diseases on the basis of experimental as well as simulated data. Therefore a lot of effort is put into the development of tools for data registration, storage, access and sharing. The most prominent data type available through the HBP to date are anatomical data and data describing single cell dynamics. However, the need to include experimental and simulated large-scale functional data, and in particular, electrophysiological activity data, has been widely recognized. Such data are primarily created in neuronal network simulations as a core part of the HBP effort. An adapted strategy for data curation is needed, as the established workflows are not yet considering the integration of electrophysiological data.

Another goal of the HBP is to provide a platform to facilitate collaborative research. For this the Collaboratory² has been set up—a web portal which provides a common online workspace (Collab) for all members of a collaboration team. The Collab combines tools which are developed in the context of the HBP platforms and by this provides access to high performance computing (HPC), simulation tools and shared datasets. In particular, it is thought to act as a platform for interactive data analysis. Next to specialized tools which can be integrated or developed for the Collab, generic analysis can be performed by using Python Jupyter Notebooks³.

Motivation: Thus, data used in the HBP must be prepared in two respects: (i) integration into the HBP databases and (ii) use in analysis processes on the Collab. Due to the diversity of data (types) in electrophysiological experiments, standardized data

1 <https://www.humanbrainproject.eu>

2 <https://collab.humanbrainproject.eu>

3 <http://jupyter.org/>

and metadata models, and tools operating on these models, have only started to be developed (Denker and Grün, 2016; Zehl et al., 2016). A crucial step in further advancing and disseminating these efforts, and to ensure that individual components can be efficiently linked, is to embed these tools into workflows that recreate the actual scientific routine of a research project.

Methods: Here we consider the combination of 4 open source projects attempt to address these issues:

- **Neo** provides a generic standardized representation for electrophysiological data, which is able to interface with a range of electrophysiological data formats (Garcia et al., 2014).
- The **Electrophysiology Analysis Toolkit** (Elephant) offers methods ranging from the analysis of spike data to population signals, e.g., local field potentials. Elephant is based on the Neo data representation format⁴.
- The **open metadata Markup Language** (odML) is based on XML and offers a hierarchical structure to store metadata related to electrophysiological experiments (Grewe et al., 2011).
- **NIX** is a file format designed to combine electrophysiological data and metadata in a single, standardized format⁵, and is linked to both the Neo and odML data models.

Results and Discussion: Here we show in 3 stages how these open source programs can interact to form a structured, comprehensible workflow for electrophysiological spike data. Firstly, we demonstrate the loading of data and metadata and their integration into a single data representation. For this we start with the conversion of the raw data into a Neo object, which is then further annotated with metadata information. To obtain the metadata information, primary metadata are first converted to the odML format using the odMLtables tool⁶, which is then queried for annotating the Neo object. In a second stage, the final Neo object is saved as NIX file, which preserves the data-metadata relations formed in the Neo structure. In a last stage, the data structure from the NIX file is used for exemplary analysis of the spiking activity using Elephant.

In addition to the implementation of such a workflow in Python for use on a local machine, we demonstrate the setup of the workflow on the Collaboratory of the HBP

4 <https://github.com/INM-6/elephant>

5 <https://github.com/G-Node/nix>

6 <https://github.com/INM-6/python-odmltables>

and indicate how the interaction of multiple collaboration partners can benefit from the workflow realized in this setting. In addition, we discuss how the data, in particular the odML-based metadata, can be used for integration in the registration processes developed by the Neuroinformatics platforms.

Acknowledgments: Helmholtz portfolio theme SMHB, EU Grant 720270(HBP), DFG Priority Program SPP 1665 (Grants DE 2175/2-1 and GR 1753/4-2).

REFERENCES

- Brochier, T., Zehl, L., Hao, Y., Duret M., Sprenger J., Denker M., et al. (2018). Massively parallel recordings in macaque motor cortex during an instructed delayed reach-to-grasp task. *Sci. Data*. (in press).
- Denker, M., and Grün, S. (2016). "Designing workflows for the reproducible analysis of electrophysiological data," in *Brain-Inspired Computing. BrainComp 2015. Lecture Notes in Computer Science*, Vol. 10087, eds K. Amunts, L. Grandinetti, T. Lippert, and N. Petkov (Cham: Springer), 58–72, doi:10.1007/978-3-319-50862-7_5.
- Garcia, S., Guarino, D., Jaillet, F., Jennings, T. R., Pröpfer, R., Rautenberg, P. L., et al. (2014). Neo: an object model for handling electrophysiology data in multiple formats. *Front. Neuroinform.* 8:10. doi: 10.3389/fninf.2014.00010 PMID:24600386
- Grewe, J., Wachtler, T., and Benda, J. (2011). A bottom-up approach to data annotation in neurophysiology. *Front. Neuroinform.* 5:16. doi: 10.3389/fninf.2011.00016 PMID:21941477
- Zehl, L., Jaillet, F., Stoewer, A., Grewe, J., Sobolev, A., Wachtler, T., et al. (2016). Handling metadata in a neurophysiology laboratory. *Front. Neuroinform.* 10:26. doi: 10.3389/fninf.2016.00026 PMID:27486397

ASSET for JULIA: Executing Massively Parallel Spike Correlation Analysis on KNL Cluster

Carlos Canova^{1,2,3}, **Wouter Klijn**⁴, **Paul Baumeister**⁵, **Alper Yegenoglu**^{1,2,3}, **Michael Denker**^{1,2,3}, **Dirk Pleiter**^{4,5}, **Sonja Grün**^{1,2,3,6}

¹*Institute of Neuroscience & Medicine (INM-6), Jülich, Germany*

²*Institute for Advanced Simulation (IAS-6), Jülich, Germany*

³*Jara Brain Institute I, FZ Jülich, Jülich, Germany*

⁴*SimLab Neuroscience, Institute for Advanced Simulation, JARA, Forschungszentrum Jülich GmbH, Jülich, Germany*

⁵*Jülich Supercomputing Centre (JSC), Jülich, Germany*

⁶*Theoretical Systems Neurobiology, RWTH Aachen University, Aachen, Germany*

c.canova@fz-juelich.de, w.klijn@fz-juelich.de

Introduction: We developed a statistical analysis method, ASSET, capable of detecting repeated sequences of synchronous events (SSE) in massively parallel spike trains (Torre et al., 2016). Yet we have not been able to apply ASSET in its full extent, given the high computational demand when assessing significance of the SSEs. This challenge, however, can now be overcome with the support from the High Performance Analytics and Computing Platform (HPAC), and their readily available modern infrastructure. Here we present the first steps towards analyzing electrophysiological recordings with ASSET on one of the new pre-commercial procurement machines, JULIA, which is based on Intel's new Knights Landing (KNL) processor.

Motivation: ASSET is an analysis designed to detect and quantify activity in a synfire chain (Abeles, 1991), a feedforward neuronal network with high convergence and divergence of connectivity between the layers (groups). Particular to such a network is that it favors the propagation of synchronous spiking activities, which appear in measurements as SSEs. In ASSET, the repetitive occurrence of an identical SSE becomes visible in an intersection matrix as a diagonal structure (DS) (Schrader et al., 2008; Gerstein et al., 2012), which is evaluated automatically for significance. Currently, the ASSET method can only be applied to time segments that are considerably shorter than the full duration of a typical session of massively parallel electrophysiological recordings due to costly numerical steps in the analysis. However, these numerical computations are composed of independent steps and thus ASSET would profit from parallelization. A second challenge is the core of the algorithm, which makes extensive use of exponential and logarithmic operations. These operations are computationally expensive and do not lend themselves to easy array vectorization on modern HPC hardware.

Methods: After analysis and instrumentation of ASSET, an MPI version of the software was implemented, distributing the workload across multiple compute instances in a round-robin manner. After the work on the nodes, the partial results are collected on the master node and summed for the final results. In a parallel effort we optimized the core of the ASSET algorithm: the exponential and logarithmic operations are typically calculated using Taylor expansions. Approximate methods perform the same mathematical operations faster at the expense of an error smaller than 1E-6. This speedup can be further improved on by (automatic) array vectorization of the code implementing these methods. These techniques were combined with C implementations using the Cython programming interface.

Results: The MPI implementation allowed us to leverage the large number of cores available in current hardware and showed an order of magnitude shorter time to solution. We will further report on the preliminary qualitative and quantitative analysis of the approximate methods and its effects on the runtime of the algorithm, including the results of running the algorithm on the KNL processors of JULIA. ASSET is currently available to the scientific community *via* the Electrophysiological Analysis Toolkit (Elephant)⁷, and as such is also available to all members of the Human Brain Project Consortium *via* the Collab.

Acknowledgments: Supported by Helmholtz Portfolio Theme Supercomputing and Modeling for the Human Brain (SMHB), EU grant 604102 (Human Brain Project, HBP), EU Grant 269912 (BrainScaleS), DFG Priority Program SPP 1665 (GR 1753/4-1 and 2175/1-1).

REFERENCES

- Abeles, M. (1991). *Corticonics*. Cambridge: Cambridge University Press.
- Gerstein, G. L., Williams, E. R., Diesmann, M., Grün, S., and Trengove, C. (2012). Detecting synfire chains in parallel spike data. *J. Neurosci. Methods* 206, 54–64. doi: 10.1016/j.jneumeth.2012.02.003 PMID:22361572
- Schrader, S., Bell, M. L., Allen, D. L., Byrnes, W. C., and Leinwand, L. A. (2008). Skeletal muscle adaptations in response to voluntary wheel running in myosin heavy chain null mice. *J. Neurophysiol.* 100, 2165–2176. doi: 10.1152/jn.01245.200 PMID:NOPMID
- Torre, E., Canova, C., Denker, M., Gerstein, G., Helias, M., and Grün, S. (2016). ASSET: analysis of sequences of synchronous events in massively parallel spike trains. *PLoS Comput. Biol.* 12:e1004939. doi: 10.1371/journal.pcbi.1004939 PMID:27420734

⁷ neuralensemble.org/elephant/

A Three-Dimensional Bayesian Spatial Variable Selection Model with Estimated HRF on fMRI Time Series Data

Nasrin Borumandnia¹, Hamid Alavi Majd¹, Farid Zayeri¹, Ahmad Reza Baghestani¹, Seyyed Mohammad Tabatabaei², Fariborz Faeghi³

¹Department of Biostatistics, Faculty of Paramedical Sciences, Shahid Beheshti University of Medical Sciences, Tehran, Iran

²Medical Informatics Department, Faculty of Paramedical Sciences, Shahid Beheshti University of Medical Sciences, Tehran, Iran

³Radiology Technology Department, Faculty of Paramedical Sciences, Shahid Beheshti University of Medical Sciences, Tehran, Iran

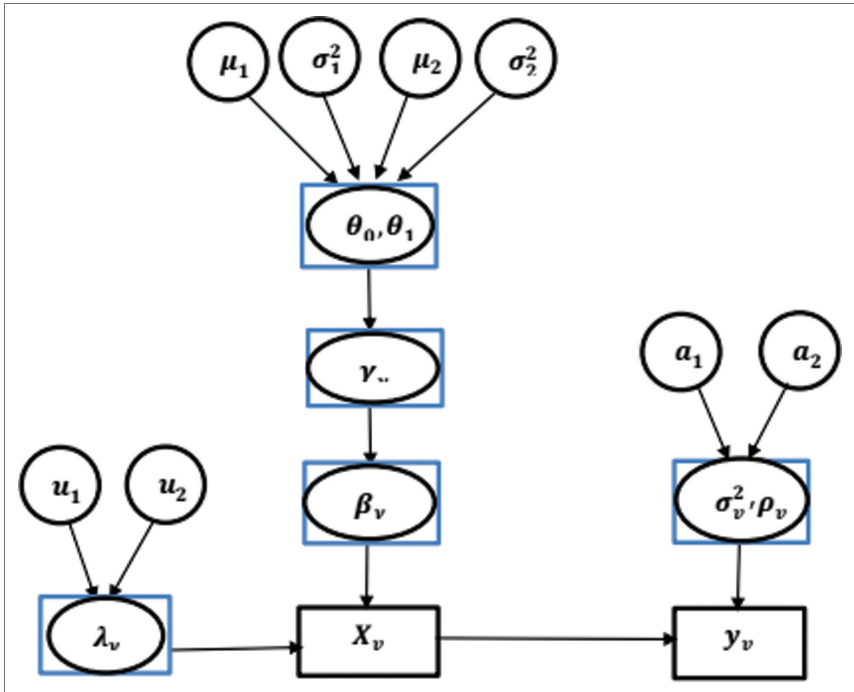
borumand.n@gmail.com

Summary: This research describes a new fully Bayesian spatiotemporal model to analyze fMRI studies. We have considered recent developments in Bayesian spatiotemporal models for detecting neuronal activation in fMRI experiments. The complete relationship between the neuronal activation and the blood oxygenation level dependent signal has not been fully modeled yet. Our goal is to provide an analytical framework that considers the complex temporal and spatial correlation structures of fMRI data as well as the complex relationship between neuronal activity and its Hemodynamic Response Function, HRF. In the temporal dimension, we assumed an autoregressive structure on error terms and also parameterize the HRF's shape parameter. So we modeled the data using the HRFs with the voxel-dependent shape parameters. We account for the complex three-dimensional spatial correlation structure of the voxels using an Ising prior on parameters that are for selecting the activated voxels. For inference, we combine the component wise Markov Chain Monte Carlo technique with the Auxiliary variable method. We investigate the properties of the model through its performance on three-dimensional simulated data sets with the block design. Also we implemented the method on two real data sets. The first one is the n -back data from My Connectome Project and the second one is the auditory data.

Method: Let y_{vt} be the time series of the observed BOLD signals for given voxel v , $y_{vt} = (y_{v1}, y_{v2}, \dots, y_{vT})^T$, where T is the number of time points and $v = 1, 2, \dots, N$. We assume a voxel-wise GLM: $y_v = X_v \beta_v + \epsilon_v$

Our proposed model allows estimating the voxel-dependent HRF's parameter. Also complex spatial and temporal correlation structures of data are captured in the model. We achieved above objects *via* the choice of appropriate priors for the model parameters.

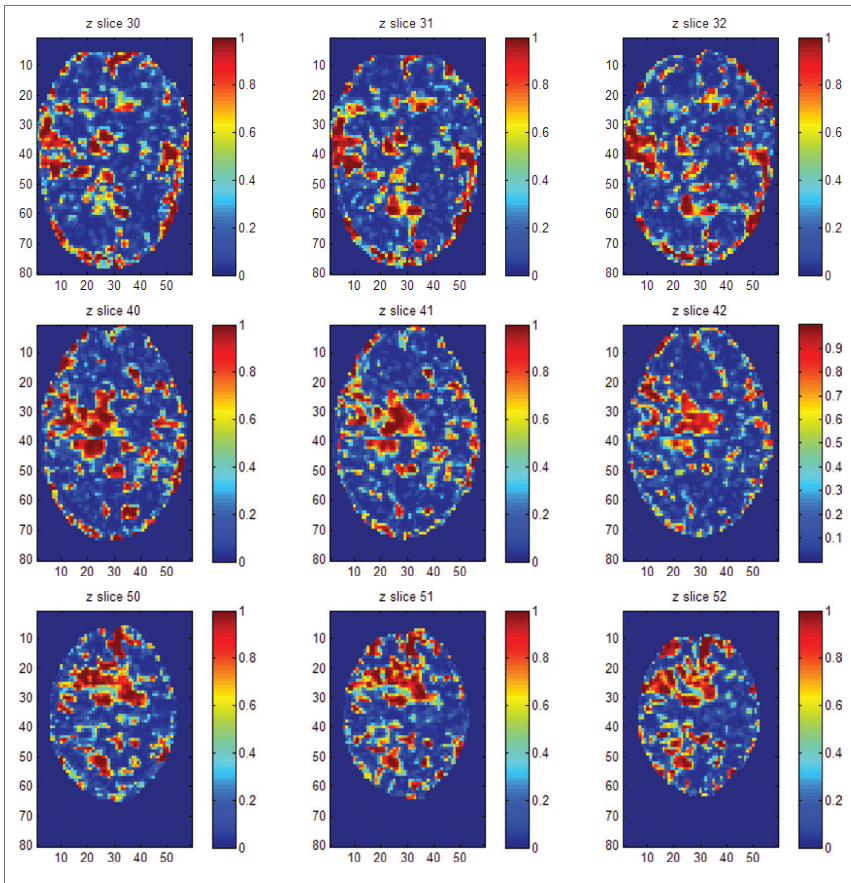
- (a) Autoregressive structure for temporal correlation
- (b) Free parameter modeling of Poisson HRF
- (c) Ising model for spatial correlation
- (d) Zellner's g-prior for regression coefficients



Simulation result: Our simulation study was designed to evaluate the performance of the proposed model in identifying the active voxels. For each scenario we simulate 10 3D images of dimension $10 \times 10 \times 10$. We performed a posterior inference on these data using our model.

θ_1	Fitted HRF		True HRF	Poisson	Canonical	Inverse Logit
0.1	Free parameter Poisson	Accuracy		95.12	99.10	99.2
		Precision		92.06	99.00	100
		FPR		1.67	0.80	0.15
		FNR		7.84	1.00	0
	Fixed parameter Poisson	Accuracy		86.65	98.40	99.00
		Precision		74.16	97.94	100
		FPR		0.77	1.12	1.86
		FNR		21.03	2.12	0
0.4	Free parameter Poisson	Accuracy		97.30	99.80	99.95
		Precision		95.97	95.65	100
		FPR		0.33	4.35	2.08
		FNR		6.22	0.1	0
	Fixed parameter Poisson	Accuracy		86.40	99.70	99.90
		Precision		78.42	95.65	100
		FPR		0.41	8.33	4.00
		FNR		26.22	0.1	0

Real data results: *n*-back data of my connectome project: The data obtained from a part of the My Connectome Project by Russell A. Poldrack to evaluate working memory. This data set is available at <https://openfmri.org/dataset/ds000031/>. An *n*-back task was performed using a blocked design, with a factorial combination of memory load (1 vs. 2 back) and stimulus type (faces, houses, and Chinese characters) across blocks. We grouped the conditions into two main categories: Images were partitioned into a $96 \times 96 \times 68$ rectangular lattice with voxel size: $2.4 \text{ mm} \times 2.4 \text{ mm} \times 2 \text{ mm}$. Data preprocessing was accomplished using FSL software. 145,122 voxels were left. Then BOLD time courses were extracted for all voxels to be analyzed. Activation probability maps for some typical slices during the *n*-back experiment are reported as follow



Discussion: Our proposed method is a truly 3D spatiotemporal model that incorporates main characteristics of the data together in statistical modeling. As an important aspect of our work, our method estimates the shape parameter of HRF as voxel-based. The other important aspect of our work is that we consider the three-dimensional spatial correlation in the data as well as temporal correlation by appropriate priors.

A Compressing Auto-Encoder as a Developmental Model of Grid Cells

Anthony Kiggundu, Cornelius Weber, Stefan Wermter

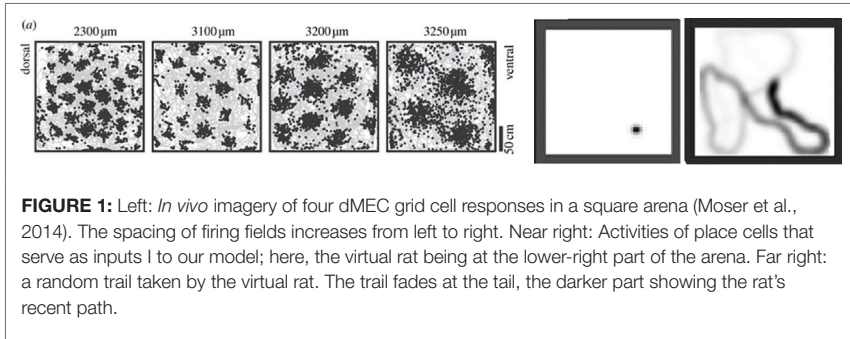
*Knowledge Technology Group, Department of Informatics, Faculty of Mathematics, Computer Science and Natural Sciences, University of Hamburg, Hamburg, Germany
antonkingdee@yahoo.com*

Introduction: The metric representation of space during navigation is attributed to grid cells in the entorhinal cortex. The cell responses form triangular grid-like patterns that tile the entire environment as an animal moves (Giocomo et al., 2011). Earlier findings suggest that the precision of place cells in the hippocampus (CA1 area) of a rodent's brain is increased by the inter-connectivity from grid cells in the parahippocampal CA3 area (Moser et al., 2014). Figure 1, left, shows the grid cells organised into modules where the receptive fields of the cells in one module have the same spacing and orientation but the scale differs in others forming multiple spatially scaled modules that together precisely encode position over a large space.

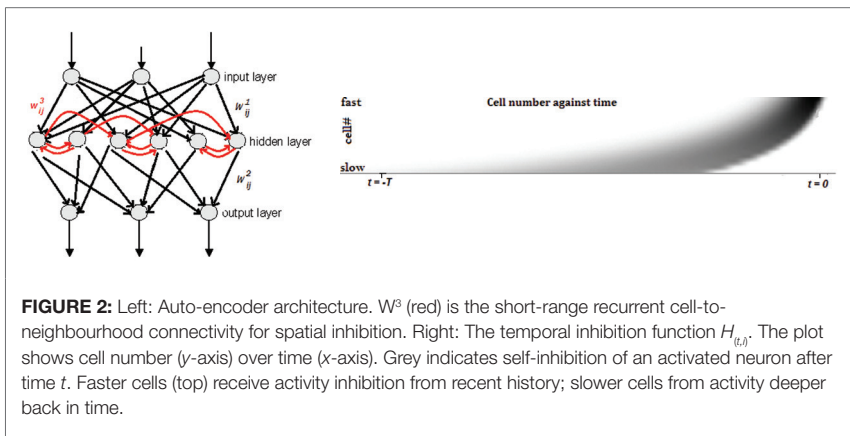
Although the mechanisms through which these multiple spatially scaled modules emerge are still unknown, existing neural models attribute this modular behaviour to odometry such that the change of the triangular tessellating grid cell firing is influenced by the animal's velocity and direction inputs.

In our auto-encoder model, we prescribe to evidence suggesting the existence of auto-associative networks within the entorhinal cortex which cohesively support the emerging activity patterns (Duigou et al., 2014; Rolls, 2007). We hypothesise that grid cell responses can arise in an auto-associative model using feed-forward circuitries and inhibition mechanisms. The inhibition is implemented at both spatial and temporal level, indirectly influencing scaling and firing field sizes within the cells. The emergent grid cells carry a compressed representation of localised place cells through trained weights that encode a virtual rat's position in the environment with varying scales of grid patterns.

Methods: Figure 1, right, shows an example input vector to the model: simulated activities I of place cells and the trajectory of the place cells as a virtual rat randomly moves with constant velocity in a box arena.



The activity is modelled as a Gaussian function centred on the position of the rat. Our auto-encoder model is a simple feed-forward architecture with additional short-range recurrent connectivity as shown in Figure 2, left. Neurons in the input layer are connected to the hidden layer with weight matrix W^1 and the hidden layer neurons to the output layer with weight matrix W^2 . A fixed recurrent or lateral weight matrix W^3 implements short-range spatial inhibition. W^1 and W^2 are randomly initialised, bias vectors b_1 and b_2 are added to the hidden and output layers. The size of the input space is 1,600 (40×40) neurons, the hidden layer has 16 neurons and the output space the same size as the input. This forms a compressing auto-encoder with strongly under-complete coding. The output layer activation is complemented with a competitive softmax function to let only those place cells fire for which grid cells of several different scales agree.



Since we assume no prior knowledge of space, we implement a temporal inhibition mechanism, which is based on the notion that grid cells of high spatial frequency will be quickly activated and deactivated as a rat moves, while cells of low spatial frequency have slow activity changes. The inhibition mechanism allows cells to remain active only for limited times. Figure 2, right, shows the function $H_{(t,i)}$ which determines how much temporal inhibition h_i neuron i receives from its previous activations S_i , inhibiting fast cells more quickly from their own activities than slow cells:

$$h_i(t) = \sum_{t'}^T H_{i,t'} \cdot S(t-t') \quad (1)$$

where T is the memory span, t is current and t' previous time-steps.

The spatial inhibition *via* short-range inhibitory recurrent weights W^3 causes distant neurons to fire independently. The net hidden layer S activity was then computed by applying a sparse transfer function g .

$$a(t) = W^1 \cdot I(t) + W^3 \cdot S(t-1) + b_1 - \eta \cdot h(t) \quad (2)$$

$$S = g(a) = a - 0.9 / (1 + a^2) \quad (3)$$

where η scales the temporal inhibition. Activation on the output layer is computed as

$$O = \text{softmax}(W^2 \cdot S + b_2) \quad (4)$$

where W^2 are the weights to the output layer with the respective bias vector b_2 . The error on the output layer $e = I - O$ is then used for learning of the weights by back-propagation using gradient descent on the sum square error.

Results: Figure 3 shows the emergent weights of the 16 hidden layer neurons after 70,000 training steps. Receptive fields of the cells are spatially organised in approximately triangular grids, showing grid cell responses. The scales of these grids increase from left to right, i.e., from grid cells with faster temporal inhibition to cells with slower temporal inhibition.



FIGURE 3: Model results. Each square shows the input weights of one of the 16 hidden layer neurons, i.e., one row of W^1 . Non-zero weights (dark) connect to isolated regions in input space forming triangular arranged grid patterns, which vary in size, from small scales of “fast” grid cells (left) to larger scales of “slow” cells (right).

Discussion: We implemented an auto-encoder that encodes a localised place cell input efficiently with fewer grid cells. Varying temporal local inhibition led to varying grid spacing, while spatial short-range inhibition enforced the coding to be performed by cells of different scales. The results simulate the emergent triangular grid pattern activity at different scales where the cells’ receptive field weight profile (Figure 3) is similar to biological findings of grid cell activations (Figure 1, left).

Our simple model does not integrate path signals from odometry to influence the behaviour of the activity bumps, as most other models of grid cells do. Nevertheless, the emergent hexagonal grid patterns are stable over time, explaining emerging and convergent connectivity between place cells and grid cells, which existing models do not yet explain. Naturally, odometric information needs to be represented within the hippocampus/dMEC to achieve accurate path integration. Introducing odometry could lead to a class of more detailed and plausible grid cell models.

REFERENCES

- Duigou, C. L., Simonnet, J., Teleńczuk, M. T., Fricker, D., and Miles, R. (2014). Recurrent synapses and circuits in the CA3 region of the hippocampus: an associative network. *Front. Cell. Neurosci.* 7:262. doi: 10.3389/fncel.2013.00262 PMID:24409118
- Giocomo, L. M., Moser, M. B., and Moser, E. I. (2011). Computational models of grid cells. *Neuron* 71, 589604. doi: 10.1016/j.neuron.2011.07.023 PMID:NOPMID
- Moser, E. I., Moser, M. B., and Roudi, Y. (2014). Network mechanisms of grid cells. *Phil. Trans. R. Soc. B* 369: 20120511. doi: 10.1098/rstb.2012.0511 PMID:NOPMID
- Rolls, E. T. (2007). An attractor network in the hippocampus: theory and neurophysiology. *Learn. Mem.* 14, 714–731. doi: 10.1101/lm.631207 PMID:18007016

Quantitative Relations between CRAIIM Human Brain Atlases

Alberto Arturo Vergani^{1,2}, **Renzo Minotto**^{3,2}, **Sabina Strocchi**^{4,2},
Elisabetta Binaghi^{1,2}

¹University of Insubria, Varese, Italy

²Centre of Research in Image Analysis and Medical Informatics (CRAIIM), Varese, Italy

³Neuroradiology – Ospedale di Circolo e Fondazione Macchi, Varese, Italy

⁴Medical Physics – Ospedale di Circolo e Fondazione Macchi, Varese, Italy
aavergani@uninsubria.it

Introduction and Motivation: We present two types of CRAIIM hybrid atlas (CRAIIM is the acronym of Centre of Research of Image Analysis and Medical Informatics at University of Insubria in Varese, Italy). Both types of atlases have in common an extensive integration of white and grey matter structures that allows representing 161 brain territories, but one with 1mm resolution and the second one with 2 mm of resolution. There are many brain templates used for image processing, that cover precise brain regions (FMRIB Software Library, Analysis Group, Medical Science Division, University of Oxford (UK), 2016): Tailarach (the more detailed with 1105 ROI), Juelich (121 ROI), Harvard-Oxford cortical (96 ROI), Harvard-Oxford subcortical (21 ROI), Montreal National Institute template (9 ROI), and other more anatomically specific such as Cerebellar-FLIRT/NIRT (28 ROI) and Subthalamic-Nucleus-Atlas (2 ROI). Therefore, the presence in the neuroinformatical context of different atlases, with diverse resolution and specialization, motivated the CRAIIM group to design a hybrid model using a number of regions oriented to the automated procedures as well as to visual inspection. Also, as presented at INCF conference 2016 (Vergani et al., 2016), the CRAIIM hybrid atlas with 1mm resolution comes from a joint operation between Juelich histological atlas and Harvard-Oxford cortical and subcortical atlases. The motivation of using them selectively emerged by a) the lack of some fundamental clinical regions in the Juelich original model, b) the high level of compatibility in terms of numerosity and volumetry of regions between H-O and Juelich, and c) the peculiarity of these two atlases of being in the same MNI 152 space, allowing the researcher to completely compare them.

Methods: There are two topics that must to be taken into account: Integration Procedure (IP) and Voxel-Label Probability (VLP).

IP: To make the integration correctly, we have to choose how to cope with atlases overlaps between brain regions belonged to Juelich and Harvard-Oxford atlases. We chose Juelich template as our reference with the purpose of completing it by regions originally

present only into the Harvard-Oxford atlas (cortical and subcortical portions), from which we selected 40 ROI, such as frontal and temporal cortexes, subcallosal portions, and cingulated gyrus and thalamus halves. The main criteria to manage partial intersection between brain structures was to save all the portions just belonged to Juelich, and then to integrate them with the selected Harvard-Oxford regions, excluding their part overlapped, in other words, we framed the Juelich template with 40 regions of Harvard-Oxford without their portions that generated the overlaps.

VLP: Another step was to decide which probabilistic version of the atlases to consider. We use atlases contained into FMRIB Software Library (FSL) (Jenkinson et al., 2012) that offers probabilistic templates that, for each of their voxel, assign a probability to fit a certain brain region. This allows giving to research the ability to use atlases that have all regions with probability major or =0%, otherwise with probability major or equal to 25% or, finally, major or =50%. Intuitively, the less is the degree of probability, the more is the volume of the atlas. We consider Juelich and Harvard-Oxford atlases with a probability threshold major or equal to 0%, i.e., their version with all of the possible labelled voxels to be shaped for their integration. We tested the CRAIIM hybrid atlases with the computerized pipeline of fMRI analysis that estimates synthetic measures, i.e., Activated Weighted Indexes and Vectors (Pedoia et al., 2011, 2012, 2013), for each of the brain regions covered by the hybrid template [cfr. (Vergani et al., 2016) for results and comments]. Also, we evaluated it with FMRIB Software Library tools for neuroimaging analysis.

Results: Figure 1 shows the difference before and after the integration of Juelich brain with the 40 regions hailing from Harvard-Oxford cortical and subcortical atlases. In the three images in the top row, there is the superimposition between the Montreal National Institute (MNI) detailed anatomical atlas, as example of possible patient brain, and the Juelich atlas. A large amount of portions is not covered with, such as frontal lobes, many temporal territories, thalamus halves, and so on. In the bottom row, there is the same MNI template, but with the superimposition of the CRAIIM hybrid atlas, that covers exactly the same volumes enclosed by Juelich one, but having extra-extended brain regions, that are the 40 added from Harvard-Oxford atlases. Tables 1 and 2 explain quantitative relations among the two type of versions of CRAIIM hybrid atlases. Table 1 illustrates how many voxels are in each template and how many of them belong to Juelich or Harvard-Oxford models. It is indicated the number of regions that come from them, that are 162 and not 161 because we counted also the empty space, i.e., the black area in the images that has not brain labels. The volume of atlases with their empty space is always the same: with 1mm length for each voxel and with 7,221,032 voxels, there is a volume of 7,221,032 mm³; equivalently, for 2mm voxel length, but with 902,629 voxels, the volume is always 7,221,032 mm³ (~ 7 L). Table 2, instead, presents the numbers of voxels of two atlases organizing the 161 brain regions

with 9 anatomo-functional meta-labels, i.e., Acoustic, Associative, Behaviour, Fascicles, Language, Limbic System, Motor, Somato-Sensitive and Visual. Figures 2 and 3 show the voxel distribution through CRAIIM hybrid atlases with 1mm and 2mm of resolution. The quantities are clustered by the 9 anatomo-functional zones and sub-grouped for their original models. There is no difference in proportion between the two figures, and this reflects the equivalence in terms of representability of CRAIIM hybrid atlas in both resolutions. What it is changed in Figures 2 and 3 is for sure the numbers of voxels that depend by voxel length. Figure 4 is a bar plot that makes in relation the voxel enumeration of the only 40 regions added to Juelich that coming from Harvard-Oxford. We selected them because the treatment of overlapping causes a reduction of the original volume of these regions added. The graph shows the difference in voxel number of 40 structures before and after the integration operation. Figure 5 highlights the better completeness of the 1mm version compared to the 2mm of the CRAIIM hybrid atlas, due to the minor gap in terms of voxel percentage in reference to the original Harvard-Oxford template. Figure 5 proved that the Juelich regions in CRAIIM hybrid atlases are the same of those in Juelich model.

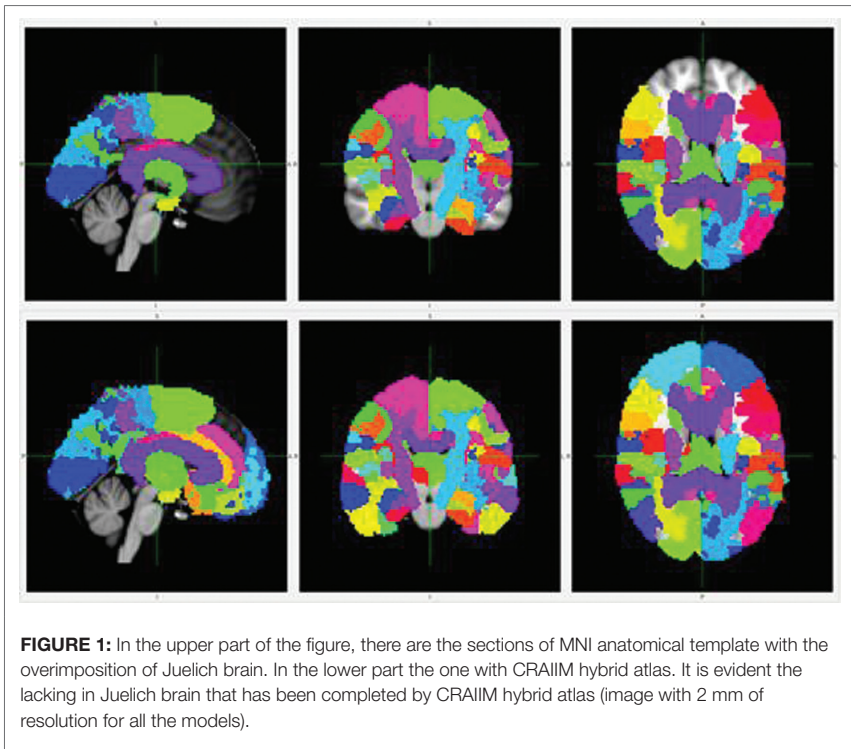


TABLE 1: Numerosity of CRAIIM voxel distinguished for resolution type and organized by anatomo-functional meta-labels (n.b. NA means empty space, i.e., black volume without brain regions).

Anatomo-Functional meta-labels	CRAIIM_VOXEL_1mm	CRAIIM_VOXEL_2mm	# Regions
ACUSTIC	42304	5667	16
ASSOCIATIVE	396253	51711	39
BEHAVIOUR	182316	23571	2
FASCICLES	25009	3579	6
LANGUAGE	166982	23216	16
LYMBIC_SYSTEM	265700	33518	42
MOTOR	203616	27727	8
NA	5616265	689415	1
SOMATO-SENSITIVE	89824	11954	16
VISUAL	232763	32271	16
Grand Total	7221032	902629	162

TABLE 2: Numerosity of CRAIIM voxel grouped for resolution type and organized by original atlases (n.b. NA means empty space, i.e., black volume without brain regions).

Original Atlases	CRAIIM_VOXEL_1mm	CRAIIM_VOXEL_2mm	# Regions
HO_cort	497974	61797	38
HO_sub	10609	965	2
JUELICH	1096184	150452	121
NA	5616265	689415	1
Total	7221032	902629	162

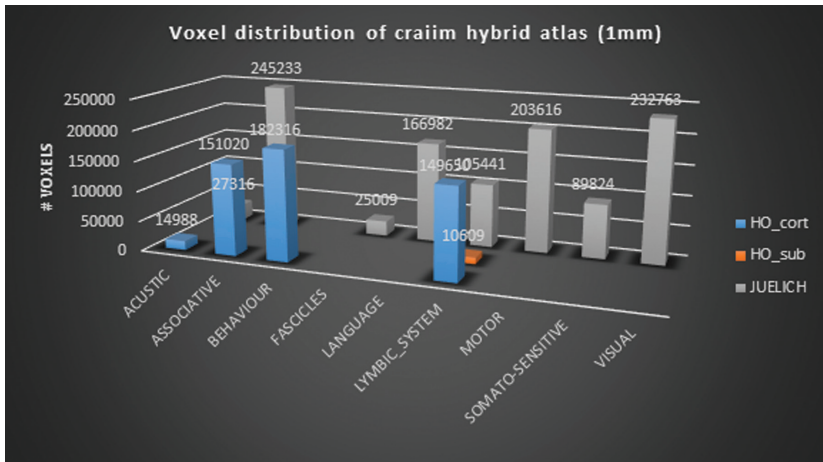


FIGURE 2: Voxel distribution clustered by 9 anato-functional meta-labels of 161 brain regions of CRAIIM Hybrid Atlas with 1mm of voxel resolution organized by their original atlas (Juelich in grey and Harvard-Oxford cortical and subcortical in orange and blue, respectively).

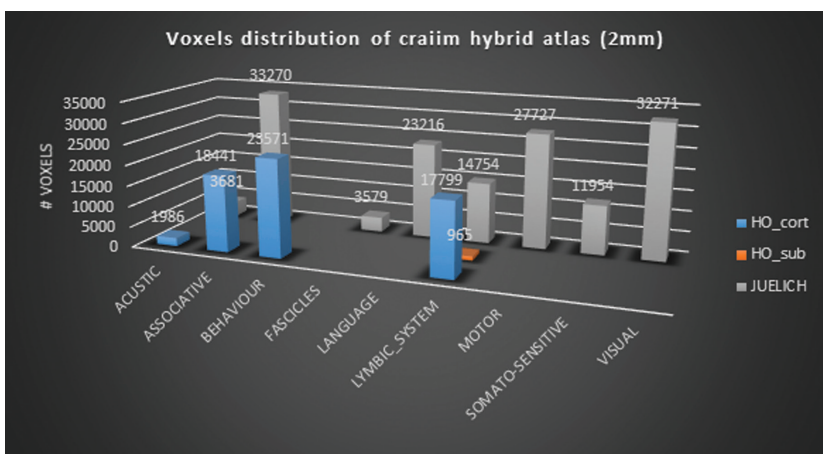


FIGURE 3: Voxel distribution clustered by 9 anato-functional meta-labels of 161 brain regions of CRAIIM Hybrid Atlas with 2 mm of voxel resolution organized by their original atlas (Juelich in grey and Harvard-Oxford cortical and subcortical in orange and blue, respectively).

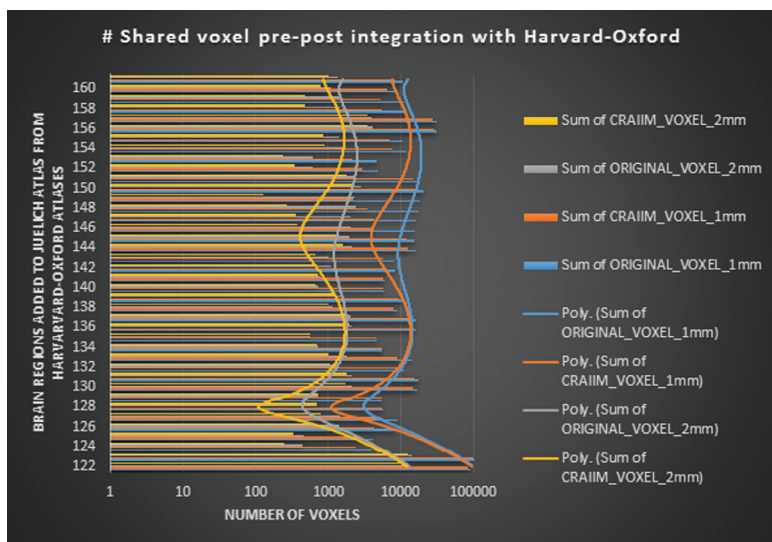


FIGURE 4: Bar plot with the 40 added regions to Juelich atlases coming from Harvard-Oxford atlases. The different bars show the original voxel value of each brain regions and the value that they have had after the overlap treatment. The main result refers that the CRAIIM hybrid atlas with 1 mm of resolution shares more with the original atlas than the CRAIIM hybrid atlas with 2 mm of resolution (cfr. the convexities among Polynomial trend lines: Orange-Blue duo (1 mm) VS Yellow-Grey duo (2 mm)).

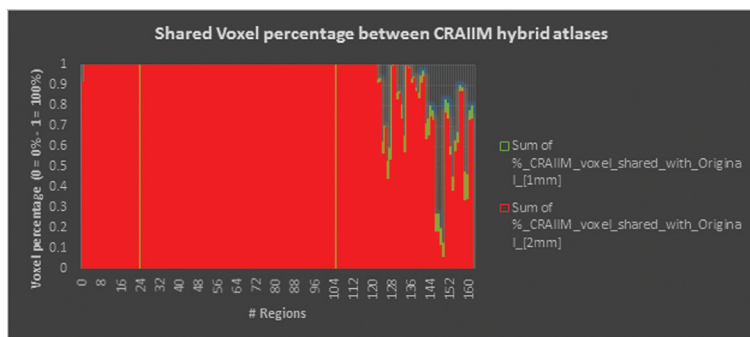


FIGURE 5: CRAIIM hybrid atlas with 2 mm of resolution (Red bars) always have minor shared voxel percentage with their own original structures (Juelich and Harvard-Oxford atlases), for the 40 added regions (122–161), then the CRAIIM hybrid atlas with 1 mm of resolution (bars in Green).

Discussion: We have presented two versions of the CRAIIM Hybrid Atlases of human brain for neuroimaging purposes. They differ for resolution, but not for representativeness of the 161 brain regions (kept 121 from Juelich and the 40 from Harvard-Oxford cortical and subcortical atlases). They are in perfectly proportions of the same brain structures (161 ROI; cfr. Figures 2 and 3), but the 40 added regions from Harvard-Oxford differ in the two version of our atlas for percentage shared with their original shapes. The CRAIIM hybrid atlas with 1mm resolution has more portions in common with the 40 Harvard-Oxford parts, then the one with 2 mm of resolution (Figures 4 and 5). This percentage variable by resolution depends properly by the length of the voxel. The presence of more voxels with the 1mm version of CRAIIM hybrid atlas has allowed to better shape the added structures, framing them more stylishly, with respect to the version with 2 mm. The “thumb rule” used states that is better to have voxel-labeled than voxel-unlabeled (i.e., black voxel). The constraint with this rule is evident when we added brain regions that are in low percentage of voxel shared with their original version, after the integration procedure. The advantage is indeed the possibility of displaying them instead the empty space. Next step could be to trace the percentage cut-off that law if or if not include regions under-represented after integration procedure. A part of these difference linked with the resolution, we have shown that CRAIIM hybrid atlases, both 1 and 2 mm version, cover extensively the Montreal National Institute anatomical template, as a model of patient brain, with respect to the Juelich atlas, safeguarding many territories otherwise lacking (Figure 1). In potential, CRAIIM hybrid atlases are very suitable to use in functional neuroimaging for severe scope, e.g., ROI masking, ROI selection, labels comparison, registration processing (Lindquist, 2008). The CRAIIM Hybrid Atlases could be used to promote dimensionality reduction of SPM volumes with the computation of synthetic indexes (Pedoia et al., 2011, 2012, 2013).

Actually, the Neuroinformatics Platform of Human Brain Project is able to display anatomical atlases of mammals such as *Mus Musculus*, *Rattus Norvegicus* and *Homo Sapiens* (e.g., BigBrain, MNI Colin27, MNI ICBM, InfantAtlas) (H. B. Project, 2016). In the future, the development of neuroinformatical tools to generate hybrid atlas, with a good rational between human usability and covered neuro-topography, and with a wise algorithm to handle overlaps, could be the right way to design purpose-based atlas with specific anatomical representativeness and normative features able to standardize and process heterogeneous functional and structural brain images.

REFERENCES

- FMRI Software Library. (2016). *Atlases Overview*. Available at: <http://fsl.fmrib.ox.ac.uk/fsl/fslwiki/Atlases>
- H. B. Project. (2016). *Neuroinformatics Platform*. Available at: <https://www.humanbrainproject.eu/nip>
- Jenkinson, M., Beckmann, C. F., Behrens, T. E. J., Woolrich, M. W., and Smith, S. M. (2012). FSL. *Neuroimage* 62, 782–790. doi: 10.1016/j.neuroimage.2011.09.015 PMID:21979382
- Lindquist, M. A. (2008). The statistical analysis of fMRI data. *Stat. Sci.* 23, 439–464. doi: 10.1214/09-STS282 PMID:NOPMID
- Pedoia, V., Colli, V., Strocchi, S., Vite, C., Binaghi, E., and Conte, L. (2011). “fMRI analysis software tools: an evaluation framework,” in *Proceedings of the SPIE 7965, Medical Imaging 2011: Biomedical Applications in Molecular, Structural, and Functional Imaging*, Lake Buena Vista, USA
- Pedoia, V., Strocchi, S., Colli, V., Binaghi, E., and Conte, L. (2013). Functional magnetic resonance imaging: comparison between activation maps and computation pipelines in a clinical context. *Mag. Reson. Imag.* 31, 555–566. doi: 10.1016/j.mri.2012.10.013 PMID:NOPMID
- Pedoia, V., Strocchi, S., Minotto, R., and Binaghi, E. (2012). “Hemispheric dominance evaluation by using fMRI activation weighted vector,” in *Computational Modelling of Objects Represented in Images - Fundamentals, Methods and Applications III, Third International Symposium, CompIMAGE 2012*, Rome, Italy, September 5–7, 2012.
- Vergani, A., Minotto, R., Strocchi, S., and Binaghi, E. (2016). FSL-based hybrid atlas promotes activation weighted vector analysis in functional neuroradiology. *Front. Neuroinform.* Conference Abstract: Neuroinformatics 2016. doi: 10.3389/conf.fninf.2016.20.00077

Activation Likelihood Estimation Based Analysis of Memory in Alzheimer Disease and Mild Cognitive Impairment Patients Using fMRI and PET Data

**Armin Vosoughi¹, Saeed Sadigh-Eteghad¹, Mehdi Farhoudi¹,
Yadollah Omid²**

¹Faculty of Medicine, Neurosciences Research Center (NSRC), Tabriz University of Medical Sciences, Tabriz, Iran

²Faculty of Pharmacy, Research Center for Pharmaceutical Nanotechnology (RCPN), Tabriz University of Medical Sciences, Tabriz, Iran
vosoughi954@gmail.com

Introduction/motivation: Human brains, their behaviors and capacities alter by aging. This is considered as the main risk factor for developing neurodegenerative diseases including Alzheimer disease (AD), mild cognitive impairment (MCI) and other types of dementia. AD is a neurodegenerative disease that can impair memory and learning processes (Dickson, 1997). The main molecular mechanisms involved in AD include the deposition of amyloid β (A β) and neurofibrillary tangles (NFTs), which are often reported in temporal lobe, and then frontal and parietal cortices. On the other hand, atrophy and neuronal death occur in the mentioned areas (Braak et al., 2006).

MCI tends to be considered as a bridge between healthy elderly and AD patients, thus pattern changes in MCI might be indicative of the emergence of AD (Petersen et al., 2001). Functional evaluation of the brain tasks is made by imaging modalities, including functional magnetic resonance imaging (fMRI) and positron emission tomography (PET). These imaging modalities are expensive and are available solely in high technology facilities. Variations in their outputs are vast and need complex analyses to demystify the raw data. Therefore, online computer-based studies have proved useful in analyzing and interpreting the existing data (Sadigh-Eteghad et al., 2014; Rombouts et al., 2005). In this study, activation likelihood estimation (ALE) is used to evaluate the overlap between foci, based on their distributions at the respective coordinates (Eickhoff et al., 2009). The coordinate-based analyses of neuroimaging data (i.e., PET and fMRI images) were investigated to find a difference in memory-related neuroimaging aspects between AD and MCI patients as well as normal elderly.

Methods: Search was conducted in BrainMap (www.brainmap.org) database using the keywords “Alzheimer disease”, “Mild cognitive impairment”, “cognition”, “memory” (including all types of memory), “fMRI” and “PET” for the case group and “normal”, “cognition”, “memory” (including all types of memory), “fMRI” and “PET” for the control group, with mean age of over 60 years for both groups. Then, the results of search

were evaluated and the studies with lower mean age than 60 and other cognitional or motor functions were excluded. Sleuth (version 2.4) and Ginger ALE (version 2.3.6) software were used for the ALE meta-analysis (Laird et al., 2005).

The ALE technique uses peak coordinates reported in functional neuroimaging studies as full-width-at-half-maximum Gaussian sphere model distribution. The ALE statistic describes the voxel-wise likelihood of activation, and is a measure of agglomeration among included coordinates in the reported area. Most studies have been conducted based on Talairach space, whereas, the threshold for p -value map is considered at the false discovery rate (FDR) of $p < 0.05$ and the clusters with a minimum size of 200 mm³. For visualization, threshold ALE maps were imported into multi-image analysis MANGO (Research Imaging Center, UTHSCSA) (<http://ric.uthscsa.edu/mango>); and overlaid onto a standardized anatomical template in Talairach space (colin1.1.nii) (Laird et al., 2005). Finally, the anatomical labels were illustrated using Talairach Daemon (Lancaster et al., 2000).

Results: Twenty-eight articles that explored the activated areas during memory tasks in normal elderly subjects, and AD and MCI patients (i.e., 14 papers each) were found. Based on these findings, left parietal lobe (angular gyrus) and left frontal lobe (middle frontal gyrus) appeared to be the most activated areas in memory-related tasks in healthy elderlylies. Further, left and right precuneus and left and right temporal lobes were activated more in AD and MCI patients. Subtracting the images of the AD and MCI patients from the normal elderly subjects showed that right temporal lobe (sub-gyral), left and right precuneus and supramarginal gyri (in right temporal and parietal lobes), as well as left superior occipital gyrus were activated in AD and MCI patients (Figure 1).

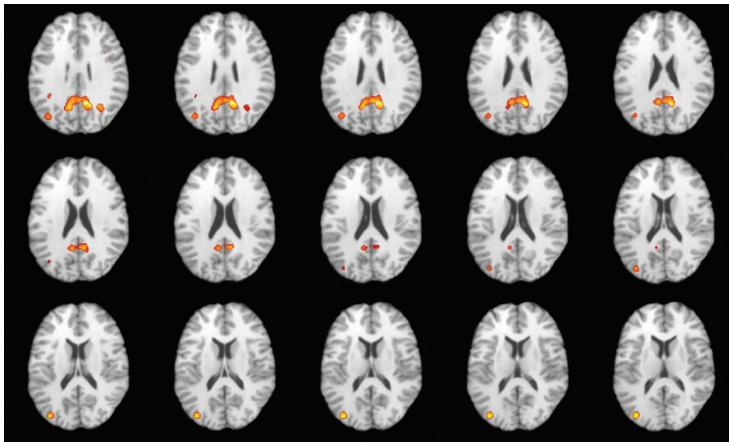


FIGURE 1: Subtraction analysis in normal elderly subjects in comparison to AD and MCI patients. Significant clusters thresholded with a FDR at $p < 0.05$.

Conclusion: Right and left precuneus and supramarginal gyri were activated in AD and MCI patients, whereas normal elderly subjects did not show such activity in those areas during memory-related tasks. Therefore, these findings suggest that memory-related functions in AD and MCI patients could be shifted to the mentioned areas and instead of the normal former areas these new sites participate in memory tasks.

Keywords: Alzheimer disease, mild cognitive impairment, PET, fMRI, activation likelihood estimation

REFERENCES

- Braak, H., Alafuzoff, I., Arzberger, T., Kretschmar, H., and Del Tredici, K. (2006). Staging of Alzheimer disease-associated neurofibrillary pathology using paraffin sections and immunocytochemistry. *Acta Neuropathol.* 112, 389–404. doi: 10.1007/s00401-006-0127-z PMID:16906426
- Dickson, D. W. (1997). Neuropathological diagnosis of Alzheimer's disease: a perspective from longitudinal clinicopathological studies. *Neurobiol. Aging* 18(4 Suppl.), S21–S26. doi: 10.1016/S0197-4580(97)00065-1 PMID:9330981
- Eickhoff, S. B., Laird, A. R., Grefkes, C., Wang, L. E., Zilles, K., and Fox, P. T. (2009). Coordinate-based activation likelihood estimation meta-analysis of neuroimaging data: a random-effects approach based on empirical estimates of spatial uncertainty. *Hum. Brain Mapp.* 30, 2907–2926. doi: 10.1002/hbm.20718 PMID:19172646
- Laird, A. R., Fox, P. M., Price, C. J., Glahn, D. C., Uecker, A. M., Lancaster, J. L., et al. (2005). ALE meta-analysis: controlling the false discovery rate and performing statistical contrasts. *Hum. Brain Mapp.* 25, 155–164. doi: 10.1002/hbm.20136 PMID:15846811
- Lancaster, J. L., Woldorff, M. G., Parsons, L. M., Liotti, M., Freitas, C. S., Rainey, L., et al. (2000). Automated Talairach atlas labels for functional brain mapping. *Hum. Brain Mapp.* 10, 120–131. doi: 10.1002/1097-0193(200007)10:3<120::AID-HBM30>3.0.CO;2-8 PMID:10912591
- Petersen, R. C., Doody, R., Kurz, A., Mohs, R. C., Morris, J. C., Rabins, P. V., et al. (2001). Current concepts in mild cognitive impairment. *Arch. Neurol.* 58, 1985–1992. doi: 10.1001/archneur.58.12.1985 PMID:11735772
- Rombouts, S. A., Barkhof, F., Goekoop, R., Stam, C. J., and Scheltens, P. (2005). Altered resting state networks in mild cognitive impairment and mild Alzheimer's disease: an fMRI study. *Hum. Brain Mapp.* 26, 231–239. doi: 10.1002/hbm.20160 PMID:15954139
- Sadigh-Eteghad, S., Majidi, A., Farhoudi, M., Talebi, M., and Mahmoudi, J. (2014). Different patterns of brain activation in normal aging and Alzheimer's disease from cognitive task: meta analysis using activation likelihood estimation. *J. Neurol. Sci.* 343, 159–166. doi: 10.1016/j.jns.2014.05.066 PMID:24950901

NestMC: A Morphologically Detailed Neural Network Simulator for Modern High Performance Computer Architectures

Wouter Klijn¹, Ben Cumming², Stuart Yates², Vasileios Karakasis³, Alexander Peyser¹

¹Jülich Supercomputing Centre, Jülich, Germany

²Swiss National Supercomputing Center, Future Systems, Zürich, Switzerland

³Swiss National Supercomputing Center, User Engagement & Support, Lugano, Switzerland

w.klijn@fz-juelich.de

NestMC is a new multicompartment neural network simulator currently under development as a collaboration between the Neuroscience SimLab at the Forschungszentrum Jülich, Barcelona Supercomputing Center and the Swiss National Supercomputing Center under the aegis of the NEST Initiative. NestMC will enable new scales and classes of morphologically detailed network simulations on current and future supercomputing architectures.

A number of “many-core” architectures such as GPU and Intel Xeon Phi based systems are currently available, to optimally use these emerging architecture new approaches in software development and algorithm design are needed. NestMC is being written specifically with this in mind; it aims to be a flexible platform for neural network simulation, while keeping interoperability with models and workflows of NEST and NEURON.

The improvements in performance and flexibility in themselves will enable a variety of novel experiments, but the design is not finalised, and is driven by the requirements of the neuroscientific community. The prototype is open source (1) and we invite you to have a look. We are interested in your ideas for features which will make new science possible: we ask you to think outside of the box and build this next generation neurosimulator together with us.

What directions do you want us to go in?

* Simulate large morphological detailed networks for longer time scales: Study of slow developing phenomena.

* Reduce the time to solution: Perform more repeat experiments for increased statistical power.

* Create high performance interfaces with other software: Perform online statistical analysis and visualization of your running models, study the brain at multiple scales with specialized tools, or embed detailed networks in physically modelled animals.

* Optimize dynamic data structures for models with time-varying number of neurons, synapses and compartments: simulate neuronal development, healing after injury and age related neuronal degeneration.

Do you have other great ideas? Let us know!

Real-Time Neuromorphic Encoding of Visual Stimuli Acquired with a Camera through Labview Interface

Martina Finocchiaro^{1,2}, Elisa Massi^{1,2}, Marcello Calisti¹, Alberto Mazzoni²

¹Department of Information Engineering, University of Pisa, Pisa, Italy

²The Biorobotics Institute, Scuola Superiore Sant'Anna, Pisa, Italy

elymas93@gmail.com

The processing of the visual information in humans ends in the cortex but already starts at the level of the retina. The first neural encoding of visual stimuli occurs at the level of the ganglion cells whose axons converge into the optic nerve. However, the firing rates of the ganglion cells carry information about the external stimulus after that this has already been processed by the complex neural circuits within the retina, made of photoreceptors, horizontal, amacrine and bipolar cells.

The aim of this work is to emulate the neural dynamics of human ganglion cells through a real time implementation of spiking neuron models. Visual data acquired by means of a webcam will be encoded in the spiking patterns of the simulated ganglion cells mimicking the way the same image would have been encoded in ganglions cells firing after reaching the retina. Our algorithm in particular aims at encoding colour features of the image with a neuromorphic approach, contributing to the quest for an innovative bioinspired artificial visual system.

Briefly, image processing and reconstruction work as follows. A grid of arbitrary size is applied on the real time acquired image, determining the resolution of the artificial sense. Each one of the regions of interest feeds a virtual neuron. The neurons are implemented on a National Instrument myRIO embedded device, which is reconfigurable and reusable and can feature parallel programming and high execution frequencies. We modelled ganglions cell with an Izhikevich neuron model, implemented in LabVIEW. A proper choice of the model parameters was selected to replicate the adaptive properties of the retina in processing to contrast and colours. For each region of the image a 16-elements colour spectrum is computed. The gain factor of the input current to each neuron is based on the major colour of the spectrum. Exploiting the adaptive dynamics of the neurons, 9 colour features, that are 7 biologically relevant colours and black and white, are encoded into different firing rates. Real time decoding of these firing rates finally leads to a colour based reconstruction of the image.

The obtained results show a real time recognition of 5 out of the 9 classes previously encoded (red, green and blue as cones photoreceptors, black and white as rods photoreceptors), under certain controlled luminosity constraints. The 20 kHz updating frequency of the decoding of the image is biologically plausible. Moreover, the achievable spatial resolutions of the grid compete, or in some cases even exceed, the ones of the available artificial retinal implants. This work offers an alternative classification method for visual features recognition, which has the potential to achieve great results, using a simpler algorithm than the traditional one. The advantage of bioinspired methods is the reduction of computational complexity, resulting in an overall optimization, keeping high efficiency. Taking advantage of the built-in Wi-Fi of the myRIO board, the developed system could be exploited in autonomously moving robots. Finally, this study may be useful for closed loop hybrid bionic systems to restore missing vision-sensory function or to augment it and it could also be integrated in neurophysiological studies.

Neurogenesis on SpiNNaker

Petruț. A. Bogdan, Stephen Furber

University of Manchester, Manchester, United Kingdom

petrut.bogdan@manchester.ac.uk

steve.furber@manchester.ac.uk

Neurogenesis is a process of nerve tissue creation taking place during prenatal development or during adulthood in two discrete areas of the brain: the subgranular zone (SGZ) of the hippocampal dentate gyrus, and the subventricular zone (SVZ), which projects through the rostral migratory stream to the olfactory bulb. In the hippocampus, newborn cell survival has been shown to increase performance in trace eyeblink conditioning, while levels of proliferation positively affects reactions to novelty [for review, see Lledo et al. (2006)], with positive correlations regarding perceptual and memory functions also identified in the olfactory bulb.

We are investigating the problem of designing structurally evolving spiking neural networks running on the SpiNNaker (Furber et al., 2013) neuromorphic computation platform, as well as the computational advantages of enabling neural populations to self organize using stochastic processes. This platform is a massively parallel system relying on low-power ARM CPUs interconnected using a custom communication fabric in order to efficiently simulate spiking neural networks in biological real time. The research revolves around enhancing the existing PyNN (Davison et al., 2008) neural simulator running on SpiNNaker to allow for structural plasticity in a biologically plausible way. More specifically, the processes to be investigated are neurogenesis and synaptogenesis as they occur post-development, in pre-existing circuits.

Initially, the process of synaptogenesis will be modeled in the context of topographic map formation (Bamford, 2010), laying the groundworks for encoding and using spatial information in spiking neural networks (SNN) simulated on this distributed neuromorphic system. Afterwards, newborn neurons will be allowed to be created at runtime, the rate of which will be controlled using a homeostasis mechanism.

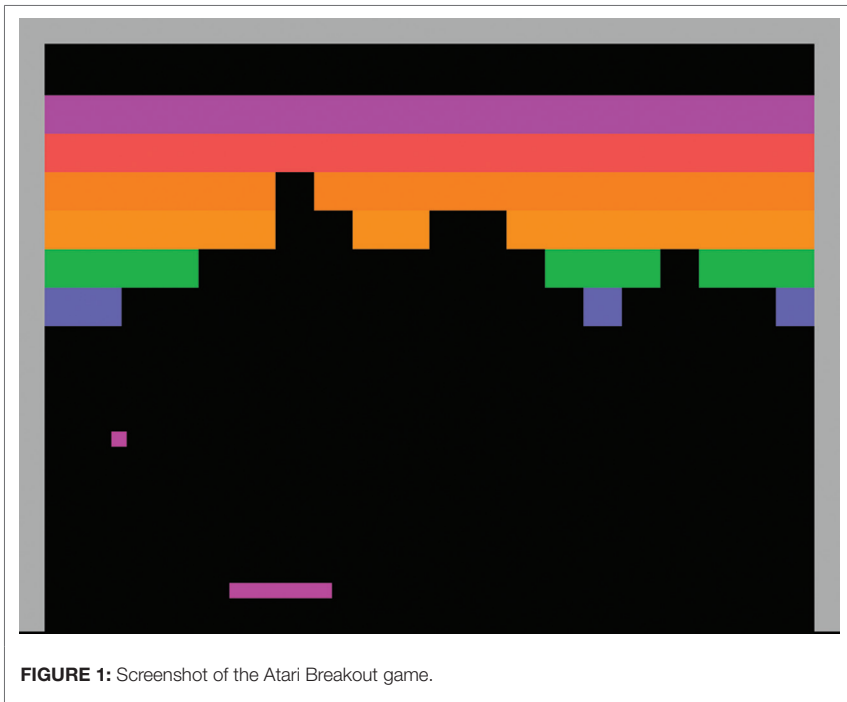


FIGURE 1: Screenshot of the Atari Breakout game.

These experiments have as a main desired outcome the exploration of additional learning mechanisms in artificial spiking neural networks, more specifically a mechanism to complement synaptic plasticity [STDP (Markram et al., 1997)]. The mechanism that we are exploring is expected to provide a longer-term type of learning, encoded by the topology of the network (from weeks to months), while STDP provides short-term learning (from minutes to hours). One application of structural plasticity on SpiNNaker will be in creating an agent that will learn to play video games (e.g. the Atari Breakout game picture in Figure 1) using a reinforcement learning algorithm implemented in spiking neurons. In the context of this task, this novel learning mechanism is expected to provide transferable skills between different games, i.e., to allow the agent to learn a new game more rapidly based on previous knowledge of a different, yet similar game. Additionally, we postulate that synaptic rewiring can, from a computational point of view, provide a form of random search of the state space of the game, thus helping in exploration.

REFERENCES

- Bamford, S. A., Murray, A. F., and Willshaw, D. J. (2010). Synaptic rewiring for topographic mapping and receptive field development. *Neural Netw.* 23, 517–527. doi:10.1016/j.neunet.2010.01.005
- Davison, A. P., Brüderle, D., Eppler, J., Kremkow, J., Müller, E., Pecevski, D., et al. (2008). PyNN: a common interface for neuronal network simulators. *Front. Neuroinform.* 2:11. doi: 10.3389/neuro.11.011.2008 PMID:NOPMID
- Furber, S. B., Lester, D. R., Plana, L. A., Garside, J. D., Painkras, E., Temple, S., et al. (2013). Overview of the SpiNNaker system architecture. *IEEE Trans. Comput.* 62, 2454–2467. doi: 10.1109/TC.2012.142 PMID:NOPMID
- Lledo, P.-M., Alonso, M., and Grubb, M. S. (2006). Adult neurogenesis and functional plasticity in neuronal circuits. *Nat. Rev. Neurosci.* 7, 179–193. doi: 10.1038/nrn1867 PMID:16495940
- Markram, H., Lübke, J., Frotscher, M., and Sakmann, B. (1997). Regulation of synaptic efficacy by coincidence of postsynaptic APs and EPSPs. *Science* 275, 213–215. doi: 10.1126/science.275.5297.213 PMID:NOPMID

Short-Term Plasticity for Neuromorphic Hardware

Sebastian Billaudelle, Johannes Schemmel, Karlheinz Meier

Heidelberg University, Heidelberg, Germany
sebastian.billaudelle@kip.uni-heidelberg.de

Increasing the size and complexity of spiking neural networks represents a growing challenge for numerical simulations. Even assuming that today's largest simulations—and the supercomputers they run on—could be scaled up straightforwardly to the size of a human cortex, running these simulations would be quite prohibitive due to both their power consumption and their slow-down with respect to biological time. State-of-the-art analog neuromorphic systems promise high execution speeds combined with a low energy footprint—mostly independent of the emulated model's size (Indiveri et al., 2011). The «physical model system» developed at Heidelberg University as part of the HBP Neuromorphic Computing Platform features a scalable computation substrate based on wafer-scale integrated neuromorphic cores. The basic building block of this platform is the High Input Count Analog Neural Network (HICANN) chip built in 180 nm CMOS technology (Schemmel et al., 2008). Its successor, the HICANN-DLS (Digital Learning System), which employs a more advanced 65 nm technology, is currently under development.

Designing scalable circuits for such a platform is challenging, as it inevitably requires a tradeoff between technological feasibility and the faithful reproduction of biological dynamics. As an example, we discuss the development of a circuit for modeling synaptic dynamics.

Starting from *in vitro* findings and their associated phenomenological model (Tsodyks and Markram, 1997), a simplified model of synaptic depression and facilitation suitable for implementation in an integrated circuit is presented (Schemmel et al., 2006). We introduce the basic building blocks of such a circuit and compare their dynamics to the reference model. Additionally, we walk through some of the design techniques and paradigms used in the development process. This includes software-assisted circuit optimizations as well as advanced pre-production verification methods. In particular, we explain how a simple evolutionary algorithm enabled us to optimize the performance of a sub-circuit as well as its area requirements by finding suitable transistor sizes that would have otherwise been difficult to infer.

REFERENCES

- Indiveri, G., Linares-Barranco, B., Hamilton, T. J., Van Schaik, A., Etienne-Cummings, R., Delbruck, T., et al. (2011). Neuromorphic silicon neuron circuits. *Front. Neurosci.* 5:73. doi: 10.3389/fnins.2011.00073 PMID:21747754
- Schemmel, J., Fieres, J., and Meier, K. (2008). "Wafer-scale integration of analog neural networks," in *2008 IEEE International Joint Conference on Neural Networks (IEEE World Congress on Computational Intelligence)* (IEEE), Hong Kong, China, pp. 431–438.
- Schemmel, J., Grubl, A., Meier, K., and Mueller, E. (2006). "Implementing synaptic plasticity in a VLSI spiking neural network model," in *The 2006 IEEE International Joint Conference on Neural Network Proceedings* (IEEE), Vancouver, Canada, pp. 1–6.
- Tsodyks, M. V., and Markram, H. (1997). The neural code between neocortical pyramidal neurons depends on neurotransmitter release probability. *Proc. Natl. Acad. Sci. U S A* 94, 719–723. doi: 10.1073/pnas.94.2.719 PMID:9012851

Neuronal Dynamics: Silicon vs. Biology

Laura Kriener, Paul Müller, Sebastian Billaudelle, Johannes Schemmel, Karlheinz Meier

Kirchhoff Institute for Physics, Heidelberg, Germany

laura.kriener@kip.uni-heidelberg.de

sebastian.billaudelle@kip.uni-heidelberg.de

In analog neuromorphic devices, the physics of neurons and synapses is replaced by the physics of semiconductors. Instead of numerically calculating (simulating) solutions to the differential equations that govern neuro-synaptic dynamics (Brette et al., 2007), analog neuromorphic circuits are built to obey these equations, thereby closely replicating (emulating) the behavior of their biological archetypes (Mead, 1990). Modern neuromorphic devices (Indiveri et al., 2011) aim to provide a configurable substrate for the study of network dynamics with the long-term aim of making use of the computational potential of spiking neural networks.

In order to achieve a good combination of configurability and precision under the constraints imposed by the available technology, we design our chips using a mix of analog and digital circuits (Schemmel et al., 2010). Our neuronal circuits, for example, model their membrane potential as an analog dynamical variable, but transmit spikes as digital events. The neuronal dynamics constitute a physical realization of the adaptive exponential integrate-and-fire model (Brette and Gerstner, 2005) that has been shown to capture relevant properties of biological neurons (Naud et al., 2008).

Our low-power accelerated implementation of the neuron model trades precision for energy efficiency and speed. In particular, the dynamics of the implemented circuits deviate from the ideal mathematical description. It is therefore essential to verify that the design still captures the most relevant behavioral characteristics of the model. This verification process additionally provides high-level test cases that are used to uncover errors in design or implementation and to test the usability of the design.

We present a verification methodology that allows evaluating the relevant properties of a neuron circuit already during the design phase. To this end we have developed a simulation setup that allows the detailed investigation of a complete neuron circuit. In the simulations individual components such as transistors are parameterized using detailed physical characteristics, including mismatch and process variations. The simulation setup is accompanied by a series of biologically-inspired single neuron benchmarks (Naud et al., 2008; Jolivet et al., 2008), which are designed to compare neuron models to each other and in particular to check them against biological data. Our most recent

circuit designs have been tested and enhanced using our method and are expected to show clear improvements over previous chip generations.

REFERENCES

- Brette, R., and Gerstner, W. (2005). Adaptive exponential integrate-and-fire model as an effective description of neuronal activity. *J. Neurophysiol.* 94, 3637–3642. doi: 10.1152/jn.00686.2005 PMID:16014787
- Brette, R., Rudolph, M., Carnevale, T., Hines, M., Beeman, D., Bower, J. M., et al. (2007). Simulation of networks of spiking neurons: a review of tools and strategies. *J. Comput. Neurosci.* 23, 349–398. doi: 10.1007/s10827-007-0038-6 PMID:17629781
- Indiveri, G., Linares-Barranco, B., Hamilton, T. J., Van Schaik, A., Etienne-Cummings, R., Delbruck, T., et al. (2011). Neuromorphic silicon neuron circuits. *Front. Neurosci.* 5:73. doi: 10.3389/fnins.2011.00073 PMID:21747754
- Jolivet, R., Schürmann, F., Berger, T. K., Naud, R., Gerstner, W., and Roth, A. (2008). The quantitative single-neuron modeling competition. *Biol. Cybern.* 99, 417–426. doi: 10.1007/s00422-008-0261-x PMID:19011928
- Mead, C. (1990). Neuromorphic electronic systems. *Proc. IEEE* 78, 1629–1636. doi: 10.1109/5.58356 PMID:NOPMID
- Naud, R., Marcille, N., Clopath, C., and Gerstner, W. (2008). Firing patterns in the adaptive exponential integrate-and-fire model. *Biol. Cybern.* 99, 335–347. doi: 10.1007/s00422-008-0264-7 PMID:19011922
- Schemmel, J., Brüderle, D., Grübl, A., Hock, M., Meier, K., and Millner, S. (2010). “A wafer-scale neuromorphic hardware system for large-scale neural modeling,” in *Proceedings of 2010 IEEE International Symposium on Circuits and Systems (IEEE)*, 1947–1950, Paris, France.

Forging an Ensemble of Neuromorphic Chips into a Large-Scale Neural Network Emulation Platform

Christian Mauch¹, Eric Müller¹, Sebastian Schmitt¹, Mitja Kleider¹, Christoph Koke¹, Vitali Karasenko¹, Johann Klähn¹, Johannes Partzsch², Stephan Hartmann², Stefan Philipp¹, Maurice Güttler¹, Dan Husmann De Oliveira¹, Andreas Grübl¹, Johannes Schemmel¹, Karlheinz Meier¹

¹*Kirchhoff Institute for Physics, Heidelberg, Germany*

²*Highly-Parallel VLSI-Systems and Neuromorphic Circuits, Technische Universität Dresden, Dresden, Germany*

christian.mauch@kip.uni-heidelberg.de

Neuromorphic devices emulate various aspects of biological neural networks in micro-electronic circuits, such as connectivity structure (Furber et al., 2012) or continuous time dynamics (Schemmel et al., 2010). Several generations of such single-chip devices have been developed in Heidelberg (Schemmel et al., 2010; Pfeil et al., 2013; Friedmann et al., 2013; Aamir et al., 2016). To facilitate scaling towards large networks, many of these devices can be integrated into a so-called wafer-scale platform such as the BrainScaleS system (Schemmel et al., 2010).

Shaping this device into an easily usable emulation platform is significantly different from interfacing a classical supercomputer architecture. Several software abstraction layers provide a high-level view of the hardware to the user, providing back-end-specific functions such as fixed-pattern noise reduction (neuron and synapse calibration) or resource allocation (mapping) (Petrovici et al., 2014).

To make efficient use of the accelerated dynamics inherent to our neuromorphic back-end, particular attention needs to be paid to the communication infrastructure, both on-wafer (chip-to-chip) and off-wafer (wafer-to-user) (Brüderle et al., 2011). In order to minimize the ratio between configuration time and execution time, the communication interface needs to have a high throughput. At the same time, a low latency is also required for enabling closed-loop interactions with simulated or physical environments.

We present an overview of the BrainScaleS software framework with particular emphasis on the communication infrastructure. Our most recent benchmark results demonstrate how this interface can achieve communication speeds of up to 2.8 GB/s, which is the equivalent of simultaneously reading out the spike trains from 72,000 neurons firing at an average of 1 Hz (bio time) on the wafer.

REFERENCES

- Aamir, S., Müller, P., Hartel, A., Schemmel, J., and Meier, K. (2016). "A highly tunable 65-nm CMOS LIF neuron for a large scale neuromorphic system," in *Proceedings of the Third International Conference on Genetic Algorithm Medings of IEEE European SolidState Circuits Conference (ESSCIRC)*, Lausanne, Switzerland.
- Brüderle, D., Petrovici, M., Vogginger, B., Ehrlich, M., Pfeil, T., Millner, S., et al. (2011). A comprehensive workflow for general-purpose neural modeling with highly configurable neuromorphic hardware systems. *Biol. Cybern.* 104, 263–296. doi: 10.1007/s00422-011-0435-9 PMID:21618053
- Friedmann, S., Frémaux, N., Schemmel, J., Gerstner, W., and Meier, K. (2013). Reward-based learning under hardware constraints – using a RISC processor in a neuromorphic substrate. *Front. Neurosci.* 7:160. doi: 10.3389/fnins.2013.00160 PMID:NOPMID
- Furber, S., Lester, D., Plana, L., Garside, J., Painkras, E., Temple, S., et al. (2012). Overview of the SpiNNaker system architecture. *IEEE Trans. Comput.* 99, 2454–2467. doi: NODOI PMID:NOPMID
- Petrovici, M., Vogginger, B., Müller, P., Breitwieser, O., Lundqvist, M., Muller, L., et al. (2014). Characterization and compensation of network-level anomalies in mixed-signal neuromorphic modeling platforms. *PLoS ONE* 9:e108590. doi: 10.1371/journal.pone.0108590 PMID:25303102
- Pfeil, T., Grübl, A., Jeltsch, S., Müller, E., Müller, P., Petrovici, M., et al. (2013). Six networks on a universal neuromorphic computing substrate. *Front. Neurosci.* 7:11. doi: 10.3389/fnins.2013.00011 PMID:23423583
- Schemmel, J., Brüderle, D., Grübl, A., Hock, M., Meier, K., and Millner, S. (2010). "A wafer-scale neuromorphic hardware system for large-scale neural modeling," in *Proceedings of the 2010 IEEE International Symposium on Circuits and Systems (ISCAS)*, 1947–1950, Paris, France.

Bayesian Computing with Spikes

Andreas Baumbach, Mihai Petrovici, Luziwei Leng, Oliver Breitwieser, David Stöckel, Ilja Bytschok, Johannes Schemmel, Karlheinz Meier

Heidelberg University, Heidelberg, Germany

andreas.baumbach@kip.uni-heidelberg.de

In view of mounting evidence that brains solve various cognitive tasks by performing Bayesian inference (Körding and Wolpert, 2004; Berkes et al., 2011), theoretical models have been developed to explain how such computations can be implemented in networks of spiking neurons (Buesing et al., 2011; Pecevski et al., 2011; Petrovici et al., 2013; Probst et al., 2015). In the neural sampling framework (Buesing et al., 2011; Pecevski et al., 2011), the activity of spiking neurons is interpreted as sampling from an underlying probability distribution that is shaped by the network's parameters. Operating under this premise, the models developed in (Pecevski et al., 2011; Petrovici et al., 2013; Probst et al., 2015) have shown how biological neural networks can make use of the high-conductance state to achieve equivalent computational capabilities. This allows, for example, the straightforward reproduction of well-known stochastic behavioral phenomena such as perceptual ambiguity with biologically plausible spiking neural networks (Petrovici et al., 2013). Here, we briefly review several applications of such spiking sampling networks, including a somewhat exotic discussion of their connection to statistical physics.

The computational abilities of these networks can be directly put to use in classical machine learning tasks such as handwritten digit recognition. In addition to achieving a similar performance when compared to traditional approaches such as Gibbs sampling, our spiking networks can profit from biology-inspired features such as short term plasticity to simultaneously provide good generative capabilities, which are otherwise difficult to achieve (Leng et al., 2015). Owing to the fact that our networks employ LIF neurons—a de facto standard model for neuromorphic devices—our networks can directly benefit from the advantages offered by these substrates. In particular, the emulation on an accelerated mixed-signal chip (Pfeil et al., 2012) has recently been demonstrated (Petrovici et al., 2015), which paves the way for larger-scale, accelerated applications for demanding computational tasks (Schemmel et al., 2008; Leng et al., 2015).

The approximate equivalence of the dynamics of LIF networks to the so-called Glauber dynamics in microscopic models of magnetic materials (Petrovici, 2016) raises the question whether macroscopic effects, such as the relationship between magnetization, external field and temperature, are also conserved. Preliminary experiments suggest consistent behavior in the perturbative limit (large temperatures, weak external excitation), but deviant behavior around critical points.

REFERENCES

- Berkes, P., Orbán, G., Lengyel, M., and Fiser, J. (2011). Spontaneous cortical activity reveals hallmarks of an optimal internal model of the environment. *Science* 331, 83–87. doi: 10.1126/science.1195870 PMID:21212356
- Buesing, L., Bill, J., Nessler, B., and Maass, W. (2011). Neural dynamics as sampling: a model for stochastic computation in recurrent networks of spiking neurons. *PLoS Comput. Biol.* 7:e1002211. doi: 10.1371/journal.pcbi.1002211 PMID:22096452
- Körding, K. P., and Wolpert, D. M. (2004). Bayesian integration in sensorimotor learning. *Nature* 427, 244–247. doi: 10.1038/nature02169 PMID:14724638
- Leng, L., Petrovici, M. A., Martel, R., Bytschok, I., Breitwieser, O., Bill, J., et al. (2015). “Spiking neural networks as superior generative and discriminative models,” in *In Cosyne Abstracts 2016* (Salt Lake City, USA).
- Pecevski, D., Buesing, L., and Maass, W. (2011). Probabilistic inference in general graphical models through sampling in stochastic networks of spiking neurons. *PLoS Comput. Biol.* 7:e1002294. doi: 10.1371/journal.pcbi.1002294 PMID:22219717
- Petrovici, M. A. (2016). “Implement DC generator devices, which were provided by the platform in the software implementation, and integrate and fire neuron dynamics,” in *Form Versus Function: Theory and Models for Neuronal Substrates* (Springer Thesis), Springer, NY, USA, doi: 10.1007/978-3-319-39552-4.
- Petrovici, M. A., Bill, J., Bytschok, I., Schemmel, J., and Meier, K. (2013). *Stochastic inference with deterministic spiking neurons*. arXiv preprint arXiv:1311.3211.
- Petrovici, M. A., Stöckel, D., Bytschok, I., Bill, J., Pfeil, T., Schemmel, J., et al. (2015). “Fast sampling with neuromorphic hardware,” in *Advances in Neural Information Processing Systems (NIPS)*, Montreal, Canada, 28.
- Pfeil, T., Grübl, A., Jeltsch, S., Müller, E., Müller, P., Petrovici, M. A., et al. (2012). Six networks on a universal neuromorphic computing substrate. *Front. Neurosci.* 7:11–11. doi: 10.3389/fnins.2013.00011 PMID:NOPMID
- Probst, D., Petrovici, M. A., Bytschok, I., Bill, J., Pecevski, D., Schemmel, J., et al. (2015). Probabilistic inference in discrete spaces can be implemented into networks of LIF neurons. *Front. Comput. Neurosci.* 9:13. doi: 10.3389/fncom.2015.00013 PMID:25729361
- Schemmel, J., Fieres, J., and Meier, K. (2008). “Wafer-scale integration of analog neural networks,” in *2008 IEEE International Joint Conference on Neural Networks (IEEE World Congress on Computational Intelligence)* (IEEE), Hong Kong, China, 431–438.

Efficiently Navigating through Structural Connectivity Parameter Spaces for Multiscale Whole Brain Simulations

Sandra Diaz-Pier¹, Christian Nowke², Alexander Peyser¹

¹Forschungszentrum Juelich, Juelich, Germany

²Visual Computing Institute RWTH Aachen University, Aachen, Germany

s.diaz@fz-juelich.de

Introduction: Simulations of the whole human brain have been suggested as a way to better understand the relationship between structural and functional connectivity (Deco et al., 2014; Schmidt et al., 2015; Sanz-Leon et al., 2015). These simulations are complex and computationally challenging due to the amount of active elements to be simulated in a human brain. Depending on the scale, these active elements can be: molecules, channels, compartments, neurons, synapses, populations, microcircuits, brain regions, etc. On top of this, the structural experimental data we have at hand today is not precise or complete enough to allow a detailed simulation at neuron level. Some strategies to overcome these problems have been suggested in the past. On one side, optimized models which simulate regions instead of neurons can be used to enhance the performance of the simulations, but loose insight on the activity at neuron level (Wong and Wang, 2006; Deco et al., 2013). On the other side, large scale simulations at neuron level are still not feasible for the whole brain and for prolonged times (Kunkel et al., 2014). However they can provide more accurate information of the activity patterns among neurons. Due to the large number of free parameters in these simulations, an efficient way to explore the possible connectivity configurations is required. In this work we show different strategies to navigate through structural connectivity parameter spaces in order to support the study of the relationships between structure and function at different scales. We tackle the exploration both at neuron level and at population level.

Methods: We work with a multiscale setup which involves neuron level simulations running on NEST 2.10.0 (Bos et al., 2015) connected to a dynamic mean field model (DMFM) simulation of the whole brain. This multiscale approach allows the analysis of the impact of different connectivity parameters on simulated functional signals which can be compared to fMRI data. Our work involves two levels of exploration: first, we use an interactive visualization tool to asses and steer the automatic generation of connectivity at neuron level. We investigate the effect of iteratively propagating the resulting connectivity data for some fixed global parameters to a higher scale by using it as input for the mean field model simulations. Second, we describe the implementation of a series of adaptive approaches designed to guide the navigation through the global

connectivity parameter space for the mean field model simulations. We analyze the efficiency and performance of the optimization using different algorithms. For this, we perform large parameter sweeps and maximize a fitness metric.

Results: We show the results of using our interactive visualization tool to generate neuron level connectivity data and reduce the times to obtain suitable local connectivity which can be propagated to the larger scale model. We also show a comparison between the adaptive algorithms and a brute force approach to optimize the selected fitness metrics.

Discussions: Efficient techniques to explore large parameter spaces such, e.g., the connectivity in whole brain simulations are of great importance to make optimal usage of computational resources and enhance the understanding of the relationships between structure and function of the system. In this work we show interactive visualization and automatic tools to aid the navigation through these complex parameter spaces.

Acknowledgments: The authors would like to acknowledge the support by the Excellence Initiative of the German federal and state governments, the Jülich Aachen Research Alliance—High-Performance Computing and the Collaborative Research in Computational Neuroscience (CRCNS) grant. In addition, this project has received funding from the European Union's Horizon 2020 research and innovation programme under grant agreement No 720270 (HBP SGA1).

REFERENCES

- Bos, H., Morrison, A., Peyser, A., Hahne, J., Helias, M., Kunkel, S., et al. (2015). *NEST 2.10.0*. Zenodo. <http://doi.org/10.5281/zenodo.44222>
- Deco, G., Ponce-Alvarez, A., Hagmann, P., Romani, G. L., Mantini, D., and Corbetta, M. (2014). How local excitation–inhibition ratio impacts the whole brain dynamics. *J. Neurosci.* 34, 7886–7898. doi: 10.1523/JNEUROSCI.5068-13.2014 PMID:NOPMID
- Deco, G., Ponce-Alvarez, A., Mantini, D., Romani, G. L., Hagmann, P., and Corbetta, M. (2013). Resting-state functional connectivity emerges from structurally and dynamically shaped slow linear fluctuations. *J. Neurosci.* 33, 11239–11252. doi: 10.1523/JNEUROSCI.1091-13.2013 PMID:23825427
- Kunkel, S., Schmidt, M., Eppler, J. M., Plesser, H. E., Masumoto, G., Igarashi, J., et al. (2014). Spiking network simulation code for petascale computers. *Front. Neuroinform.* 8:78. doi: 10.3389/fninf.2014.00078 PMID:NOPMID
- Sanz-Leon, P., Knock, S. A., Spiegler, A., and Jirsa, V. K. (2015). Mathematical framework for large-scale brain network modeling in the virtual brain. *Neuroimage* 111, 385–430. doi: 10.1016/j.neuroimage.2015.01.002 PMID:25592995
- Schmidt, M., Bakker, R., Diesmann, M., and van Albada, S. J. (2015). *Construction of a multi-scale spiking model of macaque visual cortex*. arXiv preprint arXiv:1511.09364.
- Wong, K.-F., and Wang, X.-J. (2006). A recurrent network mechanism of time integration in perceptual decisions. *J. Neurosci.* 26, 1314–1328. doi: 10.1523/JNEUROSCI.3733-05.2006 PMID:16436619

The Dynamical Response Properties of Cortical Neurons in Silico

Christophe Verbist, Michele Giugliano

Universiteit Antwerpen, Wilrijk, Belgium

christophe.verbist@uantwerpen.be

Earlier theoretical studies on simplified neuronal models suggested that the joint firing activity of ensembles of cortical neurons may relay downstream rapidly varying components of their synaptic inputs, with no attenuation. Information transmission in networks of weakly-coupled model neurons may in fact overcome the limits imposed by the spike refractoriness and the slow integration of individual cells, effectively extending their input-output bandwidth when operating as ensembles of cells. This has been first confirmed experimentally only recently but in a very limited subset of cortical neuronal types both in rodents and in human cortical cells. However, to a big surprise, neurons were found to track and relay inputs varying in time much faster (beyond 200 cycles/s) than explained by their ensemble mean firing rates (~10 spikes/s).

Such an unexpectedly broad bandwidth of neuronal dynamics has been theoretically linked to the onset rapidity of action potentials (AP) and to the features of their initiation. However competing theories explain AP fast onset by resistive impedance match between the axon and the soma, or by back propagation of the AP along the axon back to the soma, or finally by cooperative operation of sodium voltage-gated ion channels. In these perspectives, the availability of the model data set released by the Blue Brain Project is of great relevance and it offers for the first time the possibility to investigate *in silico* the input-output neuronal bandwidth and link it to the underlying biophysical properties of the model.

In this poster contribution, I will report about our recent progress in the *in silico* exploration of input-output transfer properties of morphologically detailed multi compartmental models.

Developing Software Tools for Parameter Fitting and Validation of Neuronal Models

Sára Sáray^{1,2}, **Péter Friedrich**^{1,2}, **Christian A. Rössert**³,
Márk P. Török^{1,2}, **Bence Bagi**^{1,2}, **Eilif Muller**³, **Tamás F. Freund**^{1,2},
Szabolcs Káli^{1,2}

¹Institute Of Experimental Medicine Of The Hungarian Academy Of Sciences, Budapest, Hungary

²Faculty of Information Technology and Bionics, Pázmány Péter Catholic University, Budapest, Hungary

³Blue Brain Project, École Polytechnique Fédérale De Lausanne, Geneva, Switzerland

saray.sara@koki.mta.hu

Anatomically and biophysically detailed conductance-based neuronal models can be useful tools in understanding the behavior and function of neurons. Although there are more and more experimental data available that constrain the many parameters of multi-compartmental models, there are generally several remaining parameters whose values have not been experimentally determined. The values of these unknown parameters are often set using manual, *ad hoc* procedures with the aim of reproducing the behavior of the cell in one or a few specific paradigms. However, the performance of such a model outside the original context typically remains unexplored, and systematic comparisons of different models are difficult and thus rare, limiting the reusability of these models. Recently, several solutions have been developed for the systematic optimization of neuronal parameters based on the quantitative evaluation of model performance, but customizing these tools to individual needs can be a substantial challenge. To overcome these problems we are developing software tools for automatic model validation, and for the automated, intuitive fitting of unknown model parameters.

For automatic and quantitative model validation we are developing a python test suite, called Hippounit (available at: <https://github.com/sasaray/neuronunit>), which is based on NeuronUnit, a SciUnit repository for testing neuronal models (Gerkin and Omar, 2014). Hippounit automatically performs simulations that mimic experimental protocols on detailed hippocampal CA1 pyramidal cell models built in the NEURON simulator. To test a model the user needs to create a python class for the model, including its intrinsic mechanisms, and receptor models can also be added for synaptic stimulation of the model cell. The tests of Hippounit use feature-based error functions to compare the output of the model to the results of experimental measurements on several different cells. Errors are typically measured as the difference from the mean of the experimental data, measured in the units of the experimental standard deviation (Druckmann et al. 2007). The final output of a test is an error score that is the sum of the errors of all the features tested by the given test, and a number of figures which illustrate the

model's behavior and the extracted feature values. Beside Hippounit's own functions, the Electrophys Feature Extraction Library (eFEL) of the Blue Brain Project is used for feature extraction. So far there are three different tests implemented in Hippounit. The Somatic Feature Test uses the somatic spiking features of eFEL for parameter fitting; target values for these features were extracted from recordings in rat CA1 pyramidal neurons in the laboratory of Alex Thomson. The Depolarization Block Test aims to determine whether the model enters depolarization block in response to prolonged, large-amplitude current injections to the soma, using experimental data from Bianchi et al. (2012). Finally, the Oblique Integration Test probes the integration properties of oblique dendrites according to the experimental results of Losonczy and Magee (2006). Using Hippounit, we have compared the behavior of several CA1 pyramidal cell models in these domains, and found that all of these models perform well in some domains (typically on features they were built to capture) but badly in others.

We also present the new release of the Optimizer software tool (available at: <https://github.com/KaliLab/optimizer>) and the improvements made in it since its initial release [the version described in Friedrich et al. (2014)]. Optimizer is a general-purpose tool for fitting the parameters of neuronal models. Optimizer offers a graphical user interface (GUI) for non-expert users to do optimization in several commonly used scenarios. It implements several different optimization algorithms and a number of fitness functions which can also be combined. Optimizer has a modular structure that makes it easy to extend it by adding new optimization algorithms and/or fitness functions. Recently added optimization methods include random search, and the differential evolution and particle swarm algorithms from the inspyred package. The software can now handle a combination of voltage traces and corresponding explicit spike times; this is important for the correct optimization of integrate-and-fire models. Several bugs have been fixed; most importantly, when selecting parameters for optimization in the GUI, only actual parameters (and not state variables) of Neuron models are displayed. In addition, the software now can handle abstract data that are already extracted from traces. This capability has been used to fit the behavior of a CA1 pyramidal cell model to the somatic spiking features described above. The performance of several optimization algorithms in Optimizer has been systematically compared on some benchmark problems, including the optimization of both conductance-based and integrate-and-fire models. We concluded that the classic evolutionary algorithm and the particle swarm algorithm included in Optimizer were effective in solving all types of problems, while the simulated annealing and the random search algorithms performed poorly in most of the cases.

Automated tools for model fitting and validation should enable a more principled and systematic approach to model building and validation. Together with efforts on other important components such as standardized model representation, such tools should

make possible the reproducible construction, validation, and comparison of detailed neural models, and encourage collaborative research in computational neuroscience.

REFERENCES

- Bianchi, D., Marasco, A., Limongiello, A., Marchetti, C., Marie, H., Tirozzi, B., et al. (2012). On the mechanisms underlying the depolarization block in the spiking dynamics of CA1 pyramidal neurons. *J. Comput. Neurosci.* 33, 207–225. doi: 10.1007/s10827-012-0383-y PMID:NOPMID
- Druckmann, S., Banitt, Y., Gidon, A., Schürmann, F., Markram, H., and Segev, I. (2007). A novel multiple objective optimization framework for constraining conductance-based neuron models by experimental data. *Front. Neurosci.* 1:7–18. doi: 10.3389/neuro.01.1.1.001.2007 PMID:NOPMID
- Friedrich, P., Vella, M., Gulyás, A. I., Freund, T. F., and Káli, S. (2014). A flexible, interactive software tool for fitting the parameters of neuronal models. *Front. Neuroinform.* 8:63. doi: 10.3389/fninf.2014.00063 PMID:25071540
- Geit, W. V., Moor, R., Ranjan, R., Riquelme, L., and Rössert, C. (2016). *Electrophys Feature Extraction Library v2.10.72*. Available at: <https://github.com/BlueBrain/eFEL>.
- Gerkin, R. C., and Omar, C. (2013). NeuroUnit: validation tests for neuroscience models. *Front. Neuroinform.* doi: 10.3389/conf.fninf.2013.09.00013
- Losonczy, A., and Magee, J. C. (2006). Integrative properties of radial oblique dendrites in hippocampal CA1 pyramidal neurons. *Neuron* 50, 291–307. doi: 10.1016/j.neuron.2006.03.016 PMID:16630839

Consciousness and Cortical Connectivity in Subanaesthetic Ketamine Measured by TMS and EEG

Nadine Farnes¹, Bjørn E. Juel², André S. Nilsen², Anikó Kusztor², Johan F. Storm², Luis G. Romundstad³, Pål G. Larsson³, Morten Engstrøm¹, Johan F. Storm²

¹Norwegian University of Science and Technology, Trondheim, Norway

²University Of Oslo, Oslo, Norway

³Oslo University Hospital, Oslo, Norway

nadine.farnes@gmail.com

Recent interest in the neuroscientific field of consciousness has created a surge in research trying to understand the inner workings of the mind and to objectively measure conscious states. However, little is known about the psychedelic state of consciousness produced by psychoactive drugs. The advent of methods which can more accurately determine the state of consciousness in various healthy and unhealthy populations, may allow for investigation into the psychedelic state.

Levels of consciousness have been differentiated by estimating the complexity of EEG signals after TMS stimulation with a metric called the perturbational complexity index (PCI) (Casali et al., 2013). The PCI values range from 0 to 1 and a high PCI score (closer to 1) will occur if the TMS perturbation causes EEG changes that spread widely to many unstimulated brain areas, and shows a complex pattern over time. This signifies a highly integrated and differentiated, complex network state which correlates with a high state of awareness. On the other hand, a low PCI score (closer to 0) will result from a reduction in either integration or differentiation or both, and correlates with an unconscious or reduced conscious state.

The PCI seems to give a clear indication of the consciousness level of different subject and patient groups. Previous research has focused on the lower ends of the scale, differentiating coma, vegetative state, sleep and awake state from each other. However, there is little research on states which may produce a higher conscious experience. The highest measured PCI is for awake participants and lies between 0.44 and 0.67 (Casali et al., 2013). This leaves the upper range of the index unmeasured. The question then becomes: is it conceivable that there may exist states with higher conscious experience (compared to the normal awake state) giving a measurably higher PCI value? In other words, may the brain attain states of consciousness with a higher degree of integration

and differentiation than the normal, fully alert, awake state, such that the PCI score will exceed that of the normal awake state?

Compared to the awake state, anaesthetic doses of ketamine produce a similar, high PCI score of between 0.35 and 0.55 (Sarasso et al., 2015). Anaesthetic doses of ketamine produces unresponsiveness as well as vivid dreams and hallucinations (Collier, 1972). Subanaesthetic doses of ketamine maintains an awake state with the addition of psychotomimetic effects (i.e., resembling psychosis), including disturbances in thinking and perception (Rowland, 2005). A higher PCI score might thus be attained if awake participants are given subanaesthetic doses of ketamine that give particularly vivid experiences. This is based on the assumption that the wake state combined with the perceptual change reflect a state of higher integration and differentiation in the brain's networks.

Methods: We will use the combined non-invasive techniques of transcranial magnetic stimulation (TMS) and high-density electroencephalography (hdEEG) to stimulate the cortex and measure the response. Healthy participants will be given single TMS pulses before and during administration of low dose ketamine. This allows PCI to be measured in both the awake and psychedelic state. Furthermore, continuous hdEEG recording permits the measurement of brain connectivity during each state and in the transition between the states. Psychoactive effects of ketamine will also be assessed by psychological tests.

Aims: The main aim of the study is to investigate the effects of subanaesthetic doses of ketamine on consciousness using the PCI obtained by TMS and EEG. Additional aims are to further test the validity and usefulness of PCI as an objective method for assessing the state of consciousness, and to increase our knowledge of the methods for subsequent anaesthesia trials. Finally, spontaneous hdEEG recordings can be used to measure the changes in cortical functional and effective connectivity patterns induced by subanaesthetic ketamine, which can also be compared to the measured PCI.

Predictions: We wish to test the possibility that subanaesthetic doses of ketamine may give a higher PCI value than in the normal awake state. This may happen, if ketamine is able to increase neural entropy (differentiation), producing a psychedelic experience, while at the same time maintaining integration (Gallimore, 2015).

Support: Supported by the Norwegian Research Council (NRC), and the "Conscious Brain" project (coordinator J.F. Storm) within the Human Brain Project (HBP, SP3.4).

REFERENCES

- Casali, A. G., Gosseries, O., Rosanova, M., Boly, M., Sarasso, S., Casali, K. R., et al. (2013). A theoretically based index of consciousness independent of sensory processing and behavior. *Sci. Transl. Med.* 5, 198ra105. doi: 10.1126/scitranslmed.3006294 PMID:23946194
- Collier, B. B. (1972). Ketamine and the conscious mind. *Anaesthesia* 27, 120–134. doi: 10.1111/j.1365-2044.1972.tb08186.x PMID:NOPMID
- Gallimore, A. R. (2015). Restructuring consciousness—the psychedelic state in light of integrated information theory. *Front. Hum. Neurosci.* 9:346. doi: 10.3389/fnhum.2015.00346 PMID:NOPMID
- Rowland, L. M. (2005). Subanesthetic ketamine: how it alters physiology and behavior in humans. *Aviat. Space Environ. Med.* 76(7 Suppl), C52–C58 PMID:16018330
- Sarasso, S., Boly, M., Napolitani, M., Gosseries, O., Charland-Verville, V., Casarotto, S., et al. (2015). Consciousness and complexity during unresponsiveness induced by propofol, xenon, and ketamine. *Curr. Biol.* 25, 3099–3105. doi: 10.1016/j.cub.2015.10.014 PMID:26752078

Evidence for a Novel Connectivity Gradient of Executive Function in the Mammalian Brain

Stacey A. Bedwell, Chris J. Tinsley

Nottingham Trent University, Nottingham, United Kingdom
stacey.bedwell@ntu.ac.uk

The mammalian prefrontal cortex is associated with complex, high-order processes such as decision making, forward planning, goal directed behavior, executive function and emotional control (Miller and Cohen, 2001; Alvarez and Emory, 2006; Vertes, 2006).

The organisation of connections is typically ordered throughout the cerebral cortex. Studies indicate that this is the case in Prefrontal Cortex (PFC). In a traditional model of hierarchical organisation, PFC is positioned at the top of a processing hierarchy (Alexander et al., 1986; Fuster, 2001; Botvinick, 2008). In a hierarchical model, connections would travel from primary sensory cortex, followed by secondary sensory cortex and association areas, then reaching the top of the processing hierarchy, e.g., PFC. This is followed by return connections travelling to secondary motor cortex followed by primary motor cortex (e.g., S1 → S2 → Association areas → PFC → M2 → M1), it is understood that reciprocal connections exist between source and target regions at each level of the hierarchy. Based on this understanding of cortical connectivity, it is thought that all cortical networks must contain a significant level of reciprocity in order to function, making it a fundamental structural component.

We injected the neuroanatomical tracers Fluoro-Gold and Fluoro-Ruby into sub-regions of PFC in the rat. Tracer injections were made into 3 coronal levels within the PFC (anterior, central and posterior), separated by 1mm. We found that both tracers produced prominent labelling in temporal and sensory-motor cortex. Fluoro-Gold produced retrograde labelling and Fluoro-Ruby produced largely anterograde labelling. Statistical analysis of the 3-dimensional location of these connections within temporal and sensory-motor cortex revealed consistent ordering ($p < 0.001$). At the anterior and central coronal levels, injections (i.e., equivalently located injections employing the same tracer) produced a similar pattern of ordering, this was particularly prominent within temporal cortex. However, at the posterior coronal level this pattern of ordering was reversed in temporal cortex and was also changed in sensory-motor cortex. This provides evidence for differential ordering of connections in the anterior-posterior axis of PFC, indicating a possible connectivity gradient in terms of functional complexity.

Such a functional connectivity gradient is supported by imaging studies (Taren et al., 2011) and suggestions of a gradient of abstraction (Christoff et al., 2009) in humans.

These findings imply that, in terms of decision making for instance, that decisions become more complex towards anterior PFC, or that more complicated forward planning is localised to more anterior regions of PFC. When considered alongside observations of functional gradients, our observed connectivity gradient specifically suggests that more abstract processes, e.g., highly complex abstract decisions or plans, require connections to be non-reciprocal and involve more complex circuitry.

REFERENCES

- Alexander, G. E., DeLong, M. R., and Strick, P. (1986). Parallel organization of functionally segregated circuits linking basal ganglia and cortex. *Ann. Rev. Neurosci.* 9, 357–381. doi: 10.1146/annurev.ne.09.030186.002041 PMID:NOPMID
- Alvarez, J. A., and Emory, E. (2006). Executive function and the frontal lobes: a metaanalytic review. *Neuropsychol. Rev.* 16, 17–42. doi: 10.1007/s11065-006-9002-x PMID:NOPMID
- Botvinick, M. M. (2008). Hierarchical models of behavior and prefrontal function. *Trends Cog. Sci.* 12, 201–208. doi: 10.1016/j.tics.2008.02.009 PMID:NOPMID
- Christoff, K., Keramatian, K., Gordon, A. M., Smith, R., and Madler, B. (2009). Prefrontal organization of cognitive control according to levels of abstraction. *Brain Res.* 1286, 94–105. doi: 10.1016/j.brainres.2009.05.096 PMID:19505444
- Fuster, J. M. (2001). The prefrontal cortex – an update: time is of the essence. *Neuron* 30, 319–333. doi: 10.1016/S0896-6273(01)00285-9 PMID:NOPMID
- Miller, E. K., and Cohen, J. D. (2001). An integrative theory of prefrontal cortex function. *Annu. Rev. Neurosci.* 24, 167–202. doi: 10.1146/annurev.neuro.24.1.167 PMID:11283309
- Taren, A. A., Venkatraman, V., and Huettel, S. A. (2011). A parallel functional topography between medial and lateral prefrontal cortex: Evidence and implications for cognitive control. *J. Neurosci.* 31, 5026–5031. doi: 10.1523/JNEUROSCI.5762-10.2011 PMID:21451040
- Vertes, R. P. (2006). Interactions among the medial prefrontal cortex, hippocampus and midline thalamus in emotional and cognitive processing in the rat. *Neuroscience* 142, 1–20. doi: 10.1016/j.neuroscience.2006.06.027 PMID:16887277

Markers of Consciousness before, during, and after Anesthesia; A TMS-EEG Study

André Sevenius Nilsen¹, Bjørn E. Juel¹, Anikò Kusztor², Nadine R. S. F. Farnes³, Luis Romundstad⁴, Pål Gunnar Larsson⁵, Johan F. Storm⁶

¹*Department of Molecular Medicine, Section for Physiology, University of Oslo, Oslo, Norway*

²*Department of Psychology, Institute of Social Sciences, University of Oslo, Oslo, Norway*

³*Department of Neuroscience, Norwegian University of Science and Technology, Oslo, Norway*

⁴*Department of Anesthesiology, Oslo University Hospital, Oslo, Norway,*

⁵*Department of Neurosurgery, Oslo University Hospital, Oslo, Norway*

⁶*Section for Physiology, Department of Molecular Medicine, University of Oslo, Oslo, Norway*

sevenius.nilsen@gmail.com

Introduction: Developing a valid and reliable measure of varied conscious states is not only important from a basic research perspective, but also in a clinical setting. It is of crucial importance to differentiate comatose, vegetative state (VS), minimally conscious, and locked in states in terms of conscious experience. In addition, accidental awareness during general anesthesia (Sebel et al., 2004), can cause severe pain, anxiety, and potential post-traumatic stress disorder (Osterman et al., 2001, Prendergast and Cullen-Drill, 2012).

For the clinic there exist multiple measures for assessing and monitoring conscious states, such as the bispectral index, EEG entropy, auditory evoked potentials, and several others. However, most of these measures are unreliable in combination with certain anesthetic agents, subjective factors, or external circumstances such as electrical noise (Webb et al., 1993, Bowdle, 2006, Musizza and Ribaric, 2010). Clinical diagnosis of different disorders of consciousness is also limited in terms of accuracy, with up to 41% misdiagnosis (Schnakers et al., 2009, Gawryluk et al., 2010).

Giulio Tononi has proposed a theory of consciousness based on a systems ability to integrate information (Integrated Information Theory of Consciousness; IIT, Oizumi et al., 2014). The theory offers straight forward predictions regarding the necessary structure and behavior of physical systems, for them to have conscious experience. However, calculation of the theory's proposed measure (PHI) is limited both by imaging technology and theoretical computational limits for any reasonably complex systems, thus necessitating surrogate measures.

The Perturbational Complexity Index (PCI; Casali et al., 2013) is a proposed surrogate measure of IIT's PHI. PCI is calculated from the information differentiation and integration of brain activity after perturbation by transcranial magnetic stimulation

(TMS), as measured by Electroencephalography (EEG). Earlier studies employing PCI have shown a clear and most importantly individually accurate ability to distinguish between assumed conscious states (awake, dream sleep, ketamine anesthesia), assumed unconscious states (deep sleep, coma, VS, anesthesia) and in between for assumed partially conscious states (Casali et al., 2013, Sarasso et al., 2014, Casarotto et al., 2016). However, while the PCI measure is minimally invasive, robust, and flexible, it is still in its infancy and need external validation and comparison to existing and even less invasive methods.

Aims: Our aim is to replicate and extend earlier results involving PCI and compare the measure's specificity and sensitivity in classification of conscious and unconscious states with other proposed and deployed measures of consciousness. More specifically, we aim to classify the effects of anesthetic agents propofol, ketamine, tiopental, midazolam, on human consciousness by employing the PCI, the Directed Transfer Function, and other potential measures, in healthy volunteers.

Methods: We will employ high density EEG (64 channels, BrainProducts) and TMS (BrainProducts) using a figure 8 coil in combination with motion tracking for cortical stimulation localization. 30 healthy participants will be recruited following ethical and safety guidelines (for both TMS, anesthesia, and MRI). Measures include 2 min of eyes-open, and eyes-closed passive EEG recording; 10 min of TMS to right lateral superior prefrontal cortex with 300 trials of single-pulses set at 120% intensity of the intensity of 0.5 probability of resting Motor Evoked Potential (MEP) as measured by Electromyography (EMG); administration of anesthetics until behavioral unresponsiveness with concurrent passive EEG measurement; 10 min of TMS; and a gradual ascent from anesthesia to wakefulness with concurrent EEG.

The results will be preprocessed according to standards for the respective methods employed for analysis, but mainly consisting of notch-filter (to exclude line noise), bandpass filter (0.5–80 Hz), baseline centering, pre-whitening, interpolation of TMS artefact (if applicable), ICA based noise rejection, and trial/channel inspection and rejection.

Predictions: We predict to observe similar results compared to prior findings (Casali et al., 2013, Casarotto et al., 2016), and that the other measures correlate with the PCI measure. However, we also predict that the PCI has higher sensitivity and specificity compared to other measures employed. In addition, based on pilot data, we hypothesize that the PCI measure might vary in absolute terms between institutions and setups, and therefore we might not observe similar absolute values as earlier studies report, but a similar differentiation between states.

Support: Supported by the Norwegian Research Council (NRC), and the “Conscious Brain” project (coordinator J.F. Storm) within the Human Brain Project (HBP, SP3.4).

REFERENCES

- Bowdle, T. A. (2006). Depth of anesthesia monitoring. *Anesthesiol. Clin. N. Am.* 24, 793–822. doi: 10.1016/j.atc.2006.08.006 PMID:NOPMID
- Casali, A. G., Gosseries, O., Rosanova, M., Boly, M., Sarasso, S., Casali, K. R., et al. (2013). A theoretically based index of consciousness independent of sensory processing and behavior. *Sci Trans. Med.* 5, 198ra105. doi: 10.1126/scitranslmed.3006294 PMID:23946194
- Casarotto, S., Comanducci, A., Rosanova, M., Sarasso, S., Fecchio, M., Napolitani, M., et al. (2016). Stratification of unresponsive patients by an independently validated index of brain complexity. *Ann. Neurol.* 80, 718–729. doi: 10.1002/ana.24779 PMID:27717082
- Gawryluk, J. R., D’Arcy, R. C., Connolly, J. F., and Weaver, D. F. (2010). Improving the clinical assessment of consciousness with advances in electrophysiological and neuroimaging techniques. *BMC Neurol.* 10:1. doi: 10.1186/1471-2377-10-11 PMID:20113490
- Musizza, B., and Ribaric, S. (2010). Monitoring the depth of anaesthesia. *Sensors* 10, 10896–10935. doi: 10.3390/s101210896 PMID:22163504
- Oizumi, M., Albantakis, L., and Tononi, G. (2014). From the phenomenology to the mechanisms of consciousness: integrated information theory 3.0. *PLoS Comput. Biol.* 10:e1003588. doi: 10.1371/journal.pcbi.1003588 PMID:24811198
- Osterman, J. E., Hopper, J., Heran, W. J., Keane, T. M., and van der Kolk, B. A. (2001). Awareness under anesthesia and the development of posttraumatic stress disorder. *Gen. Hosp. Psychiatry* 23, 198–204. doi: 10.1016/S0163-8343(01)00142-6 PMID:11543846
- Prendergast, K. M., and Cullen-Drill, M. (2012). Anesthesia awareness-induced posttraumatic stress disorder. *J. Psychosoc. Nurs. Mental Health Serv.* 50, 39–44. doi: 10.3928/02793695-20121003-03 PMID:NOPMID
- Sarasso, S., Rosanova, M., Casali, A. G., Casarotto, S., Fecchio, M., Boly, M., et al. (2014). Quantifying cortical EEG responses to TMS in (un) consciousness. *Clin. EEG Neurosci* 45, 40–49. doi: 10.1177/1550059413513723 PMID:24403317
- Schnakers, C., Vanhau denhuysse, A., Giacino, J., Ventura, M., Boly, M., Majerus, S., et al. (2009). Diagnostic accuracy of the vegetative and minimally conscious state: clinical consensus versus standardized neurobehavioral assessment. *BMC Neurol.* 9:1. doi: 10.1186/1471-2377-9-35 PMID:NOPMID
- Sebel, P. S., Bowdle, T. A., Ghoneim, M. M., Rampil, I. J., Padilla, R. E., Gan, T. J., et al. (2004). The incidence of awareness during anesthesia: a multicenter United States study. *Anesth. Analg.* 99, 833–839. doi: 10.1213/01.ANE.0000130261.90896.6C PMID:15333419
- Webb, R. K., Van der Walt, J. H., Runciman, W. B., Williamson, J. A., Cockings, J., Russell, W. J., et al. (1993). The Australian Incident Monitoring Study. Which monitor? An analysis of 2000 incident reports. *Anaesth. Intensive Care* 21, 529–542. doi: NODOI PMID:8273872

Spatio-Temporal Spike Pattern Recognition in Massively Parallel Spike Trains

Alper Yegenoglu^{1,2,3}, **Pietro Quaglio**^{1,2,3}, **Emiliano Torre**^{1,2,3}, **Dominik Endres**⁴, **Sonja Grün**^{1,2,3,5}

¹*Institute of Neuroscience and Medicine (INM-6), Jülich, Germany*

²*Institute for Advanced Simulation (IAS-6), Jülich, Germany*

³*JARA BRAIN Institute I, Jülich Research Centre, Jülich, Germany*

⁴*Theoretical Neuroscience Group, Dept. of Psychology, Philipps-University, Marburg, Germany*

⁵*Theoretical Systems Neurobiology, RWTH Aachen University, Aachen, Germany*

a.yegenoglu@fz-juelich.de

Introduction: Cortical neurons form a highly interwoven network. Cell assemblies (Hebb, 1949), i.e., interacting groups of neurons, were suggested as the building blocks of information processing in the brain (Singer et al., 1997; Harris, 2005). It is observed that i) spike time coordination at millisecond precision shapes synaptic efficacy (Bi and Poo, 1998), ii) neurons emit a spike more reliably upon synchronous than asynchronous input (Abeles, 1982), and iii) synchronous input may result from pre-synaptic spikes emitted at different times but arriving simultaneously at the post-synaptic site. Modern electrophysiological techniques allow to record hundreds of neurons simultaneously and thereby increasing the chances to observe neurons involved in assemblies expressed by spatio-temporal spike patterns (STPs).

Method: We developed a statistical method to detect STPs in massively parallel spike data (MPST), i.e., on the order of 100 or more neurons. The method is able to deal with the combinatorial explosion of the number of patterns occurring in such high-dimensional data by employing a combination of frequent item set mining (Torre et al., 2013) and a stability analysis algorithm (Kuznetsov, 2007), exploiting the fact that the mathematical foundation of frequent item set mining is equivalent to formal concept analysis (Ganter and Wille, 1999). Our proposed method can statistically assess the patterns and reduce considerably the multiple testing problem by use of Monte-Carlo approaches. As a result the method extracts STPs that occur significantly in excess as compared to STPs that occur by chance.

Results: We evaluate our method on ground truth MPST data generated by stochastic simulations. The performance of the method (in terms of false positive and false negative detections) is affected by a variety of parameters, such as the number of STP occurrences, the number of neurons involved in each pattern, and the firing rates of the neurons. Various features of experimental data are considered in analysis, such as non-stationary firing rate in time or inhomogeneity across neurons, and inter-spike

interval regularity. We demonstrate the robustness of our method in respect to these parameters by simulating different scenarios which replicate such features.

Our results show that the method is suited for the analysis of STPs in massively parallel spike trains thereby offering the possibility to relate such patterns to behavior and show their computational relevance.

Acknowledgments: Supported by the Helmholtz Portfolio Theme Supercomputing and Modeling for the Human Brain (SMHB), the European Union's Horizon 2020 research and innovation programme under grant agreement No 720270 (HBP SGA1), the DFG SPP Priority Program 1665 (GR 1753/4-1), and the DFG IRTG 1901.

REFERENCES

- Abeles, M. (1982). Role of the cortical neuron: integrator or coincidence detector? *Isr. J. Med. Sci.* 18, 83–92. doi: NODOI PMID:6279540
- Bi, G. Q., and Poo, M. M. (1998). Synaptic modifications in cultured hippocampal neurons: dependence on spike timing, synaptic strength, and postsynaptic cell type. *J. Neurosci.* 18, 10464–10472. doi: NODOI PMID:9852584
- Ganter, B., and Wille, R. (1999). *Formal Concept Analysis: Mathematical Foundations*. Springer Berlin Heidelberg.
- Harris, K. (2005). Neural signatures of cell assembly organization. *Nat. Rev. Neurosci.* 5, 339–407. doi:10.1038/nrn1669 PMID:15861182 PMID:NOPMID
- Hebb, D. O. (1949). *The Organization of Behavior: A Neuropsychological Approach*. New York: John Wiley & Sons.
- Kuznetsov, S. O. (2007). On stability of a formal concept. *Ann. Math. Artif. Intell.* 49, 101115. doi: 10.1007/s10472-007-9053-6 PMID:NOPMID
- Singer, W., Engel, A. K., Kreiter, A. K., Munk, M. H. J., Neuenschwander, S., and Roelfsema, P. R. (1997). Neuronal assemblies: necessity, signature and detectability. *Trends Cogn. Sci.* 1, 252–261. doi: 10.1016/S1364-6613(97)01079-6 PMID:21223920
- Torre, E., Picado-Muiño, D., Denker, M., Borgelt, C., and Grün, S. (2013). Statistical evaluation of synchronous spike patterns extracted by frequent item set mining. *Front. Comput. Neurosci.* 7:132. doi: 10.3389/fncom.2013.00132 PMID:24167487

Spatiotemporal Patterns of a Population Burst in Cultured Neuronal Networks

Dmitry Zendrikov¹, Alexander Paraskevov²

¹Moscow Institute of Physics and Technology (State University), Dolgoprudny, Russia

²National Research Centre "Kurchatov Institute", Moscow, Russia

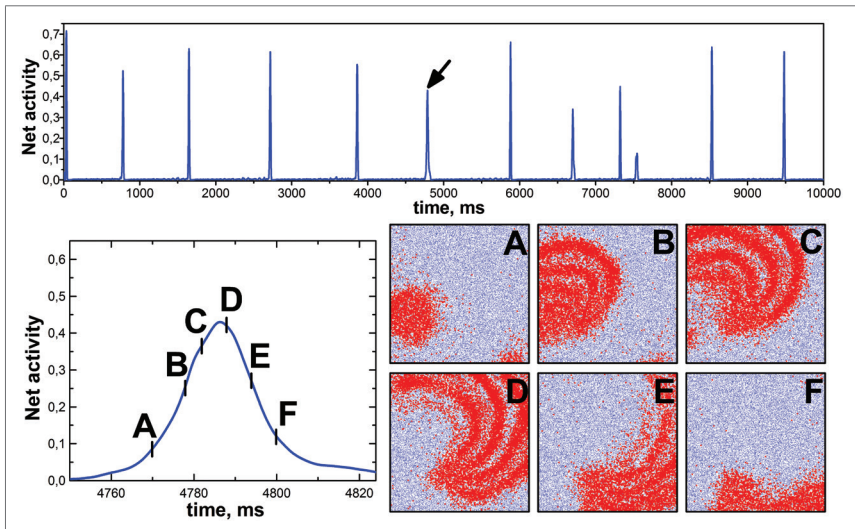
zendrikov@phystech.edu

In cultured neuronal networks one can often detect spontaneous short-term (fractions of a second) repetitive synchronization of neuronal spiking activity called a network spike or a population burst (PB). In a recent paper (Orlandi et al., 2013) it has been shown experimentally that a typical PB has a few stable spatial sources—nucleation centers of traveling waves of synchronous spiking activity. The causes of the occurrence of nucleation centers have not yet identified.

Our simulations show that in spatially uniform neuronal cultures, where the probability of interneuronal connection formation decreases exponentially with increasing distance between the neurons (Miles et al., 1988), there exists a small number of spatial nucleation centers of PBs, from where the synchronous spiking activity usually propagates in the network in the form of circular traveling waves [see Paraskevov and Zendrikov (2017) for details]. The number of nucleation centers, as well as their spatial location, is unique and unchanged for a given realization of neuronal network but is different for different networks. In contrast, if the probability of interneuronal connection formation is independent of the distance between neurons (provided that the average number of outgoing synaptic connections per neuron in the network is conserved), then the nucleation centers do not arise and the synchronization of spiking activity during a PB occurs spatially uniform throughout the network. Therefore one can conclude that spatial proximity of connections between neurons is important for the formation of nucleation centers. It is also shown that fluctuations of the spatial density of neurons at their random homogeneous distribution typical for the experiments *in vitro* do not determine the location of the nucleation centers.

Interestingly, if the average number m of outgoing connections per neuron is sufficiently large, then a drifting spiral wave can arise during some PBs (see Figure, where 50,000 neurons with $m \approx 460$ are uniformly distributed over the unit square), given that most of the PBs still start with circular traveling waves propagating from the stationary nucleation centers.

In general, these findings are in qualitative agreement with the already known. Similar effects (e.g., circular and spiral waves), regardless to the occurrence of PBs, were obtained in previous computational studies (Milton et al., 1992; Chu et al., 1994; Fohlmeister et al., 1995; Kistler et al., 1998) using different models of the neuronal network, and drifting spiral waves were observed experimentally in disinhibited neo-cortical slices (Huang et al., 2004).



Upper graph: Averaged (over 2 ms) spiking activity of the network of 50,000 neurons (20% are inhibitory neurons), with approx. 460 outgoing connections per neuron and characteristic connection length $0.04 L$. The neurons are uniformly distributed over the square area $L \times L$ of unit size ($L = 1$). Lower graph: LEFT: Network activity during the population burst (PB) marked by the arrow in the upper graph. RIGHT: Snapshots of the instantaneous spatial activity of neurons for the corresponding moments of the PB. Blue dots depict neurons and red dots highlight spiking neurons. A drifting spiral wave during the PB is clearly visible.

REFERENCES

Chu, P. H., Milton, J. G., and Cowan, J. D. (1994). Connectivity and the dynamics of integrate-and-fire neural networks. *Int. J. Bifurcat. Chaos* 4, 237–243. doi: 10.1142/S0218127494000198 PMID:NOPMID

- Fohlmeister, C., Gerstner, W., Ritz, R., and van Hemmen, J. L. (1995). Spontaneous excitations in the visual cortex: stripes, spirals, rings, and collective bursts. *Neural Comput.* 7(5), 905–914. doi: 10.1162/neco.1995.7.5.905 PMID:7584892
- Huang, X., Troy, W. C., Yang, Q., Ma, H., Laing, C. R., Schiff, S. J., et al. (2004). Spiral waves in disinhibited mammalian neocortex. *J. Neurosci.* 24(44), 9897–9902. doi: 10.1523/JNEUROSCI.2705-04.2004 PMID:15525774
- Kistler, W. M., Seitz, R., and van Hemmen, J. L. (1998). Modeling collective excitations in cortical tissue. *Physica D* 114, 273–295. doi: 10.1016/S0167-2789(97)00195-4 PMID:NOPMID
- Miles, R., Traub, R. D., and Wong, R. K. (1988). Spread of synchronous firing in longitudinal slices from the CA3 region of the hippocampus. *J. Neurophysiol.* 60, 1481–1496. doi: 10.1152/jn.1988.60.4.1481 PMID:3193167
- Milton, J. G., Chu, P. H., and Cowan, J. D. (1992). “Spiral waves in integrate-and-fire neural networks,” in *Advances in Neural Information Processing Systems 5 (NIPS 1992)*, 1001–1006. Available at: <https://papers.nips.cc/paper/689-spiral-waves-in-integrate-and-fire-neural-networks.pdf>.
- Orlandi, J. G., Soriano, J., Alvarez-Lacalle, E., Teller, S., and Casademun, J. (2013). Noise focusing and the emergence of coherent activity in neuronal cultures. *Nat. Phys.* 9, 582–590. doi: 10.1038/nphys2686 PMID:NOPMID
- Paraskevov, A., and Zendrikov, D. (2017). A spatially resolved network spike in model neuronal cultures reveals nucleation centers, circular traveling waves and drifting spiral waves. *Phys. Biol.* 14, 026003. doi: 10.1088/1478-3975/aa5fc3 PMID:28333685

Biophysical Modeling of Single-Neuron Contributions to EEG and ECoG Signals

Solveig Næss¹, Torbjørn V. Ness², Geir Halnes², Anders M. Dale³, Gaute T. Einevoll^{1,2}

¹University of Oslo, Oslo, Norway

²Norwegian University of Life Sciences, Ås, Norway

³University of California, San Diego, CA, United States

solveinae@ifi.uio.no

Electroencephalography (EEG), i.e., recordings of electrical potentials at the scalp, and electrocorticography (ECoG), i.e., potentials recorded on the cortical surface, are two prominent techniques probing brain activity at the systems level. Despite their long history and widespread use, the proper interpretation of these brain signals in terms of the biophysical activity in underlying neurons (nerve cells) and neuronal networks is still lacking. Present-day analysis is predominantly statistical and limited to identification of phenomenological signal generators without a clear biophysical interpretation. New biophysics-based analysis methods are thus needed to take full advantage of these brain-imaging techniques (Einevoll et al., 2013).

Here we used biophysical modeling based on morphologically detailed multicompartmental neuron models to explore single-neuron contributions to ECoG and EEG signals and in particular the feasibility of using the so-called current-dipole approximation in predicting these signals (Hamalainen et al, 1993). Specifically, we used the open-source Python package LFPy (lfp.github.io) which builds on Neuron (www.neuron.yale.edu) and is based on well-established volume-conductor theory for numerical calculations of extracellular potentials. The LFPy package was supplemented with new Python tools for calculating the current-dipole moment of a neuron for use of the current-dipole approximation to predict ECoG and EEG signals. Current-dipole approximations were explored in the inhomogeneous four-concentric-spheres head model (Srinivasan et al., 1998), and compared with results from using the Finite Element Method (Dhatt et al., 2012).

When comparing computed cortical-cell contributions to the EEG and ECoG signals from using the current-dipole approximation with results from the full model explicitly including all transmembrane currents, we find that the current-dipole approximation is applicable for modeling EEG signals. This allows for a drastic simplification of future biophysics-based computation of EEG signals from cortical cell populations. However, we find that the current-dipole approximation is not generally applicable for computing ECoG signals.

REFERENCES

- Dhatt, G., Emmanuel L., and Gilbert T. (2012) *Finite Element Method*. John Wiley & Sons: Hoboken, NJ.
- Einevoll, G. T., Kayser, C., Logothetis, N. K., and Panzeri, S. (2013). Modelling and analysis of local field potentials for studying the function of cortical circuits. *Nat. Rev. Neurosci.* 14, 770–85. doi: 10.1038/nrn3599
- Hämäläinen, M., Haari, R., Ilmoniemi, R. J., Knuutila, J., and Lounasmaa, O. V. (1993). Magnetoencephalography — theory, instrumentation, and application to non- invasive studies of the working human brain. *Rev. Modern Phys.* 65, 413–97.
- Srinivasan, R., Nunez, P. L., and Silberstein, R. B. (1998). Spatial filtering and neocortical dynamics: estimates of EEG coherence. *IEEE Trans. Biomed. Eng.* 45, 814–826. doi: 10.1109/10.686789

Abnormalities of Walking as a Sign of Non-Alzheimer's Dementia

Farrukh T. Fayzullaev, Aziza T. Djurabekova, Saodat S. Igamova, Farangiz S. Khamedova, Jakhongir S. Musinov, Sabina F. Ganieva, Davlatkhon A. Akramov

*Samarkand State Medical Institute, Samarkand, Uzbekistan
farfay1990@mail.ru*

Neurological abnormalities affecting walking occur early in several types of non-Alzheimer's dementias, but their value in predicting the development of dementia is uncertain.

Methods and material: We analyzed the relation between neurological walking status at base line and the development of dementia in a prospective study involving 122 patients older than 75 years of age who lived in the city and did not have dementia at base line. Methods proportional-hazards regression analysis was used to calculate hazard ratios with adjustment for potential confounding demographic, medical, and cognitive variables.

Results: At enrollment, 35 subjects had neurological walking abnormalities of the following types: unsteady gait (in 31 patients), frontal walking (in 7 patients), hemiparetic walking (in 6 patients), neuropathic gait (in 6 patients), ataxic gait (in 5 patients), parkinsonic walking (in 4 patients), and spastic gait (in 1 patients). During follow-up (median duration, 6.6 years), there were 62 newly diagnosed cases of dementia, 32 of them cases of Alzheimer's disease and 30 cases of non-Alzheimer's dementia (25 of which involved vascular dementia and 5 of which involved other types of dementia). Subjects with neurologic gait abnormalities had a greater risk of development of dementia (hazard ratio, 1.96 [95% confidence interval, 1.30 to 2.96]). These subjects had an increased risk of non-Alzheimer's dementia (hazard ratio, 3.51 [95% confidence interval, 1.98 to 6.24]), but not of Alzheimer's dementia (hazard ratio, 1.07 [95% confidence interval, 0.57 to 2.02]). Of non-Alzheimer's dementias, abnormal walking predicted the development of vascular dementia (hazard ratio, 3.46 [95% confidence interval, 1.86 to 6.42]). Among the types of abnormal walking, unsteady gait predicted vascular dementia (hazard ratio, 2.61), as did frontal gait (hazard ratio, 4.32) and hemiparetic walking (hazard ratio, 13.13).

Conclusions: The presence of neurological walking abnormalities in elderly persons without dementia at base line is a significant sign of the risk of development of dementia, especially non-Alzheimer's dementia.

Analysis on Link and Motif Asymmetry of *C. elegans* Connectome

**Pyeong Soo Kim¹, Seongkyun Kim¹, Hyoungkyu Kim¹,
Jaeseung Jeong^{1,2}**

¹Department of Bio and Brain Engineering, Korea Advanced Institute of Science and Technology, Daejeon, South Korea

²Program of Brain and Cognitive Engineering, College of Engineering, Korea Advanced Institute of Science and Technology, Daejeon, South Korea

kimvudtn@kaist.ac.kr

Majority of animal species have bilaterally symmetrical nervous system. Symmetric and asymmetric features among their morphological symmetric nervous system have been interesting issue for a long time. The simplest bilaterally symmetrical organism is nematode called *Caenorhabditis elegans*. Previously, symmetry of *C. elegans* has only been thoroughly studied in morphological and functional manner (Oliver et al., 2002). According to previous studies, *C. elegans* have highly symmetrical nervous system composed of 92 bilaterally symmetrical neuronal pairs and remaining 95 neurons which are mostly located on the axis of symmetry. Functionally there are only 2 neuronal pairs that show asymmetrical gene expression among 92 pairs of symmetrical neurons. Since investigation on network is simple but powerful tool to understand the system, we examined the symmetry of *C. elegans* nervous network which has not been studied. Total of 279 neurons and 2990 links in *C. elegans* were used. First, we defined the symmetry of each individual link according to their associated neuronal symmetry. Then we could expand that definition to define the symmetry of motif. We used structural motif of size 3 in this study (Olaf and Kötter, 2004). We analyzed how these asymmetric links are distributed throughout *C. elegans* function, neuronal type (motor neuron, sensory neuron, or interneuron), or neurotransmitter. Then, we suggested a novel approach to classify asymmetric neurons of *C. elegans* nervous system by examining asymmetric network topology for every node. We defined 5 explicit locally topological parameters for a neuron; (1) the degree is defined as the number of asymmetric links attached to the neuron, (2) the motif is defined as distribution of the numbers of asymmetric motifs for a neuron, (3) the degree ratio is defined as ratio of asymmetric links over totally attached links to the neuron including both of symmetric links and asymmetric links, (4) the motif ratio is distribution of the rates for asymmetric motifs over total motifs including both of symmetric and asymmetric motifs, and (5) the relative distance is defined by the difference of asymmetric motif fingerprint of bilaterally symmetrical neurons. Thresholds were defined using mean and standard deviation (SD) values of asymmetries to find statistically asymmetric components. Neurons with asymmetry value over the threshold were considered as

asymmetric neurons (asymmetric neurons > SD from the mean values). We checked our asymmetric neurons with ASE and AWC neurons that are only known to show bilaterally asymmetrical function induced by asymmetrical gene expression. As a result, our study suggested that (4) ratio of asymmetric motif and (5) relative distance measures successfully classified ASE and AWC as asymmetric neurons. Neurons classified as asymmetric by our measures other than ASE and AWC neurons were ALN and PLM neurons. These results could be interpreted that ALN neurons and PLM neurons might possess asymmetric features that have not been discovered. Possible functional asymmetries were suggested by investigation on individual asymmetric links they possess. ALNL neuron is connected to SMBDR neuron which is known to set the amplitude of sinusoidal movement of *C. elegans*. ALNR neuron is connected to SMDDR neuron which is associated with steep amplitude of omega turn. This suggest that ALN neurons are associated to *C. elegans* movement in different ways. PLM neuron is different from ALN that only one side neuron has many asymmetric links. PLML neuron is involved with only one asymmetric link. However, PLMR is connected to many neurons such as PVR, AVJL, AS06, AVAL/R, AVDL/R, DVA, and PDEL/R. Most of these neurons are associated with backward locomotion function and mechanosensation. We can inspect that PLM neuron have ON/OFF function that only one neurons show functionality. Our finding could be easily applied to other symmetrical networks and shed lights to understanding symmetry in our brains.

REFERENCES

- Olaf, S., and Kötter, R. (2004). Motifs in brain networks. *PLoS Biol.* 2:e369. doi: 10.1371/journal.pbio.0020369 PMID:15510229
- Oliver, H., Johnston, R. J., and Chang, S. (2002). Left-right asymmetry in the nervous system: the *Caenorhabditis elegans* model. *Nat. Rev. Neurosci.* 3, 629–640. doi: 10.1038/nrn897 PMID:NOPMID

Native Architecture for Artificial Intelligence

Dushan Balisson, Wim J. C. Melis, Simeon Keates

University of Greenwich, Chatham, United Kingdom

Dushan.Balisson@greenwich.ac.uk

Wim.J.C.Melis@gre.ac.uk

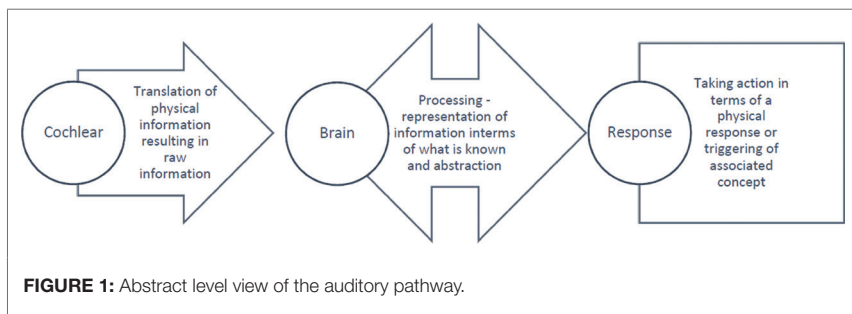
Introduction: The brain is a complex organ and even to this date, very little is known about how it works. Through the years, replicating the intelligence of the brain has puzzled many scientists, and most of this work can be broadly classified into two categories—Neurophysiological or Cognitive based. The latter approach tends to overlook the actual structure of the brain in order to focus on the behaviour itself. This is, e.g., exemplified by the Turing test (Alan, 1950), which implies that if a human interacts with an artificial machine and identifies it as a human, then this artificial machine is considered sufficiently humanlike.

Proponents of the neurophysiological approach argue that the intelligence of the brain lies in its structure, hence if this structure can be replicated, one should be able to replicate human intelligence. In this context, one of the most complete neurophysiological models of the neuron is the Hodgkin-Huxley model (Hodgkin and Huxley, 1990), which has served as a reference for biological plausibility of subsequent neural models. However, a major issue with the Hodgkin-Huxley model lies in the complexity to use it for the implementation of a complete and useful network. On the other extreme, one can find simple models such as the Leaky Integrate and Fire (LIF) model (Orhan, 2012), which is the most widely used neural model, but is commonly regarded to be oversimplified. While this model is biologically implausible, it is computationally viable and can therefore be implemented into relatively large networks to study their behaviour and dynamics.

Even further simplified networks are already used to feed the need for intelligent machines that are able to learn. Today, one of the most successful machine learning paradigms is the Artificial Neural Network (ANN). ANNs implement a self-improving function by giving a certain output, based on certain inputs, where each neuron is modelled as a transfer function. These systems have shown commendable performance and form the basis for certain popular services, such as the Google Brain Project that provides YouTube users with recommended videos based on their viewing history (Covington et al., 2016). However, the computational complexity of these tasks is not to be underestimated, as the Google Brain combines 16,000 computers to deliver the capabilities of a rat's brain (Le et al., 2012). This raises the question as to why our current systems are so largely inefficient when it comes to delivering brain-like functionality.

Considering that the theoretical limit of silicon feature sizes is getting closer and that the collapse of Moore's law is upon us, it seems more than necessary to get back to the drawing board and start considering alternative platforms that are more efficient and run without the huge semantic gap.

Method: Since the initial conceptualisation of the ANN framework, much more is now known about cognition and neurophysiology. While this knowledge covers various levels, the aim here is to look at the brain from a higher abstraction level and use that to identify the main function of the brain. This approach can also salvage knowledge from our understanding of the ANN model. Therefore, as an example, an abstract model of the auditory pathway, as shown in Figure 1, will be investigated in more detail.



The inner ear, more specifically the cochlea, transduces the received frequencies into vibrations of frequency selective hair cells; these produce electrical impulses that are then fed to the brain. The nature of this signal can be extrapolated from what is known about the functioning of the auditory pathway, however the actual representation of the information is purposefully overlooked here to maintain an abstract perspective. Within the brain, the processing that takes place is closely linked with the nature of the input signal, and so as a first step it is essential to understand and break down the processing that takes place in the brain. Being an associative memory system, the brain compares the incoming information with what is known, through similarity matching. Similarity matching is one of the most important tasks in the brain and the brain seems to excel at this task.

Implementing similarity matching can obviously be achieved through Euclidean distance calculation or various other mathematical/statistical approaches, however these seem rather brute force approaches and may not be the most efficient in their own right. Additionally, one may need to consider how information can be stored and processed

within the same location to allow suitable encoded sensory information to interact with the stored information. Obviously, storing every single possibility of a sensory item is implausible because of its impact on the required amount of memory, so one solution could be to use a hierarchical structure. This would mean that the brain breaks down its comparison into stages with different abstractions (Hawkins and Blakeslee, 2007) and so comparison at one level is performed before comparing at the next level which has a higher abstraction, and so on and so forth.

To make such an artificial system as efficient as possible, there is the need for sensory information to interact with all possibilities simultaneously at a particular hierarchical level, which then again brings along several challenges. At the same time, it is expected that this approach needs to allow learning in its broadest sense. Therefore, the memory and processing structure should be modifiable through a learning and feedback mechanism in a way similar to, but not limited by, a backpropagation algorithm.

Discussion: Today conventional computing platforms are inherently focused on arithmetic and logic operations, which seem a long way from what happens within the human brain. While there seem to be a variety of different similarity matching based approaches around, having to perform them on a one by one comparison basis, either sequentially and/or with a certain amount of parallelism has performance implications. It therefore seems essential that effort is put into the development of platforms that model the brain from a functional perspective and provide for a more direct mapping to technology. That being said, until other platforms become a reality, conventional computing platforms will remain an indispensable tool to support the exploration for alternative artificially intelligent platforms.

REFERENCES

- Alan, M. (1950). Turing. Computing machinery and intelligence. *Mind* 59, 433–460. doi: NODOI PMID:NOPMID
- Covington, P., Adams, J., and Sargin, E. (2016). “Deep neural networks for youtube recommendations,” in *Proceedings of the 10th ACM Conference on Recommender Systems – RecSys ’16*, Boston, MA, USA, 191–198.
- Hawkins, J., and Blakeslee, S. (2007). *On Intelligence: How a New Understanding of the Brain will Lead to the Creation of Truly Intelligent Machines*. Macmillan: New York.
- Hodgkin, A. L., and Huxley, A. F. (1990). A quantitative description of membrane current and its application to conduction and excitation in nerve. *Bull. Math. Biol.* 52, 25–71. doi: 10.1016/S0092-8240(05)80004-7 PMID:NOPMID
- Le, Q. V., Ranzato, M., Monga, R., Devin, M., Chen, K., Corrado, G. S., et al. (2012). “Building high-level features using large scale unsupervised learning,” in *Proceedings of the 29th International Conference on Machine Learning, ICML 2012, 38115*, Edinburgh, Scotland, 507–514.
- Orhan, E. (2012). *The Leaky Integrate-and-Fire Neuron Model*. Technical Report. University of Rochester, NY, USA. Available at: <http://hopf.cns.nyu.edu/~eorhan/notes/lif-neuron.pdf>

An Evolutionary Machine Learning Algorithm to Enhance Language Processing

Martin W. Kinch, Wim J. C. Melis, Simeon Keates

University of Greenwich, Chatham, United Kingdom

M.W.Kinch@greenwich.ac.uk

Introduction: In the current age of Artificial Intelligence (AI) there have been numerous inroads into the topic (Vinyals et al., 2016; Chan et al., 2016; Bahdanau et al., 2016), many of which have made unprecedented leaps in completing tasks that were once thought impossible; notably professional level game playing; such as: Watson (Ferrucci et al., 2010), Deep Blue (Campbell et al., 2002), or AlphaGO (Silver et al., 2016). However, despite these great leaps, nearly all these AI systems (Campbell et al., 2002; Silver et al., 2016) focus on the use of processor intensive algorithms to achieve their goals; while not necessarily an issue it requires all data to be mapped towards an arithmetic world. Since the world is not necessarily mathematical in all aspects and can only be represented in this manner as far as our current level of mathematics has been developed, which leads to the problem that any mathematical model will be limited by the development of mathematics in relation to representing the real world. The better one can make this representation, the more likely the system will operate with a good accuracy. However, as complexity increases to deal with the real world in a mathematical way, data and processing requirements increase likewise and so eventually one needs massively parallel machines consuming large amounts of power to provide for only a limited amount of intelligent functionality. Additionally, the data will be represented in a format that is optimal for that particular task, but does not necessarily allow for generalization towards other processes, and so the scope of the application is connected with the mathematical ruleset used for the AI to work from (Campbell et al., 2002; Silver et al., 2016); something that then implicitly limits the AI's ability to move from one environment to another. Which poses the question, how can something be intelligent if it cannot transfer its knowledge from one application to another, as such transference capabilities are clearly seen in humans.

Methods: To address the questions posed previously, effort will be directed towards the development of new data management models, primarily, focusing on how to best store and capture data and its complex inter-relationships and make this useful towards an intelligent system. This will require the stored data to be relational, so that meaning can be inferred more than determined. The important part is rather than perform extensive calculations to determine the importance and relevance of the information,

much of this can be determined by the relationships between data, meaning that the context is of particular importance towards the meaning of the actual data. Some of this data complexity can obviously be grasped within an artificial neural network, but these suffer from the limitation that these networks then often become black boxes making it challenging to ensure the reliability of the system. On the other hand, using mathematical approaches for machine learning requires massively parallel machines, which are great for arithmetic functionality, but struggle to efficiently deliver the intelligent functionality necessary for these type of networks.

Within the context of learning data and, storing and structuring it, it is important to understand the level of detail that is required. In a machine learning context this is often referred to as generalisation and can lead to over/under-fitting, while essentially the purpose is to find an invariant representation as mentioned in (Hawkins and Blakeslee, 2004), which has investigated this topic from a neuroscientific perspective. The more important challenge in this context is to identify the minimum required amount of data to be able to recognise something, and consequently the amount of data that really needs to be stored for recognition, even though they may both depend on the amount of context information available.

Being able to use contextual information should provide the system with a far greater understanding of the data provided to it, while also becoming more able to determine the intention behind the message that is being “translated” from human language into computational terms. The most important forms of context are probably the “hidden” elements of communication that people take for granted, such as: non-verbal cues, locational cues, situational cues and possibly even tonal or pitch cues, to name a few. The aim is to study the importance of individual elements and then select the best matches for human understanding and computational ease, to ensure that this extra information will ensure a higher accuracy rate.

While it is obviously easier to try and structure everything in a deterministic/organised world, it seems unlikely that the data and its organisation in the brain may be anywhere close to organised, and is more likely based on approximations rather than exact outcomes. This then also reflects on the data being invariant rather than very specific, although further details may be required to go from an initial “estimate” to a more detailed “result.” Even though this context suddenly becomes very unsure and unknown, due to it not being exact in nature, it is likely to be in this uncertainty that may lie the answers to some of the challenges faced. It will therefore be essential to take a more holistic approach and include the field of AI as well as other fields such as psychology, philosophy and biology to obtain the required answers.

Expected Results: This research aims to develop an algorithm that is biologically inspired, and understands and uses approximate data to achieve transferability in

its applications. Considering that all human learning is an evolutionary process, it is expected that this algorithm will have to incorporate evolutionary aspects to “fine tune” any learned data. It is in this context that language processing seems most suitable as an application as it allows for the exploration of general elements as a building block, to master one aspect of natural language while invariance and evolution can be found in secondary aspects such as interpretations and so on.

Discussion: In order to overcome some of the challenges of current research, this work will focus on developing from a data centred model, rather than a processor based one, with the aim to achieve significant savings in data storage and processing requirements for AI systems. Savings of this nature will also help improve the efficiency of such systems, while using a less deterministic approach is expected to make AI's transferability more effective; allowing them to be competent in several applications rather than just one.

REFERENCES

- Bahdanau, D., Chorowski, J., Serdyuk, D., Brakel, P., and Bengio, Y. (2016). “End-to-end attention-based large vocabulary speech recognition,” in *ICASSP (IEEE)*, Shanghai, China, 4945–4949.
- Campbell, M., Hoane, A. J., and Feng-hsiung, H. (2002). *Deep Blue*. Artificial Intelligence, 57–83. doi: 10.1016/S0004-3702(01)00129-1.
- Chan, W., Jaitly, N., Le, Q., and Vinyals, O. (2016). “Listen, attend and spell: a neural network for large vocabulary conversational speech recognition,” in *ICASSP (IEEE)*, Shanghai, China, 4960–4964.
- Ferrucci, D., Brown, E., Chu-Carroll, J., Fan, J., Gondek, D., Kalyanpur, A., et al. (2010). Building Watson: an overview of the DeepQA Project. *AI Magazine*, 59–79. doi: 10.1609/aimag.v31i3.2303.
- Hawkins, J., and Blakeslee, S. (2004). *On Intelligence*. New York: St. Martin's Griffin.
- Silver, D., Huang, A., Maddison, C. J., Guez, A., Sifre, L., van den Driessche, G., et al. (2016). Mastering the game of Go with deep neural networks and tree search. *Nature* 529, 484–489. doi: 10.1038/nature16961 PMID:26819042
- Vinyals, O., Blundell, C., Lillicrap, T., Kavukcuoglu, K., and Wierstra, D. (2016). *Matching Networks for One Shot Learning*. Available at: <https://arxiv.org/pdf/1606.04080v1.pdf>.

Creating Patterns for Machine Learning Using Multiple Alignment

Saritha Kinkiri, Wim J. C. Melis, Simeon Keates

Faculty of Engineering and Science, University of Greenwich, Chatham, United Kingdom

s.kinkiri@greenwich.ac.uk,

wim.j.c.melis@greenwich.ac.uk,

s.keates@greenwich.ac.uk

Introduction: Learning is a basic skill that helps every human on a day to day basis to improve their life. It is one of the key features to achieve knowledge and deliver intelligence. Learning involves a combination of human thoughts, thinking-process and their behaviour and that on a regular basis. This change in behaviour is achieved through the feedback of information given by and/or received from the surroundings, and that with the aim to improve the accuracy of processes. For example, sensory organs get information from the environment, but the human brain cannot take in and process all the data in one go, so it converts data into patterns, and then arranges and stores it for later retrieval. This process is continuous as these patterns are continuously adjusted to fit recent events. In order to be able to mimic this learning to artificial systems it is key to find answers to questions like: “how do humans learn with patterns?” and “how can humans improve their learning experiences?”

Method: While it is generally believed that the human brain takes most of its input from our sensory organs, it does not necessarily rely on all of them to develop and learn. For example, Helen Keller has no sight and no hearing, yet she managed to learn a language and became one of the best writers in the world (Hawkins, 2005). This shows that humans do not need all senses to become intelligent, and so while the brain is currently considered as a dark box with no knowledge, there are still time flowing patterns on its inputs from the environment. While many researchers are aiming to better understand how the brain works at the lowest level and how it provides for its learning functionalities, it may be that more suitable answers need to be searched in how the brain converts information into patterns, as it seems to be those patterns that lie at the basis of most, if not all, of our learned information. For example, if someone asks you to explain the structure of your home, you will first think about where to start from, kitchen or cellar, and from there you will work your way methodologically through the remainder. So even though all information is there, you will prioritise and then explain to your friend following a particular most often logical, pattern. Similarly, the human face is learned as a collection of patterns of nose, mouth and eyes. Here,

the question becomes, how can machine learning algorithms learn to learn like the human brain, with regards to these patterns?

One method that aims at learning patterns like the human brain is the SP theory (Wolff, 2016), which is a method of learning, where information is compressed by identifying common patterns. It operates according to the multiple alignment principle, and consequently aims to find similarities along multiple dimensions. To achieve these alignments, similarities are identified within each provided pattern during the learning phase and used to reduce storage requirements, which leads to an overall data compression. Each unique pattern is saved, and so when a new pattern is presented, the SP theory will check whether there is any similarity by identifying patterns to ensure maximum compression. The SP theory represents information through symbols, which are effectively multi-dimensional patterns. Since this theory operates similarly to how a human brain learns, it is a useful starting point to improve how machines become more able to learn like a human. The question then becomes how this machine saves and retrieves information?

Generally, the human brain retrieves information from “memory”, which for the brain are a set of interconnected neurons. While neurons are quite slow in comparison to transistors in current computers also their functionality is quite different. For example, if you want to catch a ball, you need to estimate the trajectory of the ball to be able to catch it, which happens automatically in the brain through a derivative pattern that aligns with previously learned patterns influenced by certain parameters, such as estimated weight of the ball, force of throwing and environmental conditions such as wind etc. On the other hand, computers, would need to calculate each step of the trajectory to ensure that a robot catches the same ball (Tsang, 2017). An additional difference between computers and the brain lies in the fact that a computer uses separate memory in the form of memory cards and hard drives, and does not store data automatically, while the brain seems to be one large pattern focused memory that stores/adjusts continuously.

Expected Outcome: Currently, very few machine learning algorithms care about the information coming from the environment. It would therefore be interesting to identify suitable ways to use multilevel alignment for information to create patterns like those in the brain. These machines should then also be able to retrieve data automatically, and even predict the output results based on incomplete patterns being presented. While overall, the data would be stored efficiently due to the inherent compression, the system would easily be able to learn and continuously improve its patterns. Our research will propose such a multi-level model, build a prototype simulation and evaluate its performance against baseline methods.

Discussion: Input to the human brain travels through the cerebellum and striatum, before reaching the cortex. Within the cortex, it is generally believed that there would be one unique algorithm that processes the information which is received from sensory organs. The cortex also stores information as patterns in a hierarchical structure. However, it appears that the brain does not know the difference between information received from sensory organs and virtual creations of the brain itself. Consequently, being able to create a multilevel hierarchy to store different patterns will help a machine to learn in a way like us humans, and should then also allow the machine to deliver similar functionality to that of the human brain.

REFERENCES

Hawkins, J. (2005). *On Intelligence*. New York: Holt Paperback.

Tsang, W. (2017). *The Fractal Brain Theory*, 1st Edn. Morrisville: Lulu Press Inc. Available at: <http://www.Lulu.com>

Wolff, J. G. (2016). The SP theory of intelligence and the representation and processing of knowledge in the brain. *Front. Psychol.* 7:1584. doi: 10.3389/fpsyg.2016.01584 PMID:NOPMID

The Basal Ganglia of the Hemispheres: Physiology, Function and Clinical Syndromes of Defeat

Jakhongir S. Musinov, Aziza T. Djurabekova, Sabina F. Ganieva, Farrukh T. Fayzullaev, Shokhzod Shamsiev, Jamshid Shamsiyev

*Samarkand State Medical Institute, Samarkand, Uzbekistan
musinov-92@mail.ru*

Objective: to explore the role of the basal ganglia of the hemispheres in the human organism, their physiology and pathology.

Materials and Methods: An analysis of the scientific literature.

Results and Discussion: The role of the basal ganglia in humans, despite the fact that in their origin, these formations are older, is still very high. In lower vertebrates, the basal ganglia is the main center of coordination of movements, but in humans, due to the complexity of its motor activity, these centers fall under the control of the cerebral cortex. The basal ganglia are a type of nuclear structures which are located in the white matter of the forebrain thicker closer to the base. In mammals, to the basal ganglia are strongly elongate and curved caudate nucleus and inherent in the white matter thicker lenticular nucleus. With two white plates it divided into three parts: the most major, which lies laterally shell and globus pallidus, consisting of internal and external departments. These anatomical structures form the so-called striopallidarnoy system, which also will be discussed in our work. In this study, a greater role is given to not only the anatomy as the physiology of both normal and pathological conditions. The basal ganglia play an important role in the regulation of movements and sensorimotor coordination. It is known that in case of damage striatum observed athetosis—slow worm-like movements of hands and fingers. Degeneration of the striatum cells and cause other disease—chorea, jerking expressed in facial muscles and limbs muscles, which are observed at rest and when performing voluntary movements. However, attempts to clarify the etiology of these disorders in the animal experiments described in the literature have not yielded results. Time-violation of the caudate nucleus in dogs and cats does not lead to the appearance of hyperkinesia characteristic of the above-mentioned diseases. Local electrical stimulation of certain areas of the striatum causes in animals so-called circulatory motor reactions, characterized by turning the head and torso in the opposite irritation. Irritation of the other portions of the striatum, by contrast, leads to inhibition of motor responses induced different sensory stimuli. It follows from the foregoing that these brain structures are very important for our body and their role in medicine in any case should not be leveled.

Modeling of Blood Flow in Branching Vessels of the Human Brain

Sabina F. Ganieva, Aziza T. Djurabekova, Jakhongir Sh Musinov, Farrukh T. Fayzullaev

*Samarkand State Medical Institute, Samarkand, Uzbekistan
bailando777@mail.ru*

The purpose of research—to trace changes in the Reynolds number and blood pressure, depending on the angle of the branch vessels of the brain. The method of mathematical modeling studied two-dimensional flow field velocity and pressure distribution in the field of bifurcation vascular base of the brain. Model calculations were carried out with the help of numerical simulation package COMSOL 4.0, which solves a system of nonlinear partial differential equations, finite element method in one, two and three dimensions. At the same time we took into account the fact that adult adulthood in branching vascular base of the brain (the internal carotid artery, basilar artery) have atherosclerotic plaques, that reduces the lumen of the vessel. The average speed of the blood flow at the entrance to the mother vessel in the internal carotid and basilar arteries—0.46 m/s (aged 50–55 years). Maternal vessel, we constructed geometric model, divided into two subsidiary vessel so that the sectional area of the exhaust vessel was equal to the total cross-sectional area of the parent vessel. As a result, changes in the angle of bifurcation of the received model parameters identified in the geometric form of changes in the local flow velocity and, therefore, local Reynolds number and the pressure drop. The subsidiary vessels tend to flow turbulence. The greatest pressure is observed in the apical branching angle explained that the maximum blood flow influence on its wall. By increasing the thickness “atherosclerotic plaque” (build-up of stenosis) increases the maximum Reynolds number and reduces the pressure of apical angle of vessel bifurcation, and conversely, the smaller plaque, the smaller the maximum number Re and the greater the pressure of blood. The change of the Reynolds number and blood pressure is most pronounced when you reject a vessel with a smaller diameter to 45–55°. Conclusion. Thus, from a study set optimum angle subsidiary branch vessel (smaller diameter) of the parent (about 55°), in which blood flow occurs artery stenosis place with minimal energy loss. The region of the greatest flow of blood pressure—the apical region of the bifurcation angle.

Neural Dynamics and Inter-Brain Synchronization Underlying the Use of Nonverbal Social Cues to Read Other's Intentions to Cooperate

Jaehwan Jahng¹, Dong-Uk Hwang², Jerald D. Kralik¹,
Jaeseung Jeong¹

¹KAIST, Daejeon, South Korea

²NIMS, Daejeon, South Korea

jahngjh.627@gmail.com

Social interaction is a fundamental part of our daily lives; however, exactly how our brains use social cues to read the intentions of others to determine whether to cooperate without being exploited remains unclear. In this study, we used EEG hyperscanning to investigate the effect of face-to-face contact on the brain mechanisms underlying the decision to cooperate or defect in an iterated version of the Prisoner's Dilemma Game. Participants played the game either in face-to-face (FF) or face-blocked (FB) conditions. The FF interaction led players to cooperate more often, providing behavioral evidence for the use of these nonverbal cues in their social decision making. In addition, the EEG hyperscanning identified temporal dynamics and inter-brain synchronization across the cortex, providing evidence for involvement of these regions in the processing of FF cues to read each other's intent to cooperate. Most notably, the power of the alpha frequency band (8–13 Hz) in the right temporoparietal region immediately after seeing a trial outcome significantly differed between FF and FB conditions and predicted whether an individual would adopt a 'cooperation' or 'defection' strategy. Moreover, inter-brain synchronies within this time and frequency range reflected the use of these strategies. Our study provides evidence for how the cortex uses nonverbal social cues to determine other's intentions, and highlights the significance of power in the alpha band and inter-brain phase synchronizations in high-level socio-cognitive processing.

REFERENCE

Jahng, J., Kralik, J.D., Hwang, D. U., Jeong, J. (2017). Neural dynamics of two players when using nonverbal cues to gauge intentions to cooperate during the Prisoner's Dilemma Game. *Neuroimage*, 157, 263–74. doi: 10.1016/j.neuroimage.2017.06.024.

Dissecting the Effect of 16p11.2 Gene Dosage on Brain Structure

Sandra Martin-Brevet^{1,2}, **B. Rodriguez-Herreros**^{1,3}, **C. Moreau**³, **A.M. Maillard**^{1,4}, **A. Pain**¹, **C. Modenato**^{1,2}, **S. Richetin**¹, **N. Zurcher**⁵, **16p11.2 European Consortium**⁶, **Simons Variation In Individuals Project Consortium**⁷, **A. Reymond**⁸, **N. Hadjikhani**^{5,9}, **B. Draganski**², **S. Jacquemont**^{1,3}

¹Service of Medical Genetics-CHUV, Lausanne, Switzerland

²Iren-CHUV, Lausanne, Switzerland

³Sébastien Jacquemont's Lab-Chu Sainte Justine, Montréal, QC, Canada

⁴Centre Cantonal De L'autisme-CHUV, Lausanne, Switzerland

⁵Harvard Medical School/MGH/MIT, Charlestown, MA, United States

⁶CHUV, Lausanne, Switzerland

⁷Simons Foundation, New York, NY, United States

⁸CIG, Lausanne, Switzerland

⁹Gillberg Neuropsychiatry Centre, Göteborgs, Sweden

sandra.martin15@gmail.com

Introduction: Copy Number Variants (CNVs) are major contributors to neurodevelopmental disorders-ND. CNVs represent structural variations of the chromosomes: deletion is a loss of genetic material (1 copy of the genomic region); duplication is a gain of genetic material (3 copies), while controls have usually 2 copies of each genomic region. Also, gene dosage is linked to the number of genetic copies.

Carriers of the deletion or duplication at the 16p11.2 locus (29.6–30.2 Mb-Hg 19) have a 10-fold increased risk of developing autism spectrum disorder (ASD) and ~20% of carriers ascertained of a ND meet criteria for ASDs (Zufferey et al., 2012; D'angelo et al., 2015). These 16p11.2 CNVs present an inverse gene dosage on head circumference-HC (macrocephaly for deletion and microcephaly for duplication) and on global brain metrics, as Total Intracranial Volume-TIV, Gray Matter-GM and White Matter-WM Volumes 3,4. Maillard et al. (Maillard et al., 2015) also found regional structural changes between deletion and duplication carriers in key areas of the reward system, language circuitry and social cognition, overlapping with brain regions involved in ASD. The small sample sizes of these studies did not allow to explore any other factors that may contribute to the neuroanatomic changes.

The aim of this study was to analyze a much larger sample size of 16p11.2 CNV carriers to: 1) Replicate, quantify and extend previously published findings. We pooled data from multiple cohorts and scanning sites. 2) Demonstrate that in the context of

a genetically homogeneous sample, the noise introduced by pooling multiple sites is limited in comparison to the increased power. 3) Characterize and distinguish the effect of the 16p11.2 CNVs from the effects of additional factors present in carriers who are ascertained for a neurodevelopmental disorder-ND.

Methods

Participants: Participants, above 6 year-old, were evaluated in two cohorts: the European—EU 16p11.2 consortium and the Simons VIP—SVIP study in the United States. All families were ascertained through a proband referred for genetic testing on the basis of ND. Enrollment in the SVIP cohort included referral by clinical genetic centers, web-based networks, active online registration of families, while families were directly recruited by the referring physician in the European cohort. For the familial loading analyses, the control group has been subdivided in 3 distinct groups. “Deletion familial controls” represent the controls that have one member in their family carrying the deletion mutation. “Duplication familial controls” represent the controls that have one member in their family carrying the duplication mutation. “Non-familial controls” are the extrafamilial controls, unrelated to the CNV carriers.

MRI data acquisition and processing: 361 participants were examined on 3T whole body scanner, on 7 different sites (2 sites in Europe and 5 sites in USA). T1-weighted anatomical images were acquired using a multi-echo magnetization prepared rapid gradient echo sequences (MEMPRAGE) on 264 participants and using single-echo MPRAGE sequences on 97 participants. All the ME-MPRAGE images have been averaged following a Root-Mean Square method (RMS) to obtain one echo per participant.

Global morphometric analyses were performed with FreeSurfer version 4.5.0 software package (<http://surfer.nmr.mgh.harvard.edu>), using the template of Qureshi et al. (Qureshi et al., 2014) Voxel-based morphometry (VBM) analyses were performed using the SPM12 software package (Statistical Parametric Mapping software, <http://www.fil.ion.ucl.ac.uk/spm/software/spm12>) running under Matlab 7.13 (Mathworks Inc., Sherborn, MA). The algorithm followed the default settings for the segmentation, using a novel set of brain tissue priors showing increased accuracy for subcortical structures (Lorio et al., 2016). GM probability maps were spatially registered to a standardized Montreal Neurological Institute space using the diffeomorphic algorithm based on exponentiated Lie algebra—DARTEL6. They were scaled with the corresponding Jacobian determinants and spatially smoothed using an isotropic Gaussian kernel of 8 mm full-width-at-halfmaximum.

Data analysis: Global metrics were corrected for linear and quadratic polynomial expansion of age, gender, site, Non Verbal Intelligent Quotient (NVIQ) as fixed factors.

VBM analyses used all GM data, in the General Linear Model framework of SPM12. Deletion, controls and duplication carriers were considered as the genetic groups. The model included the same regressors as the analysis of global metrics as well as TIV. Statistical thresholds were applied at $p < 0.05$ after family-wise error (FWE) correction for multiple comparisons over the whole volume of the GM mask. We computed Cohen d on FWE-corrected t-score maps to show the effect size.

Results: We analyzed MRI data in 78 16p11.2 deletion carriers and 51 of their 1st degree relatives who do not carry the deletion (familial controls), 71 duplication carriers and 21 duplication familial controls, as well as 140 controls unrelated to the CNV carriers. There were no significant differences in gender ratio across genetic groups and cohorts. Age distribution differed for deletions and controls being younger in the SVIP cohort compared to the EU cohort, and deletion carriers were overall significantly younger than the rest of the groups. Eleven deletion and 8 duplication carriers met criteria for ASD (13%).

Global brain metrics (Figure 1): Our results were in agreement with the well-established negative correlation between head circumference and the number of genomic copies at the 16p11.2 locus both in SVIP ($p < 0.0001$) and European ($p = 0.001$) cohorts. Consistently, estimated TIV also correlated negatively with the number of 16p11.2 copies, although this significance of effect was weaker in the European cohort ($p < 2e-16$ for SVIP and $p = 0.04$ for EU). Both GM and WM total volumes contributed to the observed effect on estimated TIV. Decomposition of volume in surface-based measures showed a comparable effect in cortical surface area in both cohorts, but no effect on cortical thickness.

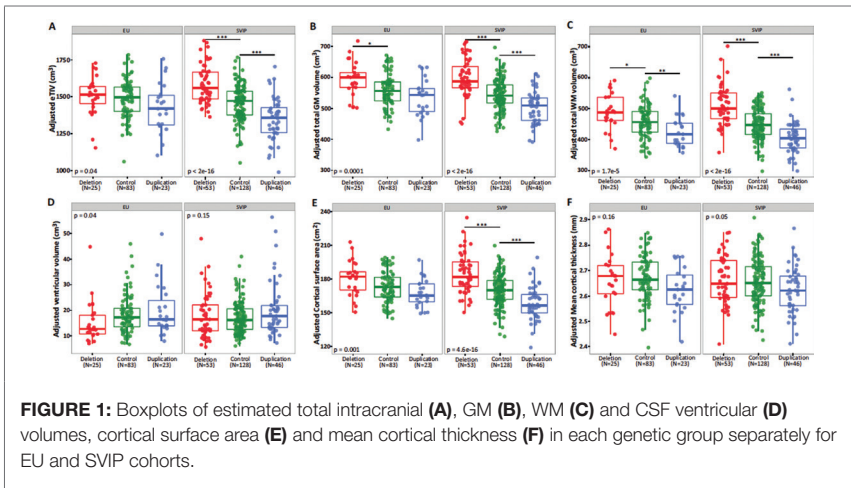
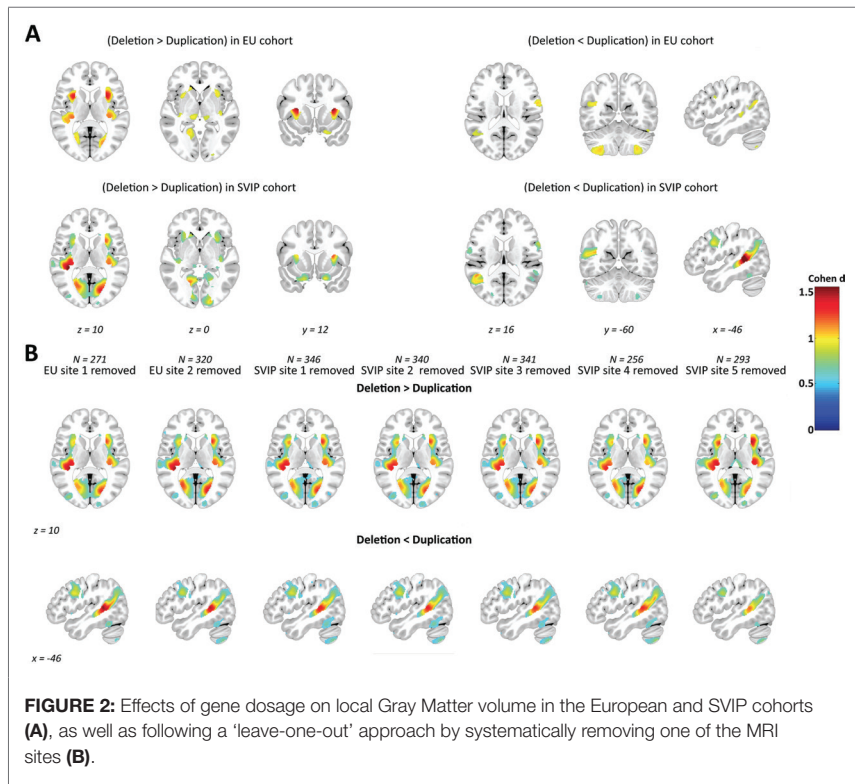
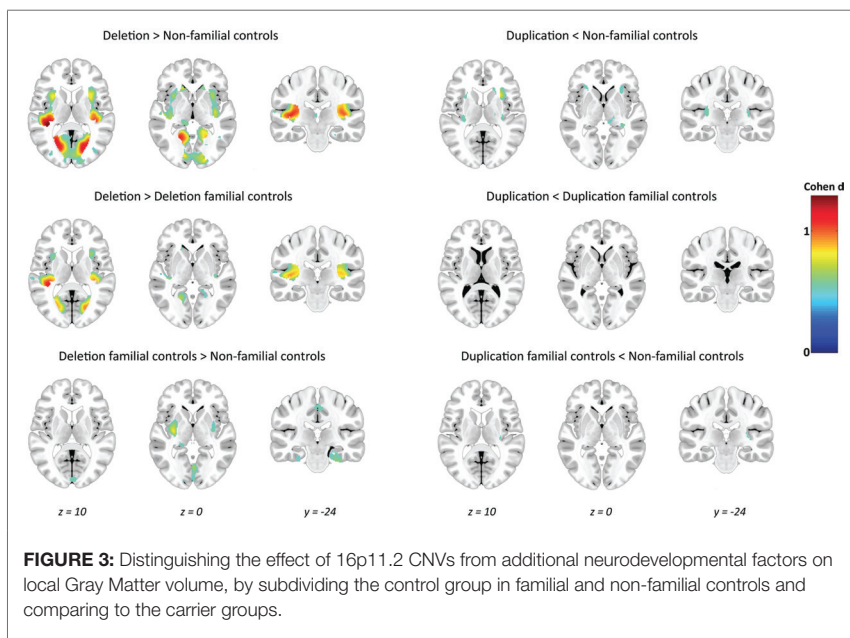


FIGURE 1: Boxplots of estimated total intracranial (A), GM (B), WM (C) and CSF ventricular (D) volumes, cortical surface area (E) and mean cortical thickness (F) in each genetic group separately for EU and SVIP cohorts.

Regional brain differences in the EU and USA cohorts (Figure 2): Voxel-based morphometry showed a pattern of regional changes which strongly correlated to the 16p11.2 gene dosage, replicating our initial findings (Maillard et al., 2015). Specifically, linear regression using the number of genomic copies (DEL=1 CTRL=2 > DUP=3) as an explanatory variable identified in both cohorts a negative relationship with the volume of bilateral anterior and posterior insula, transverse temporal gyri and calcarine cortex. Both cohorts presented a positive relationship between the number of genomic copies and the bilateral precentral gyri, left middle and superior temporal gyri and cerebellar lobule VIII. We didn't find any interaction between genetic status and the 2 cohorts, the 7 sites, gender or age. Ascertainment methods in EU and SVIP cohorts led to the same local brain differences. Results were also stable across the 7 iterative analyses successively leaving out one of the scanning sites. Results were identical across ages: subdividing the genetic group in 2 categorical age groups (below and above 16 year-old) showed the same profile of structural brain abnormalities.



Distinguishing the effect of 16p11.2 CNVs from additional neurodevelopmental factors (Figure 3): We compared the regional differences between the carriers and their respective non-carrier familial controls. Deletion carriers exhibited an increased volume in bilateral insula, calcarine cortex and left superior temporal gyrus, compared to their familial controls. In its turn, these controls showed an increased volume in bilateral fusiform gyrus, parahippocampus, amygdala, putamen, compared to the non-familial controls. The same analysis yielded weaker or non significant effects for the duplication carriers compared to their familial controls and to the non-familial controls. Alterations observed in 16p11.2 CNV carriers ascertained for a neurodevelopmental disorder should result from a cumulative effect of: (i) the 16p11.2 CNVs and (ii) additional factors.



Conclusion: The robustness and power of this combined dataset demonstrated that multi-site MRI studies are extremely relevant in autism and neurodevelopmental disorders, when neurobiological heterogeneity can be reduced by focusing on individuals who share a common ASD risk factor. The increased power of the cohort has allowed us to answer new questions: 1) The regional brain alterations were present across children, adolescents and adults. 2) Carriers of a 16p11.2 CNV demonstrated neuroanatomical

alteration due to the CNV as well as additional factors visible in first-degree relatives, suggesting an additive neurodevelopmental and possibly genetic effect.

Acknowledgment: This study was supported by a Bursary Professor fellowship of the Swiss National Science Foundation (SNSF).

REFERENCES

- Ashburner, J. (2007). A fast diffeomorphic image registration algorithm. *Neuroimage* 38, 95–113. doi: 10.1016/j.neuroimage.2007.07.007 PMID:17761438
- D'angelo, D., Lebon, S., Chen, Q., Martin-Brevet, S., Snyder, L. G., Hippolyte, L., et al. (2015). Defining the effect of the 16p11.2 duplication on cognition, behavior, and medical comorbidities. *JAMA Psychiatry* 73, 20–44. doi: 10.1001/jamapsychiatry.2015.2123 PMID:NOPMID
- Lorio, S., Fresard, S., Adaszewski, S., Kherif, F., Chowdhury, R., Frackowiak, R. S., et al. (2016). New tissue priors for improved automated classification of subcortical brain structures on MRI. *Neuroimage* 130, 157–166. doi: 10.1016/j.neuroimage.2016.01.062 PMID:26854557
- Maillard, A. M., Ruef, A., Pizzagalli, F., Migliavacca, E., Hippolyte, L., Adaszewski, S., et al. (2015). The 16p11.2 locus modulates brain structures common to autism, schizophrenia and obesity. *Mol. Psychiatry* 20, 140–147. doi: 10.1038/mp.2014.145 PMID:25421402
- Qureshi, A. Y., Mueller, S., Snyder, A. Z., Mukherjee, P., Berman, J. I., Roberts, T. P., et al. (2014). Opposing brain differences in 16p11.2 deletion and duplication carriers. *J. Neurosci.* 34, 11199–11211. doi: 10.1523/JNEUROSCI.1366-14.2014 PMID:25143601
- Zufferey, F., Sherr, E. H., Beckmann, N. D., Hanson, E., Maillard, A. M., Hippolyte, L., et al. (2012). A 600 kb deletion syndrome at 16p11.2 leads to energy imbalance and neuropsychiatric disorders. *J. Med. Genet.* 49, 660–668. doi: 10.1136/jmedgenet-2012-101203 PMID:23054248

Cytoarchitectonic Mapping and Ultrahigh-Resolution 3D Reconstruction of the Bed Nucleus of Stria Terminalis

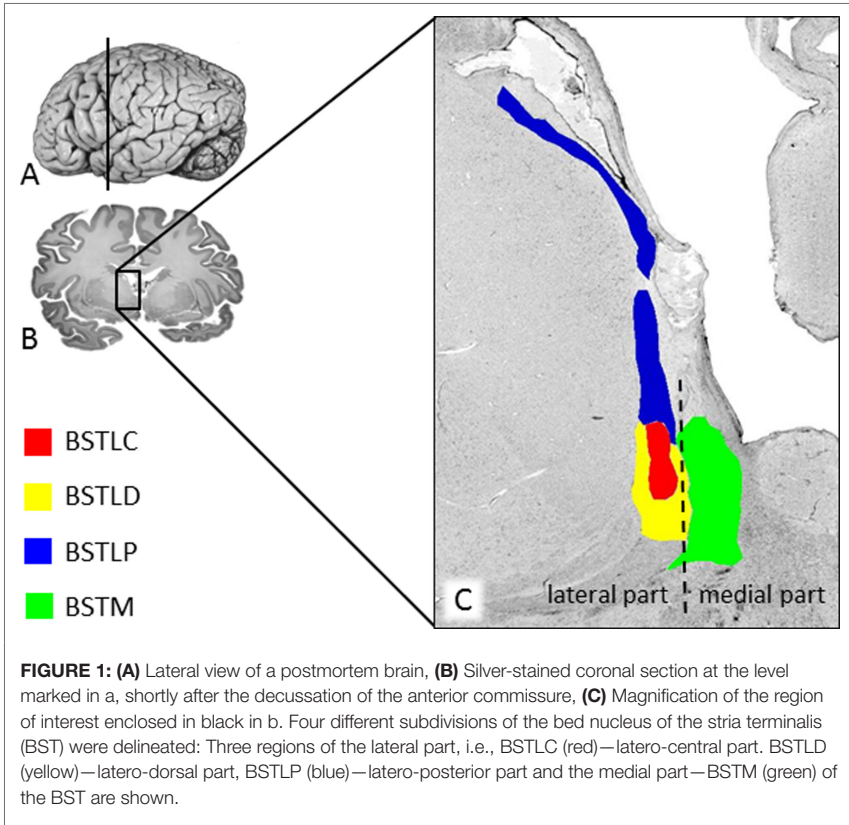
Andrea Brandstetter, Hartmut Mohlberg, Katrin Amunts

Forschungszentrum Jülich, Jülich, Germany
a.brandstetter@fz-juelich.de

Introduction/motivation: High-resolution brain atlases are a tool to find out more about human brain organization and its functions. Step by step each region of the brain has been mapped within a long-term effort to achieve this aim, and maps have been made available to public (Amunts and Zilles, 2015). The ongoing research focuses on the bed nucleus of the stria terminalis. The bed nucleus gets inputs from amygdala and hippocampus and has efferent connections to the hypothalamic region or the brainstem (Heimer and van Hoesen, 2006). The bed nucleus is involved in cortico-subcortical circuits affecting emotional processes such as fear and anxiety response, stress or motivation (Heimer and van Hoesen, 2006; Alvarez et al., 2011). The aim of this project is to delineate the bed nucleus of the stria terminalis in ten postmortem human brains, and to generate probability maps in stereotaxic space, which consider interindividual variability in size and localization of this brain region.

Methods: Ten postmortem brains, five male and five female, were fixed, paraffin-embedded and serially sectioned in coronal plane. Every 15th section (each 20 μ m thick) was mounted and silver-stained for cell bodies (Merker, 1983). Histological processing was previously described in detail (Amunts et al., 1999). The sections were digitized for tracing the structures of the bed nucleus and the subsequent 3D-reconstruction. The delineation is based on cytoarchitectonic criteria, which enable to distinguish the bed nucleus of the stria terminalis from its neighbouring structures. Criteria include the shape, size or density of the neurons, as well as the density and distribution of glial cells. When the mapping is finished in all ten brains, the bed nucleus will be 3D reconstructed, registered to the MNI (Montreal Neurological Institute) single-subject brain template and then superimposed. This leads to so-called probability maps, showing the frequency of the bed nucleus in each voxel of the MNI reference space with values ranging from 0 to 100% in a certain region (Amunts and Zilles, 2015).

Results: The bed nucleus of the stria terminalis (BST) is located in the basal forebrain, close to the striatum and the lateral ventricles (Figures 1A,B). The bed nucleus is divided into two major subnuclei, the medial (BSTM) and the lateral bed nucleus of the stria terminalis (deOlmos, 2004; Heimer and van Hoesen, 2006).



The results show that the lateral BST is further subdivided into three parts (Figure 1C): The laterocentral part (BSTLC) consists of triangular and fusiform neurons and is surrounded by a cell-poor area. In coronal sections the BSTLC appears at the level of the decussating anterior commissure. It is in most sections enclosed by the laterodorsal subdivision (BSTLD), which is characterized by frequently appearing islets, consisting of cell aggregates without any particular orientation of the neurons. Finally, the lateroposterior part (BSTLP) consists of smaller, lightly stained neurons as well as some bigger darkly stained neurons. This subdivision contains a substantial number of stria terminalis fibres, as it also extends dorsally towards the Nucleus caudatus. The BSTLP appears first shortly after the decussation of the anterior commissure in coronal sections and replaces the other subdivisions gradually. The BSTM mainly consists of small and densely packed neurons, but also contains larger more darkly stained neurons of various shapes, which leads to a heterogeneous appearance.

Discussion: Our results show four different subdivisions of the bed nucleus of the stria terminalis (BST), which were delineated according to their cytoarchitecture. Two examples regarding the cytoarchitecture as well as a functional aspect shall be briefly discussed in this passage: The BST as a whole was divided into a lateral and medial subnucleus, following the suggestions of Heimer and van Hoesen (2006), Heimer et al. (1999), and deOlmos (2004). In the lateral BST, the encapsulated central BST is classified within the dorsolateral subdivision of the BST. Avoiding one additional hierarchical step the BSTLC was considered as a part of the lateral subnucleus in this research project, equal to the other subdivisions, BSTLD and BSTLP.

On a functional level authors state, that the encapsulated central part of the BST is bigger in male than in female brains and it is responsible for sexual differentiation (Chung et al., 2002). Whether this sexual dimorphism can be confirmed will be answered as soon as all ten brains are reconstructed.

By obtaining probability maps of the bed nucleus of the stria terminalis with its distinct subdivisions will be one step forward, to achieve the overall goal of building a precise atlas of the human brain.

REFERENCES

- Alvarez, R. P., Chen, G., Bodurka, J., Kaplan, R., and Grillon, C. (2011). Phasic and sustained fear in humans elicits distinct patterns of brain activity. *Neuroimage* 55, 389–400. doi: 10.1016/j.neuroimage.2010.11.057 PMID:21111828
- Amunts, K., Schleicher, A., Bürgel, U., Mohlberg, H., Uylings, H. B. M., and Zilles, K. (1999). Broca's region revisited: cytoarchitecture and intersubject variability. *J. Comp. Neurol.* 412, 319–341. doi: 10.1002/(SICI)1096-9861(19990920)412:2<319::AID-CNE10>3.0.CO;2-7 PMID:NOPMID
- Amunts, K., and Zilles, K. (2015). Architectonic mapping of the human brain beyond Brodmann. *Neuron* 88, 1086–1107. doi: 10.1016/j.neuron.2015.12.001 PMID:26687219
- Chung, W. C. J., deVries, G. J., and Swaab, D. F. (2002). Sexual differentiation of the bed nucleus of the stria terminalis in humans may extend into adulthood. *J. Neurosci.* 22, 1027–1033. ISSN: 0270-6474 no affiliated doi
- deOlmos, J. S. (2004). "Amygdala," in *The Human Nervous System*, eds G. Paxinos and J. K. Mai (Amsterdam: Elsevier), 739–868.
- Heimer, L., deOlmos, J. S., Alheid, G. F., Pearson, J., Sakamoto, N., Shinoda, K., et al. (1999). "The human basal forebrain, part II," in *Handbook of Chemical Neuroanatomy, Volume 15: The Primate Nervous System, Part III*, eds A. Björklund and T. Hökfelt (Amsterdam: Elsevier), 57–226.
- Heimer, L., and van Hoesen, G. W. (2006). The limbic lobe and its output channels: implications for emotional functions and adaptive behavior. *Neurosci. Biobehav. Rev.* 30, 126–147. doi: 10.1016/j.neubiorev.2005.06.006 PMID:16183121
- Merker, B. (1983). Silver staining of cell bodies by means of physical development. *J. Neurosci. Methods* 9, 235–241. doi: 10.1016/0165-0270(83)90086-9 PMID:6198563

Synptology of Layer II of the Transentorhinal Cortex in Alzheimer's Disease

**Marta Domínguez-Álvarez¹, Lidia Alonso-Nanclares^{1,2,3},
Javier DeFelipe^{1,2,3}**

¹Laboratorio Cajal de Circuitos Corticales, Centro de Tecnología Biomédica, Universidad Politécnica de Madrid, Madrid, Spain

²Instituto Cajal, Consejo Superior de Investigaciones Científicas (CSIC), Madrid, Spain

³Centro de Investigación Biomédica en Red sobre Enfermedades Neurodegenerativas (CIBERNED), ISCIII, Madrid, Spain

martadominguezalvaro@gmail.com

Introduction: Alzheimer's disease (AD) is the main cause of dementia, accounting for 60–80% of cases (Alzheimer's Association, 2015). It is characterized by a progressive and persistent decline of superior cerebral functions, such as memory, language and direction. In the final stages of the disease, there is a lack of autonomy, and, in general, a lack of labor activity and social life (Prieto et al., 2011). During the course of the disease, three main histopathological alterations occur: cerebral atrophy, intracellular neurofibrillary tangles (which are made of misfolded and abnormally hyperphosphorylated tau protein) and amyloid plaques (which result from the abnormal extracellular accumulation of the amyloid- β peptide; Figure 1; Raskin et al., 2015). In addition to these three histopathological alterations, other changes have also been described: neural and synaptic loss; gliosis; vascular degeneration; cerebral amyloid angiopathy (A β peptide deposition in blood vessels); degeneration of the white matter; and aggregation of other proteins (e.g., Lewy bodies; Raskin et al., 2015).

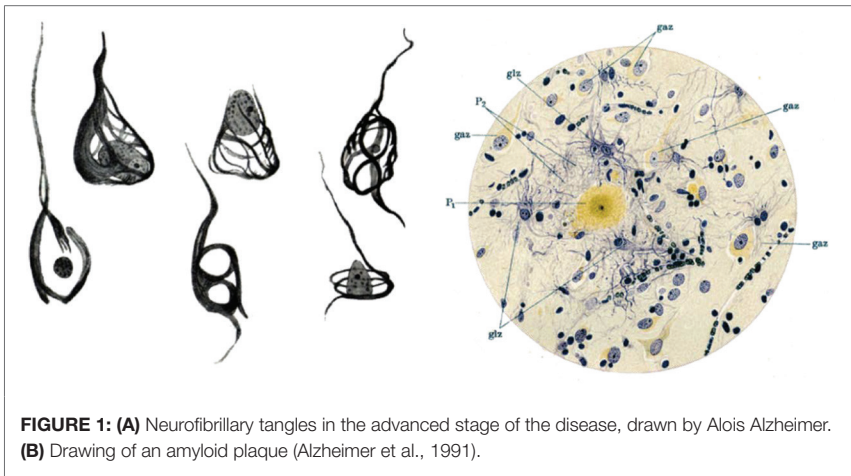


FIGURE 1: (A) Neurofibrillary tangles in the advanced stage of the disease, drawn by Alois Alzheimer. **(B)** Drawing of an amyloid plaque (Alzheimer et al., 1991).

Early loss of episodic memory in AD patients is closely associated with the progressive degeneration of the medial temporal lobe structures, with the transentorhinal cortex (TEC) being one of the first affected areas (Braak and Braak, 1991). From a cytoarchitectonic perspective, the TEC is considered as a transitional zone between the entorhinal cortex (EC) and the temporal cortex (Braak and Braak, 1985). The TEC is formed by different layers, and its main cytoarchitectonic feature is that layers III and V merge and sweep obliquely to invade layer II of the EC (Braak and Braak, 1985; Taylor and Probst, 2008; Ding and Van Hoesen, 2010).

Methods: In this study, we performed an ultrastructural analysis of the neuropil from layer II of the TEC, using human brain tissue from 5 patients with AD and from 5 subjects with no apparent neurological diseases (Figure 2). We used an instrument that combines a high-resolution field-emission SEM column with a focused gallium ion beam (FIB), which allows thin layers of material to be removed from the sample surface on a nanometer scale. As soon as one layer of material has been removed by the FIB, the exposed surface of the sample is imaged by the SEM. The sequential and automated use of FIB milling and SEM imaging allows us to obtain long series of photographs that represent a three-dimensional sample of the selected regions to be analyzed (Blazquez-Llorca et al., 2013). Customized analysis software was used for the reconstruction of synapses of the layer II neuropil, which allowed their number, morphology and spatial distribution to be calculated (EspINA software, v.2.1.9; Morales et al., 2011).

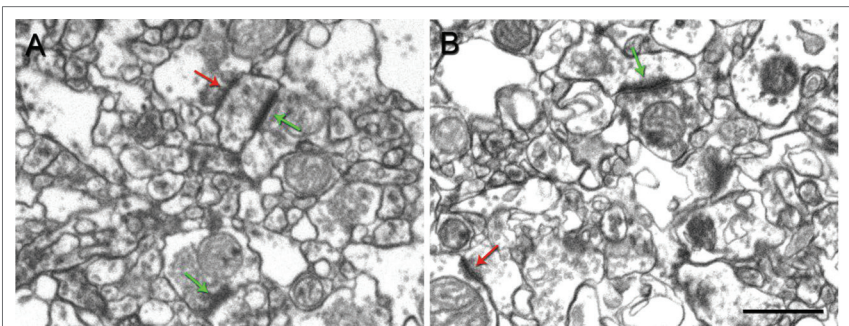


FIGURE 2: Photographs obtained by FIB/SEM microscopy illustrating the layer II neuropil of the transentorhinal cortex from a non-demented subject (**A**) and a subject with AD (**B**), showing the two types of synapses: asymmetrical (green arrows) and symmetrical (red arrow). Scale: 800 nm.

Results: Our preliminary results, from one image stack per subject, show that the total number of synapses per volume in layer II of the TEC in AD patients was significantly lower than the total number in non-demented subjects. We have not found differences in the morphology of the synapses in AD patients compared with non-demented subjects. In addition, the spatial organization of synapses in the neuropil of layer II of the TEC is random, regardless of the subject group.

REFERENCES

- Alzheimer, A., Forstl, H., and Levy, R. (1991). An English translation of Alzheimer's 1911 paper "Über eigenartige Krankheitsfalle des spateren Alters" (On certain peculiar diseases of old age). *Hist. Psychiatry* 2, 71–101. doi: 10.1177/0957154X9100200505 PMID:NOPMID
- Alzheimer's Association. (2015). Alzheimer's disease facts and figures. *Alzheimers Dement.* 11, 332–384. doi: 10.1016/j.jalz.2015.02.003 PMID:NOPMID
- Blazquez-Llorca, L., Merchán-Pérez, A., Rodriguez, J. R., Gascon, J., and DeFelipe, J. (2013). FIB/SEM technology and Alzheimer's disease: three-dimensional analysis of human cortical synapses. *J. Alzheimers Dis.* 34, 995–1013. doi: 10.3233/JAD-122038 PMID:23313928
- Braak, H., and Braak, E. (1985). On areas of transition between entorhinal allocortex and temporal isocortex in the human brain. Normal morphology and lamina-specific pathology in Alzheimer's disease. *Acta Neuropathol.* 68, 325–332. doi: 10.1007/BF00690836 PMID:4090943
- Braak, H., and Braak, E. (1991). Neuropathological staging of Alzheimer-related changes. *Acta Neuropathol.* 82, 239–259. doi: 10.1007/BF00308809 PMID:1759558
- Ding, S. L., and Van Hoesen, G. W. (2010). Borders, extent and topography of human perirhinal cortex as revealed using multiple modern neuroanatomical and pathological markers. *Hum. Brain Map.* 31, 1359–1379. doi: 10.1002/hbm.20940 PMID:NOPMID
- Morales, J., Alonso-Nanclares, L., Rodriguez, J. R., Defelipe, J., Rodriguez, A., and Merchán-Pérez, A. (2011). Espina: a tool for the automated segmentation and counting of synapses in large stacks of electron microscopy images. *Front. Neuroanat.* 5:18. doi: 10.3389/fnana.2011.00018 PMID:21633491
- Prieto, C., Eimil, M., López de Silanes, C., and Llanero, M. (2011). *Impacto social de la enfermedad de Alzheimer y otras demencias*. Fundación Española de Enfermedades Neurológicas. Available at: http://www.fundaciondelcerebro.es/docs/imp_social_alzheimer.pdf (in spanish)
- Raskin, J., Cummings, J., Hardy, J., Schuh, K., and Dean, R. A. (2015). Neurobiology of Alzheimer's disease: Integrated molecular, physiological, anatomical, biomarker, and cognitive dimensions. *Curr. Alzheimer Res.* 12, 712–722. doi: 10.2174/1567205012666150701103107 PMID:26412218
- Taylor, K. I., and Probst, A. (2008). Anatomic localization of the transentorhinal region of the perirhinal cortex. *Neurobiol. Aging* 29, 1591–1596. doi: 10.1016/j.neurobiolaging.2007.03.024 PMID:17478012

A Fusion Mechanism for Depth Cues in the Primate Brain

**Marcelo Armendariz¹, Hiroshi Ban², Andrew Welchman³,
Wim Vanduffel^{1,4,5}**

¹Laboratory of Neuro- and Psychophysiology, KU Leuven, Leuven, Belgium

²Graduate School of Frontier Biosciences, Osaka University, Osaka, Japan

³Department of Psychology, University of Cambridge, Cambridge, United Kingdom

⁴Department of Radiology, Harvard Medical School, Boston, MA, United States

⁵Athinoula A. Martinos Center for Biomedical Imaging, Massachusetts General Hospital, Charlestown, MA, United States

marcelo.armendariz@kuleuven.be

To reconstruct the third dimension from flat retinal images, the brain exploits a range of monocular and binocular depth cues. However, the neural mechanisms underlying cue integration is still poorly understood. Traditionally, this process has been broadly conceived in modular terms, with the independent processing of individual cues followed by a combination stage in which the influence of each cue reflects the reliability with which it is encoded. Computational and recent imaging studies in humans suggested the existence of a fusion mechanism that combines the information of different depth cues (Ban et al., 2012; Murphy et al., 2013). In particular, the latter studies showed, rather unexpectedly based on previous monkey research, that area V3B/KO may house neurons coding for a fusion mechanism of different depth cues. To investigate cue integration in monkeys using exactly the same paradigm as in Ban et al. (2012), we performed an equivalent fMRI study. Specifically, we showed monkeys a set of stimuli representing near or far depth planes defined by motion parallax, binocular disparity and the combination of both in either a congruent (i.e., the two cues signal the same depth planes) or incongruent fashion (i.e., the two cues signal different depth planes). We used a linear support vector machine to classify between near and far patterns in retinotopically defined regions of interest (ROI) of visual cortex. To quantify differences in prediction accuracies across conditions and to assess fusion, we conducted three test for cue integration: integration index, congruent vs incongruent cues and transfer index [similar to Ban et al. (2012)]. We found that fMRI responses are more discriminable when the two cues signal depth concurrently, and that depth information provided by one cue might be diagnostic of depth indicated by the other. We revealed that monkey area MT shows fMRI signals consistent with a fusion mechanism of independent depth cues. In fact, these results may reconcile the human imaging data with previous monkey electrophysiological studies implicating area MT in depth perception based on motion and binocular disparity signals (Nadler et al., 2008; Nadler et al., 2013; DeAngelis et al., 1998). In general, our findings together

with those obtained in humans provide evidence for a fusion mechanism for depth perception in the dorsal stream of primates. The fusion of depth cues, however, appears to be computed in different areas in humans (V3B/KO) and monkeys (MT). Therefore it is tempting to speculate that human V3B/KO may have been part of the MT cluster in an ancestor of monkeys and humans which has drifted in a caudo-dorsal direction during human evolution.

REFERENCES

- Ban, H., Preston, T. J., Meeson, A., and Welchman, A. E. (2012). The integration of motion and disparity cues to depth in dorsal visual cortex. *Nat. Neurosci.* 15(4), 636–643. doi: 10.1038/nn.3046
- DeAngelis, G. C., Cumming, B. G., and Newsome, W. T. (1998). Cortical area MT and the perception of stereoscopic depth. *Nature* 394, 677–680.
- Murphy, A. P., Ban, H., and Welchman, A. E. (2013). Integration of texture and disparity cues to surface slant in dorsal visual cortex. *J. Neurophysiol.* 110(1), 190–203. doi: 10.1152/jn.01055.2012
- Nadler, J. W., Angelaki, D. E., and DeAngelis, G. C. (2008). A neural representation of depth from motion parallax in macaque visual cortex. *Nature* 452(7187), 642–645. doi: 10.1038/nature06814
- Nadler, J. W., Barbash, D., Kim, H. R., Shimpi, S., Angelaki, D. E., and DeAngelis, G. C. (2013). Joint representation of depth from motion parallax and binocular disparity cues in macaque area MT. *J. Neurosci.* 33(35), 14061–74, 14074a.

Pre-Stimulus Brain State: A Possible Key to Vision Restoration?

Younes A. Tabi, Bernhard A. Sabel

*Institute for Medical Psychology; Otto-Von-Guericke-University, Magdeburg, Germany
younes.tabi@yahoo.de*

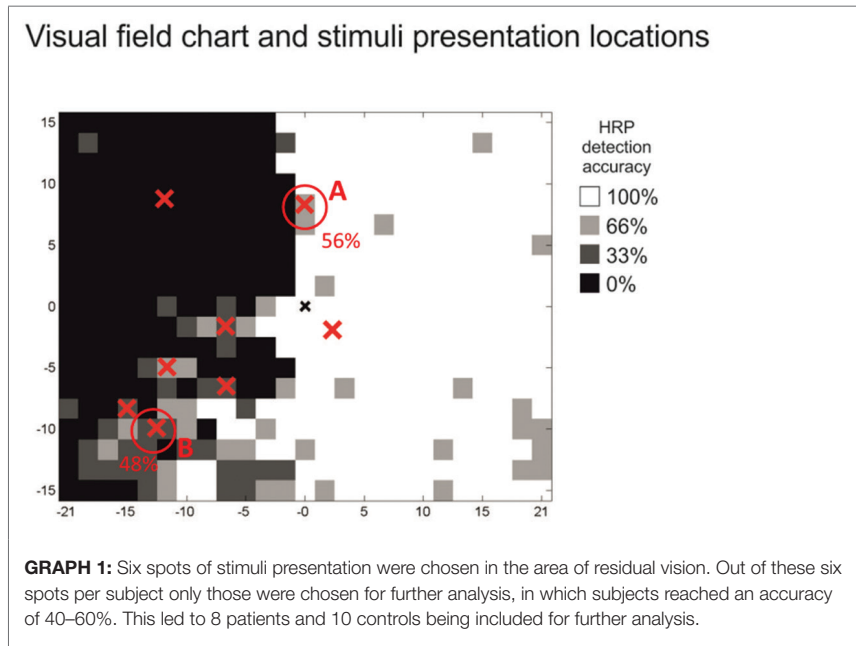
Background: There have been several near-threshold stimuli experiments that find EEG oscillations to be correlated to behavioral performance. In some of these studies the research was focused on pre-stimulus frequencies that find their correlates in cognitive discrimination such as high-alpha activity (Hanslmayr et al., 2007; van Diejk et al., 2008; Weisz et al., 2014). Though pre-stimulus investigation is becoming a more and more emerging field, there is still a gap in the present literature: There has been only very little investigation on the damaged visual system.

Aim: With High-Alpha Power as an important correlate of visual perception and previous clues for its importance in the pre-stimulus brain state, we try to frame High-Alpha oscillations not only in the context of visual discrimination in healthy controls but also in patients suffering from damage to their optic nerves. Thus previous studies show that a partially damaged visual field shows potential for recovery in training the underlying mechanisms are still broadly unknown. This study focuses on the difference of High-Alpha pre-stimulus brain states in vision of patients and healthy controls and how they might predict performance in a visual discrimination task. With this view on pre-stimulus brain state of patient's brain suffering from malfunctioned input, we try to encourage further research in this field.

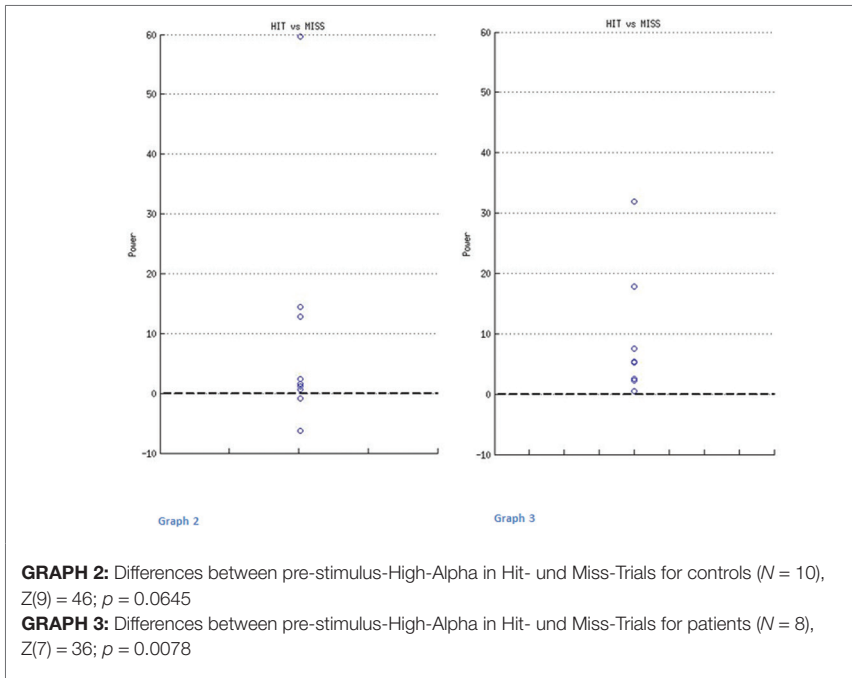
Question: Do patients suffering from vision loss due to optic nerve damage show different pre-stimulus High-Alpha power patterns than healthy controls?

Methods: We enrolled 34 subjects (19 suffering from monocular partial vision loss of different aetiologies, 15 controls) for this experiment. In patients we defined an area of no vision, an area of normal vision and a transition zone of intermediate vision. In healthy subjects we simulated this situation by defining areas of the same criterion in and around the physiological blind spot. We performed a monocular visual discrimination task while recording EEG, presenting 180 stimuli in each of six spots of "intermediate" vision. Subjects were asked to respond by button press once they see a stimulus while fixating a central fixation cross. As an ex-post threshold experiment

we only performed further investigation on spots of a.6/.4 up to .4/.6 discrimination rate to distinguish a sensitive pre-stimulus brain state (graph 1). This led to an exclusion of 11 patients and 5 controls. In a blinded analysis, individual pre-stimulus High-Alpha peaks were defined by sight for all participants (mean window size of 214.17 ms, SD = 113.68 ms and mean centre at $-262,64$ ms, SD = 94.09 ms). In a Wilcoxon-Test we compared the difference between High-Alpha amplitudes in trials in which participants detected the presented stimulus and those in which they did not for each group individually.



Results: In trials in which patients were able to see the stimulus, High-Alpha pre-stimulus amplitudes were at 1%-level significantly lower than in trials in which patients didn't see the stimuli. In controls we could not find a significant difference (Graphs 2 and 3).



Conclusion: The findings of our study support the importance of pre-stimulus brain state for visual stimulation. Based on the results, one reason for the brain's great ability to recover from malfunctioned input might be an adjustment of pre-stimulus correlates such as attention. In this model, a brain suffering from continuous malfunctioned visual input would adjust its processing resources to the source, working like an amplifier. We strongly encourage further research in this field.

REFERENCES

- Hanslmayr, S., Aslan, A., Staudigl, T., Klimesch, W., Herrmann, C. S., and Baeuml, K.-H. (2007). Pre-stimulus oscillations predict visual perception performance between and within subjects. *Neuroimage* 37, 1465–1473. doi: 10.1016/j.neuroimage.2007.07.011 PMID:NOPMID
- van Diejk, H., Schoffelen, J.-M., Oostenveld, R., and Jensen, O. (2008). Prestimulus oscillatory activity in the alpha band predicts visual discrimination ability. *J. Neurosci.* 28, 1816–1823. doi: 10.1523/JNEUROSCI.1853-07.2008 PMID:18287498
- Weisz, N., Wühle, A., Monittola, G., Demarchi, G., Frey, J., Popov, T., et al. (2014). Prestimulus oscillatory power and connectivity patterns predispose conscious somatosensory perception. *Proc. Natl. Acad. Sci. U.S.A.* 111, E417–E425. doi: 10.1073/pnas.1317267111 PMID:24474792

A Study Based on the Reconstruction of Multivesicular Bodies in the Rodent Somatosensory Cortex

Marta Turégano-López¹, Andrea Santuy¹, Javier Defelipe^{2,1}, Angel Merchán-Pérez^{1,3}

¹Centro De Tecnología Biomédica (UPM), Madrid, Spain

²Instituto Cajal (CSIC), Madrid, Spain

³Departamento De Arquitectura Y Tecnología De Sistemas Informáticos (UPM), Madrid, Spain

marta.turegano@ctb.upm.es

Multivesicular bodies (MVBs) are organelles surrounded by a single membrane containing intraluminal vesicles. They are intermediaries of the endosomal pathway and they participate in the sorting, recycling and degradation of proteins and other molecules (Von Bartheld and Altick, 2011). These organelles can fuse with the plasma membrane releasing exosomes into the extracellular space (Chivet et al., 2013). MVBs store and transport damaged cargo from mitochondria, helping them to maintain normal function (Sugiura et al., 2014). They are also known to accumulate the protein aggregates that are involved in Alzheimer's disease and Parkinson disease (Schreij et al., 2016).

We have analyzed the density, volume and spatial distribution of MVBs, as well as their location within axons or dendrites. We used three-dimensional electron microscopy with combined focused ion beam milling and scanning electron microscopy (FIB/SEM) (Merchán-Pérez et al., 2009)—a method that allows us to obtain long series of consecutive sections in an automated way. These stacks of serial sections can later be reconstructed and examined in 3D. We obtained 29 such stacks from the neuropil of the six cortical layers of the rat somatosensory cortex. Using specifically developed software (Espina) (Morales et al., 2011), we segmented and three-dimensionally reconstructed 2120 MVBs.

We found that MVBs located in dendrites outnumber those located in axons approximately 2:1, and dendritic MVBs are also twice as large as axonic MVBs. When studying the relation with mitochondria, we found that 18% of MVBs were docked to these organelles, and they were significantly larger than undocked ones. This relation between mitochondria and MVBs was more frequently found in dendrites than in axons. Another interesting finding was that about 7% of MVBs showed tubular extensions.

This kind of MVB is considered to be involved in recycling, and our results indicate that they are larger than those without tubular extensions.

Although it has previously been described that MVBs are related to synapses (Kneussel and Hausrat, 2016), we found no relationship between the density of MVBs and the density of synapses in the different layers. We also studied the spatial distribution of MVBs, and we found that in 70% of our stacks, MVBs were randomly distributed in space, while they showed a tendency to cluster in the remaining 30%. The quantitative method that we have developed in the present study will help determine the possible alterations of the endosomal pathway in pathological conditions.

REFERENCES

- Chivet, M., Javalet, C., Hemming, F., Pernet-Gallay, K., Laulagnier, K., Fraboulet, S., et al. (2013). Exosomes as a novel way of interneuronal communication. *Biochem. Soc. Trans.* 41, 241–244. doi: 10.1042/BST20120266 PMID:23356290
- Kneussel, M., and Hausrat, T. J. (2016). Postsynaptic neurotransmitter receptor reserve pools for synaptic potentiation. *Trends Neurosci.* 39, 170–182. doi: 10.1016/j.tins.2016.01.002 PMID:26833258
- Merchán-Pérez, A., Rodríguez, J.-R., Alonso-Nanclares, L., Schertel, A., and Defelipe, J. (2009). Counting synapses using FIB/SEM microscopy: a true revolution for ultrastructural volume reconstruction. *Front. Neuroanat.* 3:18. doi: 10.3389/neuro.05.018.2009 PMID:19949485
- Morales, J., Alonso-Nanclares, L., Rodríguez, J.-R., Defelipe, J., Rodríguez, A., and Merchán-Pérez, A. (2011). Espina: a tool for the automated segmentation and counting of synapses in large stacks of electron microscopy images. *Front. Neuroanat.* 5:18. doi: 10.3389/fnana.2011.00018 PMID:21633491
- Schreij, A. M. A., Fon, E. A., and McPherson, P. S. (2016). Endocytic membrane trafficking and neurodegenerative disease. *Cell. Mol. Life Sci.* 73, 1529–1545. doi: 10.1007/s00018-015-2105-x PMID:26721251
- Sugiura, A., McLelland, G.-L., Fon, E. A., and McBride, H. M. (2014). A new pathway for mitochondrial quality control: mitochondrial-derived vesicles. *EMBO J.* 33, 2142–2156. doi: 10.15252/embj.201488104 PMID:25107473
- Von Bartheld, C. S., and Altick, A. L. (2011). Multivesicular bodies in neurons: distribution, protein content, and trafficking functions. *Prog. Neurobiol.* 93, 313–340. doi: 10.1016/j.pneurobio.2011.01.003 PMID:21216273

Comparing Synaptic Connectivity of Stress-Resilient and Stress-Susceptible Rats in the Default Network after Applying Learned-Helplessness Paradigm

Annika Utz, Svend Davanger

Institute of Basic Medical Sciences, University Of Oslo, Oslo, Norway.

julia.wrzo@gmail.com

Background/Idea: In the last decades many attempts have been made to find the physiological changes underlying psychological disorders. Among those disorders, depression is the most prevalent one, affecting between 4 and 15% of the population during their lifetime. Besides the psychological aspect physical health issues like diabetes and coronary artery diseases coincide with depression leading to higher morbidity and mortality (Moussavi et al., 2007). Causes for developing depression are numerous. Susceptibility to this illness differs within the population. The reasons for this variation are still not sufficiently understood.

Studies showed that the prefrontal cortex, hippocampus and amygdala have altered activity in patients with major depressive disorder (MDD) (Palazidou, 2012). Several animal models were developed to investigate the occurred changes in more detail. One of those is the learned helplessness paradigm, in which an inescapable foot shock is applied until the animal does not try to escape anymore even when given the possibility. As a consequence those animals show a decreased interest in sucrose-consumption resembling anhedonia as well as REM-sleep changes which can be seen in humans with MDD. By using only a moderate foot shock the animals show more varied responses, some developing depression-like symptoms while others do not (Vollmayr and Gass, 2013). Rats which underwent this procedure showed a decrease in synapse number within the hippocampus, while treatment with antidepressants restored the number of synapses in some hippocampal areas (Hajszan et al., 2009). Similar changes in synaptic connectivity could possibly also be observed in the default network regions of the brain. These structures decrease their activity during attention-demanding tasks and are more active during resting-state (Raichle, 2015). The default network activity has also been found in rats (Lu et al., 2012). Changes in connectivity have been found in meditation practitioners compared to control (Jang et al., 2011) and in schizophrenic patients (Pankow et al., 2015). Functional connectivity studies found that MDD resulted in a hyperconnectivity within the default network (Kaiser et al., 2015).

The rats which are used for this project underwent a learned-helplessness paradigm with moderate foot shocks. To investigate molecular changes at synapses within the default network I will quantify the relative concentration of several proteins associated with the strength in synaptic connectivity within the cingulate cortex of rats, a key region of the default network. Those proteins include presynaptic and postsynaptic proteins.

Glutamatergic synapses show a dense post-synaptic structure called post-synaptic density (PSD). The PSD is located close to the membrane and serves among other functions as an anchoring structure for glutamate receptors. PSD95 is one of most abundant proteins in this protein complex and can be used as an indicator for the number of excitatory synapses (Chen et al., 2015). To determine the strength of a glutamatergic synapse the quantity of AMPA (α -amino-3-hydroxy-5-methyl-4-isoxazolepropionic acid) receptor subunits is analyzed. The abundance of AMPARs is the major factor in determining the size of an excitatory post-synaptic potential. Strengthening of synapses goes along with higher densities of AMPARs in the post-synaptic membrane, while weakening results in a decrease of number. AMPA receptors are important for several forms of learning (Keifer and Zheng, 2010). There are different signaling pathways to change the strength of synaptic connections, one of those being NMDAR (*N*-methyl-D-aspartic acid)-dependent potentiation/depression. NMDARs only open when the post-synaptic membrane is depolarized and glutamate simultaneously binds to the NMDAR. The channel is permeable to sodium and, importantly, calcium ions. A high rise in calcium ions leads over a signaling cascade to phosphorylation of AMPARs and an increase of AMPARs in the post-synaptic membrane (Nicoll and Roche, 2013). Early life events can result in changes of NMDAR-subunit composition. During a critical period a genetic switch ensures a change from primarily GluN2B subunits to primarily GluN2A subunits. Maternal deprivation was shown to impair this genetic switch (Timmermans et al., 2013). Implementation of GluN2A as opposed to GluN2B subunits results in a change of NMDAR-kinetics. This probably changes the calcium-influx at the post-synaptic membrane and thus the threshold for long-term potentiation (Cull-Candy et al., 2001).

It is also interesting to see whether synaptic changes coincide with extracellular alterations. The perineuronal net (PNN) is a type of extracellular matrix which is assumed to be involved in stabilizing neuronal connections in the brain (Morawski et al., 2012). The PNN consists in big parts of chondroitin sulphated proteoglycans (CSPG) like aggrecan, hyaluronic acid (HA) and tenascin-R. In the visual cortex of cats aggrecan expression starts to increase when experience-dependent synaptic plasticity begins to decline (Kind et al., 2013). It was also found that plasticity-resistant excitatory CA2 pyramidal neurons in the hippocampus could undergo synaptic potentiation after impairing the PNN (Carstens et al., 2016). The cartilage link protein (Crtl1) stabilizes

connections between CSPG and HA in the PNN and might be necessary to form the PNN in the first place (Carulli et al., 2010). For this reason I will quantify the relative concentration of Crtl1 to check for extracellular differences. Additionally, presynaptic proteins, like vesicle proteins (e.g., synaptotagmin and synaptophysin) and presynaptic membrane proteins (e.g., SNAP25) as well as metabotropic glutamate receptor 1 and 7 are quantified relatively.

Aims: The aim of this study is to compare changes in concentration of proteins linked to synaptic strength of depression-resilient and depression-susceptible rats after receiving learned-helplessness treatment. The concentrations of the above mentioned proteins will be quantified by western blot referenced to whole protein concentration. The crude synaptosomal fractions of the following areas are being analyzed: cingulate cortex, hippocampus, primary somatosensory cortex and primary motor cortex.

Hypothesis: I hypothesize a difference in protein concentrations within the cingulate cortex and the hippocampus in depression-susceptible rats compared to resilient ones. There should be no significant difference within the primary somatosensory and motor cortex.

Possible implications: Investigating synaptic protein concentrations within the default network will contribute to a better understanding of the role played by the default network in depression disorders. These regions of the brain should thus be targeted in future therapeutic interventions. It will also be interesting to see whether presynaptic terminals or postsynaptic membrane proteins differ in their protein composition when comparing stress-resilient to stress-susceptible rats. The comparison between established plasticity markers like AMPAR subunits and GluN2A/GluN2B ratio as well as Crtl1 concentrations will hopefully elucidate their role in synaptic plasticity as well.

REFERENCES

- Carstens, K. E., Phillips, M. L., Pozzo-Miller, L., Weinberg, R. J., and Dudek, S. M. (2016). Perineuronal nets suppress plasticity of excitatory synapses on ca2 pyramidal neurons. *J. Neurosci.* 36, 6312–6320. doi: 10.1523/JNEUROSCI.0245-16.2016 PMID:27277807
- Carulli, D., Pizzorusso, T., Kwok, J. C., Putignano, E., Poli, A., Forostyak, S., et al. (2010). Animals lacking link protein have attenuated perineuronal nets and persistent plasticity. *Brain* 133, 2331–2347. doi: 10.1093/brain/awq145 PMID:20566484
- Chen, X., Levy, J. M., Hou, A., Winters, C., Azzam, R., Sousa, A. A., et al. (2015). Psd-95 family maguks are essential for anchoring ampa and nmda receptor complexes at the postsynaptic density. *Proc. Natl. Acad. Sci. U. S. A.* 112, E6983–E6992. doi: 10.1073/pnas.1517045112 PMID:26604311
- Cull-Candy, S., Brickley, S., and Farrant, M. (2001). Nmda receptor subunits: diversity, development and disease. *Curr. Opin. Neurobiol.* 11, 327–335. doi: 10.1016/S0959-4388(00)00215-4 PMID:11399431

- Hajszan, T., Dow, A., Warner-Schmidt, J. L., Szigeti-Buck, K., Sallam, N. L., Parducz, A., et al. (2009). Remodeling of hippocampal spine synapses in the rat learned helplessness model of depression. *Biol. Psychiatry* 65, 392–400. doi: 10.1016/j.biopsych.2008.09.031 PMID:19006787
- Jang, J. H., Jung, W. H., Kang, D. H., Byun, M. S., Kwon, S. J., Choi, C. H., et al. (2011). Increased default mode network connectivity associated with meditation. *Neurosci. Lett.* 487, 358–362. doi: 10.1016/j.neulet.2010.10.056 PMID:21034792
- Kaiser, R. H., Andrews-Hanna, J. R., Wager, T. D., and Pizzagalli, D. A. (2015). Large-scale network dysfunction in major depressive disorder: Meta-analysis of resting-state functional connectivity. *JAMA Psychiatry* 72, 603–611. doi: 10.1001/jamapsychiatry.2015.0071 PMID:NOPMID
- Keifer, J., and Zheng, Z. (2010). Ampa receptor trafficking and learning. *Eur. J. Neurosci.* 32, 269–277. doi: 10.1111/j.1460-9568.2010.07339.x PMID:NOPMID
- Kind, P. C., Sengpiel, F., Beaver, C. J., Crocker-Buque, A., Kelly, G. M., Matthews, R. T., et al. (2013). The development and activity-dependent expression of aggrecan in the cat visual cortex. *Cereb. Cortex* 23, 349–360. doi: 10.1093/cercor/bhs015 PMID:22368089
- Lu, H., Zou, Q., Gu, H., Raichle, M. E., Stein, E. A., and Yang, Y. (2012). Rat brains also have a default mode network. *Proc. Natl. Acad. Sci. U. S. A.* 109, 3979–3984. doi: 10.1073/pnas.1200506109 PMID:22355129
- Morawski, M., Bruckner, G., Arendt, T., and Matthews, R. T. (2012). Aggrecan: beyond cartilage and into the brain. *Int. J. Biochem. Cell. Biol.* 44, 690–693. doi: 10.1016/j.biocel.2012.01.010 PMID:22297263
- Moussavi, S., Chatterji, S., Verdes, E., Tandon, A., Patel, V., and Ustun, B. (2007). Depression, chronic diseases, and decrements in health: results from the world health surveys. *Lancet* 370, 851–858. doi: 10.1016/S0140-6736(07)61415-9 PMID:17826170
- Nicoll, R. A., and Roche, K. W. (2013). Long-term potentiation: peeling the onion. *Neuropharmacology* 74, 18–22. doi: 10.1016/j.neuropharm.2013.02.010 PMID:23439383
- Palazidou, E. (2012). The neurobiology of depression. *Br. Med. Bull.* 101, 127–145. doi: 10.1093/bmb/lds004 PMID:NOPMID
- Pankow, A., Deserno, L., Walter, M., Fydrich, T., Bermpohl, F., Schlagenaus, F., et al. (2015). Reduced default mode network connectivity in schizophrenia patients. *Schizophr. Res.* 165, 90–93. doi: 10.1016/j.schres.2015.03.027 PMID:25892719
- Raichle, M. E. (2015). The brain's default mode network. *Annu. Rev. Neurosci.* 38, 433–447. doi: 10.1146/annurev-neuro-071013-014030 PMID:25938726
- Timmermans, W., Xiong, H., Hoogenraad, C. C., and Krugers, H. J. (2013). Stress and excitatory synapses: from health to disease. *Neuroscience* 248, 626–636. doi: 10.1016/j.neuroscience.2013.05.043 PMID:23727506
- Vollmayr, B., and Gass, P. (2013). Learned helplessness: unique features and translational value of a cognitive depression model. *Cell Tissue Res.* 354, 171–178. doi: 10.1007/s00441-013-1654-2 PMID:23760889

Neuropeptide Y and Y2R in Emotional and Non-Emotional Learning

Birgit A. Hörmer¹, Dilip Verma¹, Elisabeth Gasser¹, Herbert Herzog², Ramon O. Tasan¹

¹Medical University Innsbruck, Institute of Pharmacology, Innsbruck, Austria

²Garvan Institute of Medical Research, Neuroscience Division, Darlinghurst, Sydney, NSW, Australia
birgit.hoermer@i-med.ac.at

Introduction: Neuropeptide Y (NPY) is highly enriched in limbic brain areas and well known for its anxiolytic and fear-suppressing properties. These effects are predominantly mediated by Y1 receptors. The role of the extensively expressed pre-synaptic Y2 receptors (Y2R) is, however, not clear yet. We aimed at investigating the role of hippocampal Y2R in fear learning as well as non-emotional learning.

Methods: Wildtype and Y2KO mice were subjected to different forms of hippocampus-dependent Pavlovian fear conditioning and the Barnes maze test for non-emotional learning. Furthermore, we combined cell-type specific viral vector-mediated rescue of Y2 receptor expression in Y2KO mice with immunohistochemical methods and receptor binding to differentiate the Y2-mediated effects in different hippocampal subfields and cell types. We further conducted neuronal tract tracing studies using transgenic mice, viral vectors and immunohistochemistry to identify different populations and synaptic partners of NPY-expressing neurons of the hippocampus.

Results: Y2KO mice did not differentiate between similar fear contexts in a pattern separation paradigm. In addition, the temporal precision and stimulus specific expression of freezing behaviour in trace fear conditioning was lost, suggesting fear generalization. When Y2R were reintroduced specifically in the dorsal dentate gyrus of Y2KO mice, freezing behaviour was significantly reduced and temporal precision was largely restored. Interestingly, re-expression of Y2R in the dorsal hippocampus of Y2KO mice also reduced the consolidation of spatial memory in the Barnes maze. Immunohistochemical analysis showed co-expression of NPY with Parvalbumin (Pvalb) as well as Somatostatin (Sst), but not Calretinin in the mouse dentate gyrus. Furthermore, in addition to their local function as interneurons, both, SST as well as Pvalb-neurons of the dentate gyrus were sending projections to other brain areas, such as the medial septum and the cortical amygdala.

Discussion These data indicate that Y2R are crucial for differentiating similar fear contexts, while their absence may result in fear generalization, a hallmark of anxiety

disorders. On the other hand, Y2R may be crucial for memory consolidation. Thus, NPY neurons of the dentate gyrus may control memory formation in the hippocampus also by activation of pre-synaptic Y2 receptors. Further investigations will address the role of NPY-expressing projection neurons of the dentate gyrus in memory formation. *Supported by FWF-P25851.*

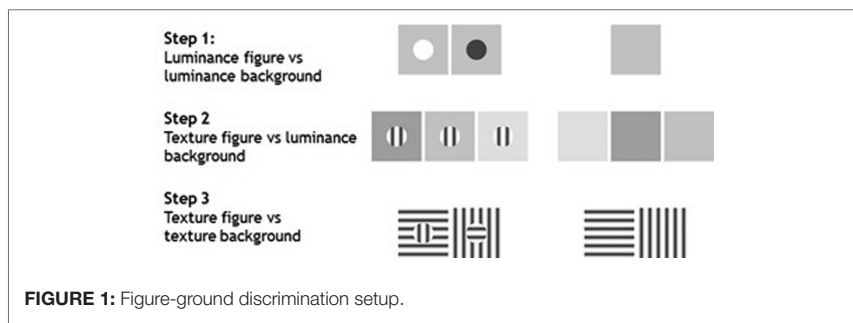
Assessment of Mid-Level Vision Segregation in Mice

William John Redmond, Christophe Bossens, Hans Op De Beeck;

*Ku Leuven, Leuven, Belgium
william.redmond@mq.edu.au*

The ease and rapidity with which we perceive and compute our environment keeps puzzling vision scientists to this day, and the ability of rodents to perceive and categorize objects, long neglected, has now resurfaced. A recent paper from our group showed that rats are able to dissociate visual presentation based on second-order variables such as textures. Once this initial learning is acquired, they can generalize this discrimination in various ways with surprising ease (De Keyser et al., 2015). The broad objective of our project is to unravel the neural correlates of visual perception and image segmentation in the mouse primary visual cortex. In this preliminary work, the development of visual stimulations and training procedures to assess mid-level vision segregation in mice is described. Animals performed discrimination tasks in eight automated touch screen operant chambers. 8 mice were trained with figure-ground discrimination in 3 incremental steps in order to dissociate second-order texture based features (Figure 1). Mice reached a threshold performance of 80% correct after 9.0 SD = 3.3 sessions on average for discrimination involving only luminance cues. Average discrimination performance for the new stimuli in step 2 during the first session that they were introduced was 84.3% SD = 0.1, indicating that they were able to generalize based on the stimuli from step 1. In contrast, discrimination performance for the new stimuli in the first session of step 3 dropped to 64.3% SD = 1.1, before rising. On average, mice needed 5.8 SD = 1.1 training sessions to get back to threshold performance of 80%.

The preliminary data shown therein indicate that mice are able to distinguish mid-level vision features through an incremental learning procedure.



The Presence of Corpora Amylacea and Microglial Cells in Individuals with Unspecified Encephalopathy

Iveta Beinarovica, Sandra Skuja, Valerie Groma

*Riga Stradins University, Riga, Latvia
iveta.beinarovicha@gmail.com*

Introduction: Corpora amylacea (CA) is translucent spherical structure that is easily detectable on routine preparations. The cellular origin of CA is not yet clearly defined. The previous studies showed that CA is aging or cellular stress indicator, but the presence of CA in neuroinflammation remains unclear (Hoyaux et al., 2000; Rohn, 2015). Still, it has been suggested that CA are inclusions, which are observed in greatest numbers in astrocytic foot processes, particularly around blood vessels and beneath the pia mater (Mills, 2012). In the central nervous system, microglial cells are the resident phagocytes of the innate immune system. Microglial cells are traditionally referred as a key of the inflammatory process developing in nervous tissue response to various harmful agents (Korzhevskii and Kirik, 2016). In this activated state microglia produce various proinflammatory cytokines and immune mediators that create a neurotoxic milieu leading to the progression of diseases (Krause and Muller, 2010). The purpose of this study is to investigate the presence of CA as cellular stress indicators, thus correlating astrocytic and microglial response in individuals with unspecified encephalopathy.

Materials and Methods: Brain tissues autopsy samples were selected from 25 individuals with unspecified encephalopathy and 30 controls; age range was between 42–76 and 49–74 years, respectively. Thereafter, the gray and the white brain matter obtained from temporal and frontal lobes were sectioned. The post-mortem interval allowed for this study was 24–96 h. The inclusion criteria were pathomorphological signs of an unspecified encephalopathy on tissue examination. The individuals with inflammatory and non-inflammatory hepatic diseases were excluded from the study. CA quantification was carried out in 10 vision fields of routine histology slides. Immunohistochemical reactions using anti-CD68 monoclonal antibody were performed for decoration of the activated microglia/macrophages. Quantitative estimation of immunopositive cells in 10 randomly selected vision fields of each specimen was performed. All tissue sections were analysed using a Leica microscope (×400).

The results are presented as medians with interquartile values [IQR (25%;75%)]. Chi-Square test was used for comparison of several categorized variables. Immunoreactivity values between groups were analysed with Mann Whitney U test, in group—with Wilcoxon Signed Ranks test. Spearman's rank correlation coefficient

was used to estimate a relation between CA and CD68 expression. The significance level (p) with value, which is less than 0.05 is assumed as statistically significant. Calculations were performed using SPSS 23.0 programme.

Results: Our investigation showed that a higher number of CA, located in the white matter of the frontal and temporal lobes are observed in the individuals with the unspecified encephalopathy when compared to the control group. Statistically higher ($p < 0.001$) numbers of CA were observed in the white matter of the frontal and temporal lobes in the individuals with unspecified encephalopathy (1.00 (0.00; 1.00) and 0.00 (0.00; 0.00); 1.00 (0.00; 2.00) and 0.00 (0.00; 1.00), respectively), and controls (0.00 (0.00; 1.00) and 0.00 (0.00; 0.00); 0.00 (0.00; 2.00) and 0.00 (0.00; 1.00), respectively), when compared to the gray matter. CA mostly displayed perivascular location both, within the gray and white matter, and were found in higher numbers in pial, subpial, and periventricular regions of the brain. The number of microglial cells was significantly higher ($p < 0.001$) in the white than in the gray matter in the frontal (12.00 (8.00; 15.00) and 4.00 (2.00; 7.00), respectively) as well as in the temporal lobe 9.00 (6.75; 12.00) and 3.00 (2.00; 5.00), respectively) in encephalopathy group. Similarity was found in controls presented as 8.00 (5.00; 12.00) and 4.00 (2.00; 6.00) in the frontal, and temporal lobe 9.00 (6.00; 12.00) and 3.00 (2.00; 6.00), respectively. Statistically higher ($p < 0.001$) numbers of microglial cells were detected in the white matter of individuals with unspecified encephalopathy when compared with controls—12.00 (8.00; 15.00) and 8.00 (5.00; 12.00), respectively, although there are no significant differences when comparing the numbers of microglia in temporal lobe between individuals of both encephalopathy and control groups. There are positive correlations found between number of microglia located in gray and white matter of frontal lobe in the individuals with unspecified encephalopathy and controls ($r = 0.575$, $p < 0.001$, and $r = 0.481$, $p < 0.001$, respectively). There were no correlations between CA and microglia in the frontal lobe in both encephalopathy and control cases. There are positive correlations found between number of microglia located in gray and white matter of temporal lobe in the individuals with unspecified encephalopathy and controls ($r = 0.349$, $p < 0.001$, and $r = 0.171$, $p < 0.001$, respectively). There were negative correlations ($r = -0.135$, $p < 0.001$) found in the white matter between CA and microglia in the temporal lobe in control cases.

Conclusions: Our study showed higher number of CA and microglial cells located in the white matter of frontal and temporal lobes in case of unspecified encephalopathy when compared to controls. The higher numbers of CA were observed in temporal lobe within the white matter when compared with frontal lobe. Increasing evidence of CA may reflect chronic neurodegenerative damage, whereas elevation in a number of microglial cells may be associated with inflammatory processes affecting the frontal lobe of the brain.

REFERENCES

- Hoyaux, D., Decaestecker, C., Heizmann, C. W., Vogl, T., Schafer, B. W., Salmon, I., et al. (2000). S100 proteins in *Corpora amylacea* from normal human brain. *Brain Res.* 867, 280–288. doi: 10.1016/S0006-8993(00)02393-3 PMID:10837826
- Krause, D. L., and Muller, N. (2010). Neuroinflammation, microglia and implications of anti-inflammatory treatment in Alzheimer's disease. *Int. J. Alzheimer Dis.* 2010, 732806. doi: 10.4061/2010/732806 PMID:NOPMID
- Mills, S. E. (2012). *Histology for Pathologists*, 4th Edn. Philadelphia: Lippincott Williams & Wilkins, a Wolters Kluwer Business, 311.
- Rohn, T. T. (2015). Corpora amylacea in neurodegenerative diseases: cause or effect? *Int. J. Neurol. Neurother.* 2, 031. doi: 10.23937/2378-3001/2/2/1031 PMID:26550607

From Membranes to Transistors: A Physical Model of Spiking Neurons

Gerd Kiene, Paul Müller, Johannes Schemmel, Karlheinz Meier

*Heidelberg University, Heidelberg, Germany
gerd.kiene@kip.uni-heidelberg.de*

To expand our understanding of the underlying mechanisms governing information processing and especially learning in neural networks, the ability to employ large-scale simulations is essential. Current trends in conventional processor technology indicate that general-purpose processors will face significant difficulties in achieving both the cost-efficiency and the performance required for human-brain-size neural network simulations. In particular, the simulation of slow processes such as learning and development appears particularly unfeasible. As a potential solution, the development of specialized neuromorphic hardware has been proposed, containing circuitry that mimics neuronal and synaptic dynamics while operating with significantly lower power consumption and at much higher speeds than conventional simulation platforms (Schemmel et al., 2008).

Here, we focus on the design of such a neuromorphic neuron circuit: starting from specifications given in seminal literature from both experimental and computational neuroscience, we sketch how neuronal dynamics can be implemented in a micro-electronic circuit. This neuron model is an integral part of the newest generation of HICANN-DLS (High Input Count Analog Neural Network-Dynamic Learning System) chips developed at the Heidelberg University as part of the HBP Neuromorphic Computing Platform (Aamir et al., 2016).

The chip aims at implementing a highly configurable physical representation of the adaptive exponential integrate-and-fire neuron model (Brette and Gerstner, 2005). The neuron on the HICANN-DLS mixes analog as well digital building blocks to efficiently represent the model's dynamics—while optimally using the timescales and possibilities available in microelectronics. Since the technology used for implementing the chip has been updated from a 180 nm to a 65 nm process, design trade-offs have shifted, requiring a fundamental redesign of the neuron circuit. We discuss how technology scaling impacts the balance between digital and analog submodules for executing computations and storing results, and how this provides access to new levels of model precision and system performance.

REFERENCES

- Aamir, S.A., Mueller, P., Hartel, A., Schemmel, J., Meier, K. (2016). "A highly unbalanced 65-nm CMOS LIF neuron for a large scale neuromorphic system," in *Proceedings of IEEE European Solid-State Circuits Conference (ESSCIRC)*, IEEE, Lausanne, Switzerland, 71–74.
- Brette, R., and Gerstner, W. (2005). Adaptive exponential integrate-and-fire model as an effective description of neuronal activity. *J. Neurophysiol.* 94, 3637–3642. doi: 10.1152/jn.00686.2005 PMID:16014787
- Schemmel, J., Fieser, J., Meier, K. (2008). "Wafer-scale integration of analog neural networks," in *2008 IEEE International Joint Conference on Neural Networks (IEEE World Congress on Computational Intelligence)*, Hong Kong, China, 431–438.

The Play Pen – Accelerated Embodiment for Accelerated Hardware

Korbinian Schreiber¹, Johannes Schemmel, Karlheinz Meier

¹University of Heidelberg, Heidelberg, Germany

k.schreiber@kjp.uni-heidelberg.de

The complete spectrum of phenomena relevant for understanding brain function comprises not only physiological aspects of neuro-synaptic dynamics on a microscopic scale, but also the functional properties of the system as a whole. For embodied neural networks—which is the case for all biological brains - these can only be understood in the context of behaviour, which almost by definition requires an interaction with the external world. Learning is an essential component of behaviour development and can be viewed as continuously updating an internal model of the external world as a consequence of the ongoing agent- environment interaction (Rao and Ballard, 1999; Hawkins and George, 2006; Friston, 2010).

While experimental data does provide some information about the plasticity mechanisms underlying learning in the brain, it does not fully constrain the learning rules and associated parameters required for ultimately producing the targeted behaviour. Simulations of learning networks will therefore need to perform some form of learning rule optimization, which in turn is likely to require a large number of training scenarios.

One solution is offered by accelerated neuromorphic hardware (Schemmel et al., 2008). The HICANN-DLS (High Input Count Analog Neural Network—Dynamic Learning System)—a neuromorphic system developed for flexible high-speed learning tasks—offers an accelerated emulation platform for spiking neural networks operating at a 1,000-fold speed-up compared to biological real-time (Aamir et al., 2016). As the system also contains a digital processing unit that is tightly coupled to all relevant parts of the neural network and optimized for parallel computing tasks, it enables the application and adjustment of learning rules during runtime.

Combining this hardware with a virtual, i.e., simulated habitat for a neuromorphic agent would require a fast low-latency link to an equally accelerated environment simulation. Alternatively, instead of connecting the hardware to a simulation, it could also be directly connected to a set of real-world actuators and sensors.

Our approach for such a real-world environment is called the Play Pen, a physical experimentation platform specifically designed for high-speed neuromorphic systems.

With the Play Pen, a large number of possible control and learning problems can be realized in a very direct and user-interactive way. A Play Pen experiment runs continuously and produces output, not only in the form of recorded time series of internal dynamical variables, but also in terms of physical movement, which in turn affects the agent's environment, thus closing the sensor-actuator loop. We discuss the fast mechanical components required to realize the Play Pen and also describe several interactive learning scenarios that we envision for our embodied neuromorphic agents.

REFERENCES

- Aamir, S. A., Mueller, P., Hartel, A., Schemmel, J., and Meier, K. (2016). "A highly unstable 65-nm CMOS LIF neuron for a large scale neuromorphic system," in *Proceedings of IEEE European Solid-State Circuits Conference (ESSCIRC)* (Lausanne, Switzerland: IEEE), 71–74.
- Friston, K. (2010). The free-energy principle: a unified brain theory? *Nat. Rev. Neurosci.* 11, 127–138. doi: 10.1038/nrn2787 PMID:20068583
- Hawkins, J., and George, D. (2006). *Hierarchical Temporal Memory: Concepts, Theory and Terminology*. Redwood City: Numenta. Technical Report.
- Rao, R. P. N., and Ballard, D. H. (1999). Predictive coding in the visual cortex: a functional interpretation of some extra-classical receptive-field effects. *Nat. Neurosci.* 2, 79–87. doi: 10.1038/4580 PMID:10195184
- Schemmel, J., Fieres, J., and Meier, K. (2008). "Wafer-scale integration of analog neural networks," in *2008 IEEE International Joint Conference on Neural Networks (IEEE World Congress on Computational Intelligence)* (Hong Kong, China), 431–438.

Advantages of publishing in Frontiers



OPEN ACCESS

Articles are free to read,
for greatest visibility



COLLABORATIVE PEER-REVIEW

Designed to be rigorous
– yet also collaborative,
fair and constructive



FAST PUBLICATION

Average 85 days from
submission to publication
(across all journals)



COPYRIGHT TO AUTHORS

No limit to article
distribution and re-use



TRANSPARENT

Editors and reviewers
acknowledged by name
on published articles



SUPPORT

By our Swiss-based
editorial team



IMPACT METRICS

Advanced metrics
track your article's impact



GLOBAL SPREAD

5'100'000+ monthly
article views
and downloads



LOOP RESEARCH NETWORK

Our network
increases readership
for your article

Frontiers

EPFL Innovation Park, Building I • 1015 Lausanne • Switzerland
Tel +41 21 510 17 00 • Fax +41 21 510 17 01 • info@frontiersin.org
www.frontiersin.org

Find us on

